S
u

FACULTY OF SCIENCE AND TECHNOLOGY

MASTER THESIS

Study programme / specialisation:
Environmental Engineering / Offshore
Technology

The spring semester, 2022.

Open

Author: Audun Undheim

....
(signature author)

Course coordinator: Malcolm Kelland

Supervisor(s): Malcolm Kelland

Thesis title: A Study on Multi-Functional Oilfield Production Chemicals for Scale, Corrosion and Gas Hydrates

Credits (ECTS): 30

Keywords:

Multi-functional
Corrosion
Kinetic gas hydrate
Scale
Polymer
Green chemicals
Oilfield production chemicals

Pages: 72
....

+ appendix: 8 ....

Stavanger, 15/06/2022
....
date/year

Abstract

Oilfield production chemistry is a wide field which includes many different areas and related difficulties. In this work, focus is on mitigating scale, corrosion, and gas hydrates using chemical inhibitors. Production lines often require chemical treatment for several problems simultaneously, which may cause incompatibility issues. The development of multi-functional inhibitors is based on the idea of treating all three issues simultaneously and avoiding incompatibility. As a part of this development, the ability to test the corrosion inhibition of a compound was paramount. Using the Gamry EuroCell Electrochemical Cell a CO_2 corrosion testing method was reviewed and optimized to reduce deviation and increase replicability. The optimized method was used to test various compounds to investigate which functional groups that could be interesting to include in future inhibitor syntheses. The major results found from this testing were that 500 ppm of a commercial imidazoline exhibited a corrosion inhibition efficiency of 85.4 ± 2.2 %, and that none of the synergists by themselves tested achieved higher efficiency. The compound with highest efficiency was found to be sodium lignosulfonate which exhibited an efficiency of 95.9 ± 1.6 %. An experimental polymer based on polymaleic anhydride reacted with 3,3-dibutylaminopropylamine (DBAPA) and vinylcaprolactam (VCap), abbreviated PMA:VCap-DBAPA, was tested as a CI, both by itself and with various synergists. While the polymer by itself at 500 ppm exhibited an efficiency of 18.1 ± 6.6 %, this was increased to above 90 % by the addition of five separate synergists at 100 ppm, of which the highest was ammonium thiocyanate at 96.0 ± 1.5 %. Overall, synergists with thiol functional groups seemed to generally provide good synergism with PMA:VCap-DBAPA. While synergists with functional groups embedded within a ring structure generally provided poor synergism with PMA:VCap-DBAPA.

Two other projects to synthesise polymers with multi-functional character were also carried out. The synthesis of poly(1-oxy-3-lactam vinylene) was successful for polyoxyvinylcaprolactam (POVCap) and polyoxyvinylpiperidone (POVPip). Copolymers of POVCap and POVPip were tested as corrosion and gas hydrate inhibitors. It was found that a copolymer of 36 % POVCap and 64 % POVPip exhibited a hydrate onset temperature of 11.6 ± 0.1 °C, and corrosion inhibition efficiency of 15.4 ± 3.6 % for pure POVPip. While corrosion results were somewhat higher for copolymers at different ratios, the increased efficiency is likely due to the insoluble part of copolymers with a high molar fraction of OVCap. None of the synergists tested managed to achieve a similar synergism with POVCap as with other polymeric caprolactam containing kinetic gas hydrate inhibitors. Finally, the synthesis of hyperbranched polyamine containing imidazolidine rings based on a publication from a Chinese group was unsuccessful. Many attempts were made with different variations of the synthesis, but none were found to produce the described product.

Acknowledgements

Table of Contents

Table of Figures

Table of Tables

Abbreviations

AA	Anti-agglomerate
AIBN	Azobisisobutyronitrile
AMT	3-Acetamidotetrahydro-2-thiophenone
APIM	1-(3-aminopropyl)imidazole
BID	1-butylimidazole
BOD	Biological oxygen demand
BTG	Butyl thioglycolate
CI	Corrosion inhibitor
CMC	Critical micelle concentration
DBAPA	3,3-dibutylaminopropylami
DCM	Dichloromethane
DIW	Deionized water
DMH	N,N-Dimethylhydrazine
FFCI	Film-forming corrosion inhibitor
GPC	Gel permeation chromatography
GTC	Guanidine thiocyanate
HBGC	Hexabutylguanidinium chloride
iBGE	Iso-butyl glycol ether
IBT	Isobutylthiadiazole
ICI	Iodine monochloride
i-PrCN	Isobutyronitrile
KHI	Kinetic gas hydrate inhibitor
LAWS	Low aromatic white spirit
LPR	Linear polarizaiton resistance
MCSA	Mercaptosuccinic acid
mmpy	Millimetre per year
MPO	4-Methyl-1-pentanol
NMR	Nuclear magnetic resonance
OECD	Organisation for Economic Co-operation and Development
PI	Polymeric inhibitor
PMA	Polymaleic anhydride
PMA:VCap-DBAPA	Polymaleic anhydride reacted with 3,3-dibutylaminopropylamine and N-Vinylcaprolactam
PMA-DBAPA	Polymaleic anhydride reacted with 3,3-dibutylaminopropyla
POVCap	Polyoxyvinylcaprolactam
POVPip	Polyoxyvinylpiperidone
i-PrOH	Isopropanol
PVCap	Poly(N-vinylcaprolactam)
RBF	Round bottom flask
SD	Standard deviation
SFI	Surfactant inhibitor
SI	Scale inhibitor
SLS	Sodium lignosulfonate
SNG	Synthetic natural gas
SRB	Sulfate-reducing bacteria
STF	Sodium thiosulfate
TAO	Tributyl amine oxide in i-PrOH
TBA	2-thiobarbituric acid
TCI	Tokyo Chemical Industry
TDD	2,4,7,9-Tetramethyl-5-decyne-4,7-diol
TGA	Thioglycolic acid
THI	Thermodynamic inhibitor
ThOD	Theoretical oxygen demand
TPAB	Tetrapentylammonium
TPPeAO	Tri-n-pentylamine oxide
UiS	University of Stavanger
VCap	N-vinylcaprolactam

1. Introduction

Oilfield production chemicals is a wide field which includes many more areas than will be described in this thesis. In this work, focus will be maintained on scale, corrosion, and gas hydrates, which has all been described as a severe form of formation damage, critical issue occurring in petroleum production, or extremely undesirable phenomenon (Kamal, 2018, p. 127; Migahed et al., 2018, p. 10; Zhukov et al., 2017, p. 377). This chapter will begin by describing the fundamentals of scale and review a selection of common scale inhibitors (SI). Thereafter fundamentals of corrosion and a selection of common film forming corrosion inhibitors (FFCI) are reviewed. Additionally, both surfactant and polymer based FFCIs are reviewed and discussed. Afterwards, fundamentals of gas hydrates and a selection of common kinetic gas hydrate (KHI) inhibitors are reviewed. Associated with these three types of inhibition are environmental concerns from the possible effluent into offshore waters. Some of these concerns and recent development of green alternatives are therefore investigated. Chemical solutions for scale, corrosion, or gas hydrates may also be incompatible with each other (Kelland et al., 2021, p. 1). The importance of developing a multi-functional inhibitor is based in the idea of treating all three issues simultaneously and avoiding incompatibility. The development of various multi-functional inhibitors for these three types of inhibitors are reviewed.

The chapters following chapter 1, are divided into each of the projects that will be worked for this thesis, in which all projects are a part of the same parent project to develop a multi-functional inhibitor. In chapter 2, we will start by reviewing the method for corrosion testing developed by Undheim (2021), before any steps at optimization of said method are described. The method will then be put into practice and a selection of inhibitors and synergists are tested for their ability to inhibit corrosion, the results from this test are described and discussed in chapter 3. Further on in chapter 4, an experimental polymer which was synthesised at UiS by Janronel Pomicpic, and is a part of the project worked on by Kelland et al. (2021) to develop multi-functional oilfield production chemicals will also be tested. This polymer is based on polymaleic anhydride reacted with 3,3-dibutylaminopropylamine (DBAPA) and vinylcaprolactam (VCap), abbreviated PMA:VCap-DBAPA. In chapter 5, the syntheses of poly(1-oxy-3-lactam vinylene) with 6- and 7-ring structures are described. The resulting polymer- and copolymers are also tested for their ability to inhibit corrosion and gas hydrates, in addition to results from OECD306 seawater test for biodegradability and gel permeation chromatography. The final project worked on is presented in chapter 6, which describes the attempts at synthesising hyperbranched polyamine containing imidazolidine rings. Chapter 7 describes the financial overview over chemicals and items consumed, and chapter 8 describes the major sources for electricity consumption and sources of climate gases for the project. Finally at the end of the thesis, all references and appendices are presented.

1.1. Scale

Deposition of scale is considered a major problem in the production of oil and gas wells (Mpelwa & Tang, 2019, p. 830), as well as in industrial wastewater treatment (Mazumder & A, 2020, p. 1). The formation of scale may lead to restricted flow, breakdown of equipment, and increased operational costs (MacAdam & Jarvis, 2015, p. 5). There may also be high costs associated with the use of cleaning chemicals to remove scale deposits (Mpelwa & Tang, 2019, p. 831). Scale may be one of the three largest water-related production problems, along with corrosion and gas hydrates (Kelland, 2014, p. 51). In this subchapter the fundamentals of scale and a review of common scale inhibitors are presented.

1.1.1. Fundamentals of Scale

Scaling is the deposition of inorganic salt from aqueous solutions (Kelland, 2014, p. 51; P. Zhang et al., 2015, p. 603), but may be used to refer to any hard deposit on the surface of equipment in aqueous environments (Chilingar et al., 2008, p. 118). In the oil industry, the most encountered scales are calcium carbonate, sulfate salts, sulfide scales, and sodium chloride, as listed in Table 1.1.

Table 1.1 Common scale types. Adapted from (Kelland, 2014, p. 51; Mazumder & A, 2020, pp. 5–6; Olajire, 2015, p. 725).

Scale type	Chemical Formula	Mineral
Calcium carbonate	$CaCO_3$	Calcite, aragonite, vaterite
Calcium sulfate	$CaSO_4$	Gypsum, Anhydrite,
Barium sulfate	$BaSO_4$	Barite
Strontium sulfate	$SrSO_4$	Celestite
Lead(II) sulfide	PbS	Galena
Zinc sulfide	ZnS	Sphalerite
Iron sulfide	Fe_xS_x	Pyrrhotite, Troilite, Mackinawite, Pyrite, Marcasite, Greigite
Sodium chloride	$NaCl$	Halite

1.1.1.1. Calcium Carbonate Scales

The formation of calcium carbonate scales is dependent on pH, temperature, ionic strength, calcium cation concentration and bicarbonate concentration (Chilingar et al., 2008, pp. 118–119). Formation of carbonate scaling is a result of changes in temperature and pressure (P. Zhang et al., 2015, p. 603). A pressure loss resulting in calcium scales may occur anywhere in the production system. On an oil production platform, this could for example be across the perforations, at a choke, or anywhere in production tubing, downhole, or topside (Kelland, 2014, p. 52). Calcium carbonate is insoluble in water, and deposits may occur as the equilibrium reaction (1.1) moves to the right (Kelland, 2014, p. 52).

$$2HCO_3^- \leftrightarrow CO_3^{2-} + H_2O + CO_2\ (g) \tag{1.1}$$

If a pressure drop occurs, the equilibrium moves to the right to increase the pressure by forming gaseous CO_2. This in turn increases the concentration of carbonate ions and pH, which eventually might be high enough to precipitate calcium carbonate (Kelland, 2014, p. 52), as given in reaction (1.2).

$$Ca^{2+} + CO_3^{2-} \rightarrow CaCO_3\ (s) \tag{1.2}$$

1.1.1.2. Sulfate Scale

Sulfate scaling may occur due to mixing incompatible brine solutions, such as high sulfate concentration brines mixing with brines high in barium or calcium. Sparingly soluble sulfate scales formed by such mixing (Kelland, 2014, p. 53), as given in reaction (1.3).

$$M^{2+} + SO_4^{2-} \rightarrow MSO_4\ (s) \tag{1.3}$$

1.1.1.3. Sulfide Scales

Sulfide scales are indirectly formed by the activity of sulfate-reducing bacteria (SRB). Although formation waters naturally contain hydrogen sulfide (H_2S), most of it is formed as SRB reduce sulfate ions to hydrogen sulfide. SRB reduce sulfate ions to hydrogen sulfide,

which is in equilibrium with hydrosulfide and sulfide ions (Kelland, 2014, p. 54), as given in reaction (1.4) and (1.5).

$$H_2S + H_2O \leftrightarrow H_3O^+ + HS^- \tag{1.4}$$

$$HS^- + H_2O \leftrightarrow H_3O^+ + S^{2-} \tag{1.5}$$

Through corrosion of steel in the production system, iron(II) ions are be formed. These iron ions may react with the sulfide ions and form iron sulfide scale (Kelland, 2014, p. 54), as given in reaction (1.6).

$$Fe^{2+} + S^{2-} \rightarrow FeS \ (s) \tag{1.6}$$

1.1.2. Scale Inhibitors

Scale inhibitors (SI) are a group of water-soluble chemicals with the capability of reducing the precipitation and deposition of scale (P. Zhang et al., 2015, p. 607). This may be achieved through prevention or retardation of nucleation and/or crystal growth (Kelland, 2014, p. 56). SIs have proven to be a cost-effective and economic way of treating scale deposits (Mpelwa & Tang, 2019, p. 831). Although there is an increasing concern for the environmental impact associated with the discharge of many of these compounds (Hasson et al., 2011, p. 7606). Due to the toxicity and low biodegradation of some SIs, there is a move to replace these with green chemicals (P. Zhang et al., 2015, p. 608). SIs are commonly derived from three groups: organophosphates, polyelectrolytes, and condensed polyphosphates (Shemer & Hasson, 2015, p. 3479). Phosphonate or polymer-based SI form complexes with the Ca^{2+} or Ba^{2+} ions, or they may adsorb onto the barium or calcium salts to prevent their growth (Mékarbané et al., 2019, p. 2).

1.1.2.1. Polyphosphates and Phosphate Esters

Polyphosphates and phosphate esters as presented in Figure 1.1 and Figure 1.2, respectively, are both able to prevent deposition of calcium carbonate scales. If the brine conditions are not very acidic, some of these compounds may also function as an inhibitor for barite scale formation (Kelland, 2014, p. 58; P. Zhang et al., 2015, p. 842). Polyphosphate anions are effective SIs and may be used as CIs (Mpelwa & Tang, 2019, p. 840) while also being nontoxic and cost-effective (Mazumder & A, 2020, p. 928). Although they are mainly used in boiler water treatment at low calcium concentrations, because there are more thermally stable products with better compatibility for oilfield applications (Kelland, 2014, p. 58). There has been reported problems of eutrophication associated with the effluent of desalination plants where polyphosphates have been used. Polyphosphates easily hydrolyse into orthophosphate, which is a nutrient for primary producers (Lattemann & Höpner, 2008, p. 9). Phosphate esters are more tolerant of low pH conditions, generally compatible with high-calcium brines and exhibit more environmentally friendly properties, although they are only stable up to 95 – 110 °C (Kelland, 2014, pp. 58–59).
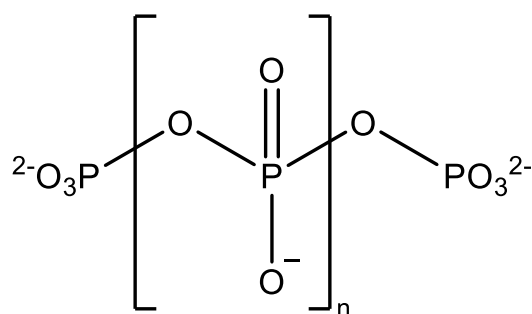
Figure 1.1 Structure of polyphosphate anion.
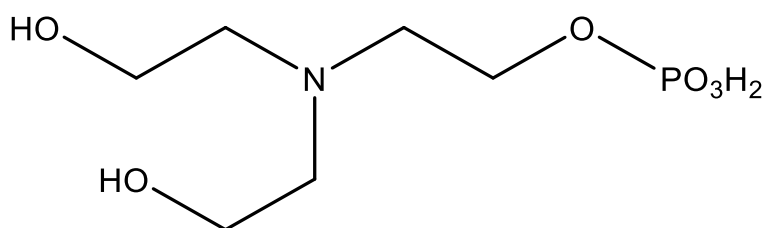
Figure 1.2 Structure of triethanolamine phosphate ester.

1.1.2.2. Nonpolymeric Phosphonates and Aminophosphonates.

A commonly used phosphonate is 2-phosphonobutane-1,2,4-tricarboxylic acid, as presented in Figure 1.3, is mostly used as a calcite SI. Another common phosphonate is 1-hydroxyethylidene-1,1-diphosphonic acid (P. Zhang et al., 2015, p. 608). The metal binding ability can be greatly increased by introducing an amine group (Kelland, 2014, p. 60).

This paragraph is adapted from Zhang et al. (2015, pp. 607–608). While diethylenetriamine-pentakis(methylenephosphonic acid exhibit great inhibition for barite and calcite scale, bis-hexamethylenetriaminepentakis (methylenephosphonic acid) can be useful for high temperature conditions and exhibit improved calcium tolerance. Although aminophosphonates typically have low bioaccumulation and toxicity, they also have low biodegradability. Due to this, in environmentally sensitive areas they may need to be replaced with green inhibitors.
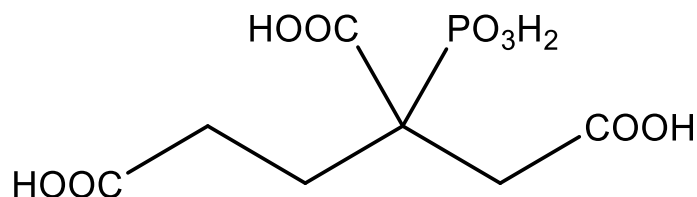
Figure 1.3 Structure of 2-phosphobutane-1,2,4-tricarboxylic acid.

1.1.2.3. Phosphino Polymers and Polyphosphinates

Polyphosphinocarboxylic acid (PPCA), as presented in Figure 1.4, is the most used phosphino polymer for scale inhibition. PPCA exhibit enhanced calcium compatibility and inhibition performance due to the presence of phosphorus. Attachment to formation rocks is also increased, which extends the squeeze lifetime (Ghorbani et al., 2017, p. 310; P. Zhang et al., 2015, p. 608).
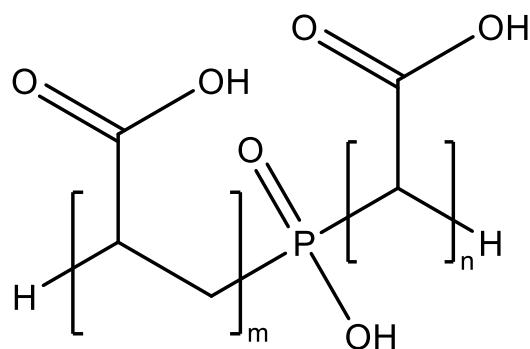
Figure 1.4 Structure of polyphosphinocarboxylic acid.

1.1.2.4. Polysulfonates

Polysulfonates are sulfonated polymeric SIs which exhibit high thermal stability and calcium tolerance. Most commercial polysulfonates have a polyvinyl backbone and adsorbs poorer to rock than phosphonates (Kelland, 2014, p. 68). The structure of styrene sulfonic acid is presented in Figure 1.5.
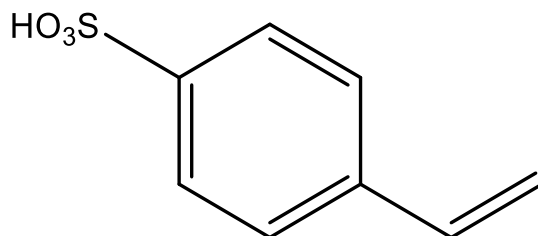
Figure 1.5 Structure of styrene sulfonic acid.

1.2. Corrosion

Corrosion is an electrochemical reaction with the environment which cause degradation in a material's properties. In most cases corrosion means electrochemical oxidation of metal (Tang, 2019, p. 1). In the petroleum industry, corrosion is a major problem and may occur in storage tanks, pressure vessels, pipelines, or in downhole tubing and equipment (Kelland, 2014, p. 191). In a study by National Association of Corrosion Engineers (NACE) the global cost of corrosion was estimated to be \$2.5 trillion annually, which is equivalent to 3.4 % of the 2013 global Gross Domestic Product (GDP) (Koch et al., 2016, p. 4). There are several different methods to control corrosion, where prevention is considered the best way (Galio & Dariva, 2014, p. 365). For carbon steel, inhibition is often considered the most practical and cost-effective method (Jaal et al., 2014, p. 1). Corrosion inhibitors are generally divided into four groups: anodic, cathodic, vapor phase, and film forming. Anodic and cathodic inhibitors are not used in production operations, and vapor phase are occasionally used in wet gas lines or gas coolers (Kelland, 2014, pp. 194–195). In this work, focus will be maintained on the utilisation of film-forming corrosion inhibitor (FFCI) for CO_2 corrosion, which is the main tool used in the oil and gas industry (Olvera-Martínez et al., 2015, p. 1). This chapter will begin by exploring the fundamentals of corrosion, which includes subchapters on sweet and sour corrosion, as well as corrosion inhibitors (CIs) in general and a brief explanation of adsorption. Thereafter, a selection of both surfactant and polymeric based FFCI will be reviewed and discussed.

1.2.1. Fundamentals of Corrosion

The redox reaction of corrosion occurs between anodic and cathodic sections on a metal surface. In an acidic solution the general cathodic reaction is as given in reaction (1.7) and (1.8). This subchapter is based on the work of Kelland (2014, p. 191), unless otherwise noted.

$$2H^+ + 2e^- \rightarrow 2H \tag{1.7}$$

$$H + H \rightarrow H_2 \tag{1.8}$$

In neutral or basic solution, the cathodic reaction is as given in reaction (1.9).

$$O_2 + 2H_2O + 4E^- \rightarrow 4OH^- \tag{1.9}$$

At the anode, iron is oxidised as given in reaction (1.10).

$$Fe \rightarrow Fe^{2+} + 2e^- \tag{1.10}$$

The generated hydroxide ions react with iron(II) ions to form insoluble iron(II) hydroxide (ferrous hydroxide), as given in reaction (1.11).

$$Fe^{2+} + 2OH^- \rightarrow Fe(OH)_2 \tag{1.11}$$

While iron(II) hydroxide can be oxidised to iron(III) hydroxide (ferric hydroxide) in the presence of oxygen, produced fluids are usually anaerobic. Under anaerobic conditions the Schikorr reaction may occur, where iron(II) hydroxide are oxidised by the protons of water to form iron(II,III) oxide (magnetite) (Ma et al., 2013, p. 1), as given in reaction (1.12).

$$3Fe(OH)_2 \rightarrow Fe_3O_4 + H_2 + 2H_2O \tag{1.12}$$

1.2.1.1. Sour Corrosion

Sour corrosion is the degradation of a metal in the presence of hydrogen sulfide (H_2S), and at a sufficient concentration to significantly affect corrosion behaviour and products (Kvarekvål & Moloney, 2017, p. 113). The corrosion process occurs through a series of complex chemical and electrochemical reactions, although they may be simplified to the oxidation of iron and reduction of protons (Kvarekvål & Moloney, 2017, p. 114). The dissolution of hydrogen sulfide in aqueous environment release bisulfide (HS^-) and sulfide (S^{2-}) species (Santos et al., 2021, p. 2), as given by reaction (1.13), and (1.14).

$$H_2S \rightarrow H^+ + HS^- \tag{1.13}$$

$$HS^- \rightarrow S^{2-} + H^+ \tag{1.14}$$

The combination of free iron(II) ions and sulfide may form iron sulfide scale as previously described in chapter 1.1.1.3. And the overall corrosion reaction may be simplified as given in reaction (1.15) (Kvarekvål & Moloney, 2017, p. 114).

$$Fe + H_2S \rightarrow FeS + H_2 \tag{1.15}$$

Hydrogen released from this reaction may form as H_2 gas, or absorb into the metal, causing hydrogen embrittlement (Kvarekvål & Moloney, 2017, p. 114). Sour corrosion may also cause localised pitting where SRBs are concentrated, typically in the anaerobic section of a biofilm.

1.2.1.2. Sweet Corrosion

Sweet corrosion originates from the dissolution of carbon dioxide (CO_2) in an aqueous environment, which forms carbonic acid (H_2CO_3) (Santos et al., 2021, p. 1), as given in reaction (1.16).

$$CO_2 + H_2O \rightarrow H_2CO_3 \tag{1.16}$$

Bicarbonate (HCO_3^-) and carbon trioxide (CO_3^{2-}) are formed from the dissociation of the carbonic acid (Santos et al., 2021, p. 1), as given in reaction (1.17) and (1.18).

$$H_2CO_3 \rightarrow H^+ + HCO_3^- \tag{1.17}$$

$$HCO_3^- \rightarrow H^+ + CO_3^{2-} \tag{1.18}$$
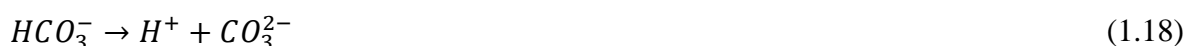
As the steel surface corrodes iron(II) ions are released. The free iron(II) can react with carbon trioxide, which may precipitate as iron(II) carbonate (ferrous carbonate) (Santos et al., 2021, p. 2) and deposit as scale, as given in reaction (1.19).

$$Fe^{2+} + CO_3^{2-} \rightarrow FeCO_3 \ (s) \tag{1.19}$$

1.2.1.3. Corrosion Inhibitors

Corrosion inhibitors (CIs) may be passivating (anodic), cathodic, vapor phase/volatile, or film forming (FFCI). In oil and gas production FFCIs are the most common, while passivating CIs are not used at all (Kelland, 2014, p. 194). Cathodic inhibitors have been used in drilling fluids, but are not used in production operations (Kelland, 2014, p. 195). FFCIs contains a polar head and hydrophobic tail, which allows the polar head to adsorb onto a metal surface, forming a protective film with the hydrophobic tail (Usman & Ali, 2018, p. 5).

Imidazolines are a well-known group of FFCIs, which is commonly used in the oil and gas industry (Kelland, 2014, p. 203). Imidazolines readily adsorbs onto a metal surface and forms a protective barrier (Usman & Ali, 2018, p. 6). Although imidazolines are an efficient group of CIs, they generally also show high acute toxicity (Kelland, 2014, pp. 203–207). Phosphate esters show good corrosion inhibition (Kelland, 2014, p. 199), which is thought to be due to complexation with metal ions on steel surfaces (Yu et al., 2006, p. 262). Although phosphate esters are good FFCIs the environmental concerns described in chapter 1.1.2.1, also applies here. Amine salts of (poly)carboxylic acids can be produced to have excellent film-forming and film-persistent characteristics, and some amine salts has been claimed as an environmentally friendly alternative (Kelland, 2014, p. 200). Amide derivates of long-chain amines have also been proposed to be environmentally acceptable FFCI, but the separation process of oil and water may be adversely affected (Kelland, 2014, p. 207). Some amides have been claimed to exhibit low-marine toxicity, while others are claimed to show high biodegradability (Kelland, 2014, p. 207). Some polymeric compounds can form more effective films on metal surfaces than small molecule CIs (Usman & Ali, 2018, p. 17). Polyaspartic acid combined with the amino acids cystine and cysteine, and their decarboxylated analogues cystamine and cysteamine, are particularly effective and show very environmentally friendly compositions with low toxicity and good biodegradability (Kelland, 2014, p. 211).

1.2.1.4. Adsorption

The first step in the adsorption of an organic inhibitor onto a metal surface is generally accepted to involve displacement of adsorbed water molecules on the metal surface (Oguzie

et al., 2007, p. 93). This substitution process between the organic compound and water molecules are given in reaction (1.20), where x is the ratio size in terms of the number of water molecules replaced by the adsorbed molecules (Obot, 2009, p. 544).

$$Org_{aq} + xH_2O_{ads} \rightleftarrows Org_{ads} + xH_2O_{aq} \tag{1.20}$$

Adsorption of various surfactant FFCI compounds have been shown to fit the Langmuir adsorption isotherm (Heydari & Javidi, 2012, p. 153; Obot, 2009, p. 544). The Langmuir isotherm assumes that the energy of adsorption is dependent of the coverage or atomic arrangement of species on the surface (Belton, 1976, p. 36). The formation of an adsorbate monolayer on the surface of an adsorbent is described by the model and assumes that no further adsorption occurs. Thus, the isotherm is valid for monolayer adsorption, and assumes that the surface contains a finite amount of adsorption sites. Uniform energies are also assumed, and that no transmigration of adsorbate occurs (Dada et al., 2012, p. 41).

Adsorption of a polymeric FFCI have been shown to fit the Temkin isotherm (Palumbo et al., 2020, p. 21). The Temkin isotherm consider interactions between adsorbent and adsorbate. Through exclusion of high and low extremes, the model assumes that for all molecules in the layer, the heat of adsorption would decrease linearly with coverage rather than logarithmic (Dada et al., 2012, p. 41).

The formation of a protective film by an inhibitor may occur through physisorption or chemisorption (Tiu & Advincula, 2015, p. 28). Physisorption typically involves ionic or electrostatic interactions with anions, which rapidly attach through van der Waals forces to positively charged surfaces. Although, while this bond may attach rapidly, it may also easily be broken by increasing temperature due to larger thermal motion (Palumbo et al., 2020, p. 7; Tiu & Advincula, 2015, p. 28). Chemisorption involves the replacement of water as mentioned above, and the electron sharing between heteroatoms and iron (Singh et al., 2015, p. 347). Chemisorption forms slower than physisorption, but the covalent bond increases with temperature (Tiu & Advincula, 2015, p. 28). A hydrophobic film may be formed in contact with the metal surface through donor-acceptor interactions between vacant d-orbital of iron and π-electrons of nitrile and carbonyl groups. The dπ-dπ bonds are also formed by the overlap of 3d-electrons of iron atom to vacant orbital of nitrogen and oxygen atoms (Singh et al., 2015, p. 347).

1.2.2. Film-Forming Inhibitors

In general, FFCIs inhibit corrosion through reducing contact between a brine and the metal. Most commercial FFCIs are organic compounds which contain some atoms of oxygen, nitrogen, sulfur, or phosphorus, they may also contain double bonds or aromatic rings. The inhibitor molecules in acidic environments are adsorbed onto the metal surface, separating it from the brine (Al-Shihry et al., 2020, p. 1; Askari et al., 2018, p. 102). Many FFCI are surfactant, although some are polymeric (Kelland, 2014, p. 196), in this chapter we will review a selection of inhibitors of each kind.

1.2.2.1. Surfactant Inhibitors

Surfactant FFCI consists of a polar head group and a hydrocarbon tail. The polar head group generally contain heteroatoms which adsorbs to the metal surface (Kelland, 2014, p. 196). While the hydrocarbon tail exhibit hydrophobic properties, which allows an oil film to form on the surface, effectively reducing contact between the water phase and the metal (Bajpai & Tyagi, 2006, p. 326). In this subchapter we will review a selection of surfactant FFCI.

1.2.2.1.1. Imidazolines

Imidazolines are thermally stable organic nitrogenous bases (Bajpai & Tyagi, 2006, p. 323). This group of cationic surfactants are commonly used as CI in the oil and gas industry (Jaal et al., 2014, pp. 1–2). Imidazoline are heterocyclic compounds with five membered ring which contain two nitrogen atoms. The basic structure is as presented in Figure 1.6, where R is the hydrocarbon tail, and R^1 is the pendant side chain (Bajpai & Tyagi, 2006, p. 321). This structure makes imidazolines strongly cationic, which allows them to adsorb strongly on negatively charges surfaces (Bajpai & Tyagi, 2006, p. 323).
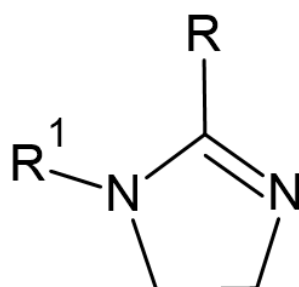
Figure 1.6 General structure of imidazolines.

In a study by Edwards et al. (1994) the mechanism of oleic imidazoline were investigated. Oleic imidazoline contains oleyl hydrocarbon tail, and a CH_2CH_2-NH_2 pendant group (Edwards et al., 1994, p. 318). They found that the corrosion inhibition performance increased with the presence of a pendant side chain, although the chemistry of the active group, or number of carbons in the chain were not critical. They also found that bonding of oleic imidazoline primarily occurred through the heterocyclic ring, which lies planar to the metal surface. And that the hydrocarbon chain plays an important role in the inhibition mechanism (Edwards et al., 1994, p. 324). This result is in agreement with other studies which propose that the surfactant nature of imidazoline allows lipophilic properties of the hydrocarbon tail to form a hydrophobic surface, effectively forming a barrier between the brine and the metal (Usman & Ali, 2018, p. 5). The length of the hydrocarbon tail has been shown to be critical for the inhibitory effect where a tail with fewer than 12 carbons show no inhibition, and a length of 18 gives the best performance and worst environmental properties (Kelland, 2014, p. 205). In a study by Zhang et al. (2010) it was shown how all the imidazoline derivatives investigated in the study had larger adsorption energy than water, and how inhibitor molecules would be preferentially adsorbed onto the metal surface (J. Zhang et al., 2010, p. 2062). The authors also note that van der Waals force is principal in the interaction between the heterocyclic ring of imidazoline and the iron surface.

In a review by Askari et al. (2018) they found that the surfactant properties of imidazolines increases the free energy of the system as dissolution occurs, this results in an increased inhibitor concentration at the interface. The surface tension is reduced as the surfactant molecules are preferable located at the air-solution interface. Surface tension decreases until the concentration of the surfactant reaches critical micelle concentration (CMC). A complex will form at sufficient concentrations, which reduce the dissolution of the surface layer and increases the corrosion inhibition ability (Askari et al., 2018, p. 112).

1.2.2.1.2. Amine

This subchapter is adapted from (Askari et al., 2018, pp. 99–102), unless otherwise noted. Amines used as FFCI may be aliphatic or ethoxylated. Aliphatic amine are simple molecules where the nitrogen is only connected to two hydrogen atoms and an alkyl group, as presented

in Figure 1.7. Although being quite cheap, there are problems with using aliphatic amines, especially types containing 14 to 18 carbons, as FFCI. Their quite high melting point of 25 – 50 °C makes them solid at room temperature, which in addition to their usually low solubility in organic solvents, makes their formulation for syntheses as corrosion inhibitors difficult.
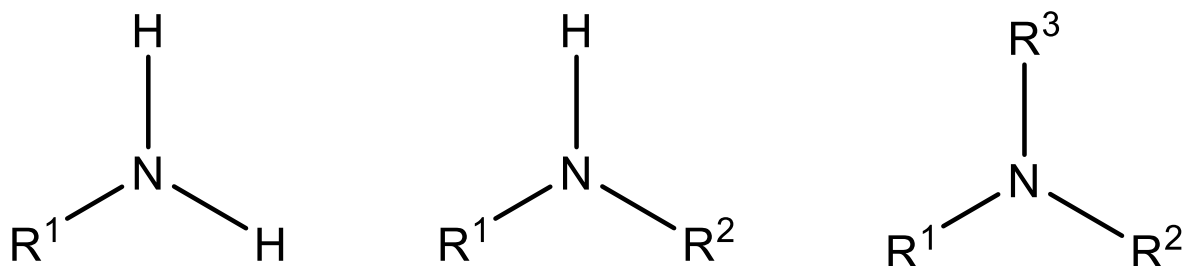
Figure 1.7 General structure of primary, secondary, and tertiary amine.

The inhibition efficiency of aliphatic amines is thought to be related to the nitrogen in the amino functional group. Due to the high electron density, the nitrogen atoms in aliphatic amines acts as a reaction centre. Ethanolamine has been shown to exhibit high corrosion inhibition in HCl, which is thought to be because the hydroxyl group acts as an electron repellent, leading to increased protection. Aliphatic amines may be made more water soluble through a reaction with ethylene oxide, forming ethoxylated amines. Ethoxylation gives the amine extra oxygen containing sites for adsorption to the metal surface (Kelland, 2014, p. 208). Water solubility may be increased further by the incorporation of hydroxyl groups into the amine (Kelland, 2014, p. 208). Because of the larger size and ease of polarizability, there has also been found a synergistic effect with the addition of iodine ions (Heydari & Javidi, 2012, p. 149). This has led researchers to conclude that the inhibitory effect of amines may be increased by the addition of iodine ions, because the synergistic effect makes chemisorption more stable (Askari et al., 2018, p. 112).

1.2.2.1.3. Quaternary Ammonium Compounds
This subchapter is adapted from (Askari et al., 2018, pp. 102–103), unless otherwise noted. Quaternary ammonium compounds, as presented in Figure 1.8, are a group of cationic surfactants with corrosion inhibiting properties. The adsorption mechanics of quaternary ammonium compounds are a combination of physical and chemical adsorption, which follows the Langmuir isotherm. Due to the strong cationic charge of these compounds, they tend to strongly adsorb to negative charged metal surfaces. The inhibition of positively charged quaternary ammonium compounds are considered to work by competing with protons for binding sites on the metal surface. As the inhibitor molecules adsorb and forms a hydrophobic layer, the binding of protons is reduced. To from a strong bond with the metal surface, at least one aromatic ring must be present in the compound. Because these compounds are highly soluble in water, they exhibit poorer film forming properties than imidazoline, although they may act as a surfactant. Quaternary ammonium compounds are usually quite toxic, and rarely used alone (Kelland, 2014, p. 200).
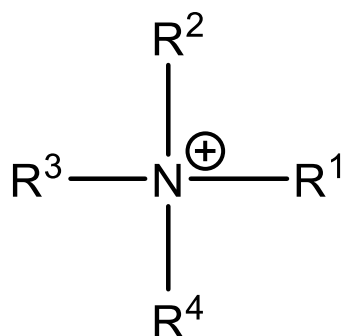
Figure 1.8 General structure of quaternary ammonium.

1.2.2.1.4. Phosphate Esters

Phosphate esters a group of good FFCI which are often use in combination with other classes of FFCI (Kelland, 2014, p. 199). In a study by Gao et al. (2015) corrosion inhibition by phosphate esters of different chain lengths were experimentally tested. The chain lengths investigated were butyl, hexyl, and octyl, represented by R in Figure 1.9. Although the corrosion inhibition of this study was done in an 0.5 M H_2SO_4 solution, phosphate esters are also used to inhibit CO_2 corrosion (Foss et al., 2010, p. 1). It seems likely that the results found by Gao et al. (2015) regarding chain length may also be true for CO_2 corrosion, as similar results are found for other inhibitors, such as imidazolines in chapter 1.2.2.1.1. Gao et al. (2015) found a correlation between alkyl chain length and inhibition efficiency, where the butyl chain exhibited much lower results than the longer chains. The hexyl and octyl chains showed similar efficiency and behave like surfactants once the concentrations reach their CMC, which aggregate at the electrode/solution interface (Gao et al., 2015, p. 1947). The hexyl and octyl chains were also found to more easily adsorb onto the metal surface compared to the butyl chain (Gao et al., 2015, p. 1951). Adsorption of all three molecules were found to fit with the Langmuir isotherm (Gao et al., 2015, p. 1950).
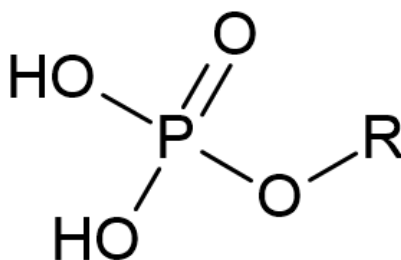
Figure 1.9 General structure of phosphate ester.

1.2.2.2. Polymeric Inhibitors

Polymeric inhibitors reduce corrosion by forming a barrier between the metal and the brine. Typically, these inhibitors contain functional anchoring groups which adsorb onto the meal surface. The anchoring groups can be ampholytic, anionic, cationic, or non-ionic. The interaction between the polymer and the metal are generally dispersion, dipole interactions, van der Waals forces, or may also be of hydrogen-bridge type (Ali Fathima Sabirneeza et al., 2015, p. 233). The adsorption of the anchoring groups is correlated to the presence of aromatic/heterocyclic rings, or heteroatoms such as nitrogen, sulfur, and oxygen (Singh et al., 2015, p. 347). The possible reactions centres are π-electrons of aromatic/heterocyclic rings and unshared electron pairs of heteroatoms (Singh et al., 2015, p. 347). Polymeric inhibitors

may be designed with moieties capable of forming complexes with metals and are considered to have increased number of attachment points to metal surfaces, multi-functionality, better film forming capabilities, flexible viscosity, and solubility (Askari et al., 2018, p. 112; Tiu & Advincula, 2015, p. 28). In this chapter we will review a selection of polymeric inhibitors.

1.2.2.2.1. Polycarboxylates/Polycarboxylic Acids

This paragraph is adapted from Tiu & Advincula (2015, p. 38). Derivatives of fatty acid and carboxylic acid are conventional molecular species used in corrosion inhibition. Polyamide inhibitors may be formed through the reaction of oleic acids with alkylene. The inhibition mechanism is correlated to the adsorption capabilities of oxygen on the metal surface. Another inhibition mechanism has also been proposed where the carboxylic acids react with iron cations to form iron carboxylate species at the anodic side, as given in reaction (1.21) and (1.22). This mechanism is supported by the positive shift of the corrosion potential corresponding to the anodic protection provided by the molecules.

$$Fe_{ads}^{2+} + R(COOH)_{2,aq} \rightarrow R(COO)_2Fe_{ads} + 2H_{aq}^+ \tag{1.21}$$

$$Fe_{ads}^{3+} + R(COOH)_{2,aq} + A_{aq}^- \rightarrow \{Fe(COO)_2R\}_{ads}^+ + 2H_{aq}^+ \tag{1.22}$$
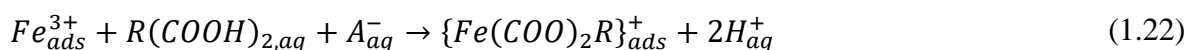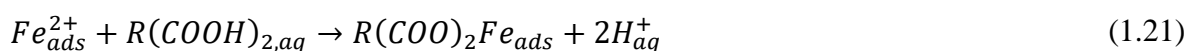
1.2.2.2.2. Polymeric Phosphate Esters

This paragraph is adapted from Tiu & Advincula (2015, p. 39). The surfactant properties of phosphate esters may be used with various polymeric materials to form an effective FFCI. The polymer can function as a protective inhibitor for ferrous metal surfaces in deep gas wells. The water solubility of the inhibitor is controlled by the level of oxyalkylation, and too high will prohibit transport of the inhibitor to the oil phase, affecting adsorption onto the metal surface. Amine and quaternary groups may also be added to control the solubility.

In a study by Yu et al. (2006), corrosion inhibition by the utilisation of polyhydric alcohol phosphate ester were investigated, structure presented in Figure 1.10. They found that the inhibition is of an anodic and cathodic negative catalytic effect interface type, and that the inhibitor adsorbs onto the metal surface and follows the Langmuir isotherm. They also found that the inhibitor immediately adsorbs to the surface with a film thickness which increased over time, and that the adsorption is attributed to complexation of the H_2O_3P functional group with accumulated metal ions on the surface (Yu et al., 2006, p. 262).
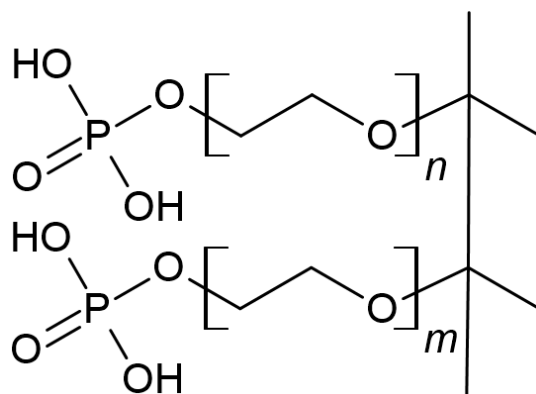
Figure 1.10 Structure of polyhydric alcohol phosphate ester, adapted from (Yu et al., 2006, p. 259).

1.2.2.2.3. Polysaccharide
In an effort to develop more environmentally friendly inhibitors with high biodegradability, polysaccharides have been considered. A polymeric inhibitor may be constructed with a polysaccharide backbone fitted with quaternary amine functional groups (Tiu & Advincula, 2015, p. 42), as presented in Figure 1.11.
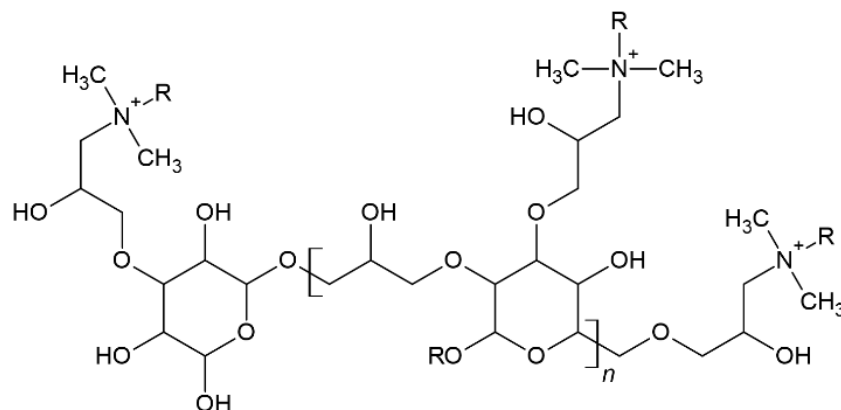
Figure 1.11 Structure of polysaccharide with quaternary amine groups, adapted from (Tiu & Advincula, 2015, p. 42).

Another promising polysaccharide inhibitor is hydroxyethyl cellulose, which contain several electron-donating sites, as presented in Figure 1.12. Hydroxyethyl cellulose also has a large molecular size and exhibit good corrosion inhibition properties. In a study by EL-Haddad (2014), potentiodynamic polarization showed that the inhibition by hydroxyethyl cellulose is of a mixed type. These results were also in agreement with results from electrochemical frequency modulation and electrochemical impedance spectroscopy (EL-Haddad, 2014, p. 601). The adsorption fit with the Langmuir isotherm (EL-Haddad, 2014, p. 598) and was suggested to be spontaneous physisorption based on Gibbs free energy calculations (EL-Haddad, 2014, p. 599). Through quantum chemical calculations it was found that adsorption of the inhibitor onto metal may occur by the interaction between d-orbitals of iron atoms and the unshared electron pairs in oxygen atoms (EL-Haddad, 2014, p. 600). Hydroxyethyl cellulose exhibit good inhibition efficiency of 99.7 % at 0.1 mM and 298 K, although the efficiency was found to decrease with increasing temperature (EL-Haddad, 2014, p. 599).
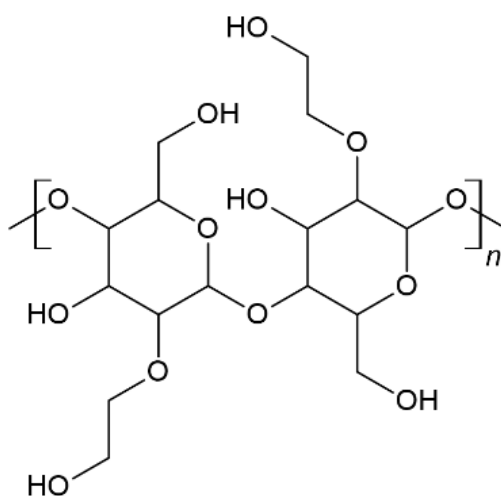
Figure 1.12 Structure of hydroxyethyl cellulose, adapted from (EL-Haddad, 2014, p. 596).

Acacia gum has been investigated as a possible environmentally friendly CI in saturated CO_2 (Palumbo et al., 2019) and CO_2-water saline environments (Palumbo et al., 2020). In both studies acacia gum was found to be an efficient CI, with an efficiency of 85 % at $P_{CO_2} = 40$ bar after 24 hours of immersion in one of the studies (Palumbo et al., 2020, p. 21). They also found that the adsorption of acacia gum fits with the Temkin adsorption isotherm and spontaneously adsorb strongly onto the metal surface. Both studies also found the inhibitor to act as a mixed-type, and indications of the adsorption to mainly occur through physisorption (Palumbo et al., 2019, p. 6469, 2020, pp. 10, 21).

1.2.2.2.4. Polysulfide

In comparison to polymeric inhibitors which adsorb onto the metal surface, polysulfide ions chemically react with iron to form iron disulfides or polysulfides, which retards the corrosion process in extreme conditions (Tiu & Advincula, 2015, p. 40). With the continuous addition of reactants, the insoluble coating may be constantly replenished.

1.2.2.2.5. Poly(urethane-semicarbazides)

In a study by Al-Shihry et al. (2020) poly(urethane-semicarbazides) was investigated as a possible inhibitor for CO_2 corrosion on carbon steel in oilfield systems. Two polymers of this group were selected for experimentation, which share a similar structure. The difference between these molecules is that the one denoted SR-16 has cyclohexyl moiety, which are replaced by a phenyl ring in SR-17 to increase rigidity and stability, as presented in Figure 1.13 (Al-Shihry et al., 2020, p. 3).
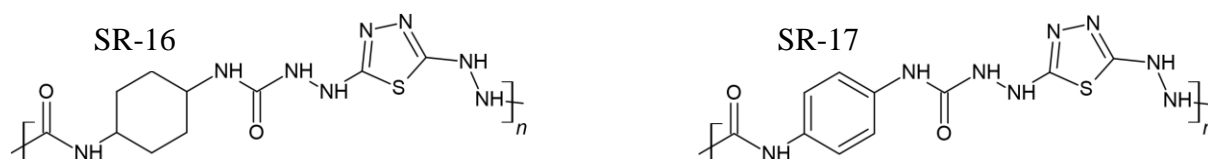
Figure 1.13 Structure of poly(urethane-semicarbazides), adapted from (Al-Shihry et al., 2020, p. 3).

Initially, chloride ions are adsorbed onto the metal surface, giving it a negative charge. The -NH- in both inhibitors are protonated, and physically adsorbed onto the cathodic sections on the metal surface by electrostatic interaction. The inhibitors also adsorb through chemisorption which occurs by donor-acceptor interactions among the unoccupied d-orbitals of iron and π-electrons of sulfur, nitrogen, and oxygen atoms. Due to the benzene ring of SR-17, the authors found that additional chemisorption occurs between the π-electrons of the ring and unoccupied d-orbitals of the iron (Al-Shihry et al., 2020, p. 8). The authors conclude that SR-17 shows excellent inhibition of CO_2 corrosion on carbon steel, with an efficiency of 95.5 % at 100 ppm. The superiority of SR-17 over SR-16 is attributed to the aromatic rings in the backbone, which makes the polymer more stable and increases rigidity (Al-Shihry et al., 2020, p. 3).

1.2.3. Surfactant and Polymeric Inhibitor Discussion

Surfactant inhibitors (SFI) are conventionally used as they provide a wide range of properties such as thermal stability, strong adsorption, water solubility and exceptional inhibitory performance. Although, some of these compounds are quite toxic and exhibit poor biodegradability, which has fuelled the search for environmentally friendly inhibitors with low toxicity and high biodegradability. Bioaccumulation may also be of concern but is often avoided by increasing the molecular mass to avoid transgression into cell membranes.

Utilisation of polymeric inhibitors (PI) is viewed as a possible way of avoiding the aforementioned concerns, while still providing acceptable inhibition efficiency. The polymeric backbone generally consists of a hydrocarbon chain which is nontoxic, and on this chain functional groups may be added to give it corrosion inhibition properties. Although, if a PI is constructed with only a few biodegradable groups, then the same issues as with SFI will persist here as well.

SFI are monomeric and generally adsorb to a surface by heteroatoms in their polar head, and makes the surface hydrophobic with their hydrocarbon tail, or by the formation of precipitants or complexes which creates a physical barrier between the metal and the brine. PI generally also adsorb onto a surface by heteroatoms, and some chemically react to form a protective barrier such as with polysulfides. Although instead of having a hydrocarbon tail, PI generally contain several anchor groups which may adsorb, these anchors adsorb the polymer in a horizontal direction rather than vertical, relative to the surface plane. This causes a film of polymers to build up onto the surface, rather than attract oil to form a film such as SFI. As PI often contains more anchoring groups than the monomeric SFI, they should in theory adsorb stronger to the surface.

The backbone of a PI may be designed to hold a wide variety of functional groups in comparison with SFI. Such as moieties capable of forming complexes with metals, increased number of attachment points, multi-functionality, better film forming capabilities, flexible viscosity, and solubility. Several of the reviewed PI adsorb through physisorption onto the surface, this makes them thermally unstable in which the inhibition efficiency decreases with temperature. For low temperature operations this does not necessarily pose an issue, but for high temperature operations one would need to utilise a PI which favours chemisorption. Polymerisation of the monomers used as SFI seems like a simple way of creating a PI with the necessary properties. With the addition of quaternary ammonium on a polysaccharide backbone, one has a functional polymeric inhibitor synthesised from mostly natural compounds. But with a PI like this, other issues will arise such as biodegradability of the polysaccharide backbone and toxicity of the quaternary ammonium groups. Poly(urethane-semicarbazides adsorbs through chemisorption, which allows the polymeric film to adsorb stronger and remain stable at higher temperatures. This PI contains many nitrogen atoms embedded in the polymeric backbone, which if oxidised to nitrate, may lead to eutrophication if released into ocean waters.

1.2.4. Summary
Polymeric FFCI seems like a promising alternative to surfactant FFCI. They can be constructed to hold a wider variety of functional groups, such as moieties capable of forming complexes with metals, increased number of attachment points, multi-functionality, better film forming capabilities, flexible viscosity, and solubility. Polymeric FFCI may also exhibit better environmental properties, such as lower toxicity, although biodegradation is still a concern. While there exists polymeric FFCI with good performance and low toxicity, research is still needed to develop inhibitors which exhibit lower environmental impact and higher biodegradation.

1.3. Gas Hydrates
This subchapter is adapter from (Kelland, 2014, p. 219), unless otherwise noted. Gas hydrates are ice-like clathrate structures which are made up of a lattice of water cages held together by hydrogen-bonding. Within these cages, small gas molecules such as methane or propane may be trapped. Gas hydrate plugging of flowlines is a major flow assurance problem, particularly

subsea and in deep water environments. Plugging may also occur in upstream transportation mixtures of unprocessed oil, condensate gas and water. There has been developed several methods to prevent plugging of flow lines. The utilisation of thermodynamic inhibitors (THIs) is the most common chemical method. THIs generally work by shifting the equilibrium such that formation of gas hydrates is less favourable. Another chemical method is the utilisation of anti-agglomerates (AAs) which generally work by dispersing the hydrate particles enough to inhibit electrostatic interaction and as such reducing the likelihood of agglomeration. The final chemical method is the utilisation of kinetic hydrate inhibitors (KHIs), which generally works by attaching onto the gas hydrate surface, making it more difficult for the hydrate to grow. Of these methods, only KHIs will be described further in this chapter.

1.3.1. Fundamentals of Gas Hydrates

The clathrate solids of gas hydrates are formed from small hydrocarbons and water at decreased temperature and elevated pressure. Formation of gas hydrates may form in temperatures as high as 25 – 30 °C with sufficient pressure. Gas hydrates are typically encountered in cold climates, subsea, wet gas, or multiphase flowlines where they may block the fluid flow. Although, gas hydrates may also be formed during completion and workover operations, during drilling, or at gas processing facilities and injection lines. In the right pressure-temperature conditions, formation may also occur in aqueous chemical injection in gas lift lines. While hydrate formation may form from free water, a hydrate plug may also form when no liquid water phase is present. Such formation may occur as the liquid water saturation curve is crossed and the water coalescence, or by dissolved water in the hydrocarbon phase. Typical formation of a hydrate plug in multiphase flow is described in Figure 1.14.
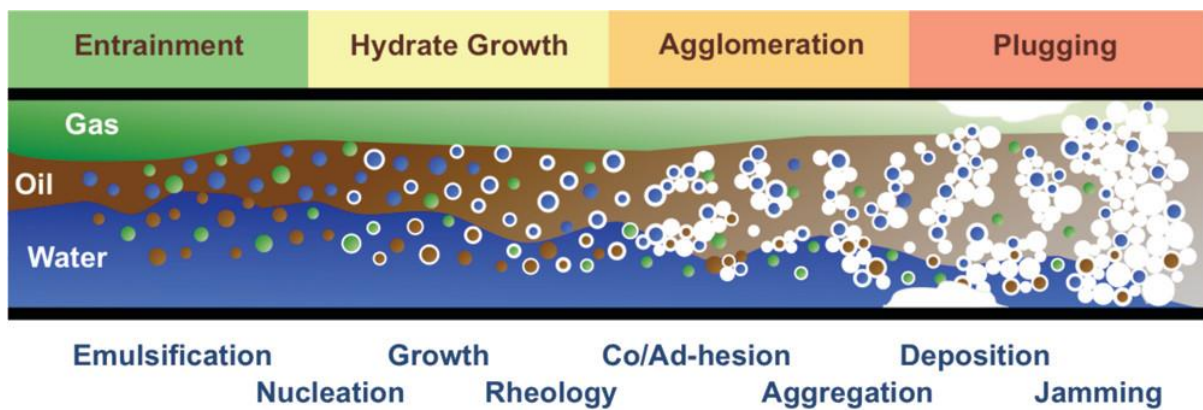
Figure 1.14 Gas hydrate growth in multiphase flowline (Sum et al., 2012, p. 4047).

Many multiphase production lines are designed to largely avoid formation of gas hydrates, problems may occur during shut-in operations and cooling of the fluid to within the hydrate-forming envelope. Unless necessary precautions are taken, a gas hydrate plug may also be formed beneath the wellhead. Prevention of plugging in flowlines is considered one of the main production issues in deepwater field developments. The clathrate structure of gas hydrates is formed when an open structure containing cages held together by hydrogen bonding is formed by the water molecules. These cages contain typically small hydrocarbons which stabilize the clathrate structure through van der Waals interactions.

While three main gas hydrate structures are known, sI, sII and sH, which all exhibit different pressure temperature equilibrium curves, sH is seldom an issue in the oil and gas industry and will therefore not be described further. Structure I and II, as presented in Figure 1.15, are a known problem in the oil and gas industry where they may form in flow lines. While both structures may be kinetically formed with all gas mixtures, sI is thermodynamically favoured for methane rich natural gas that contains almost no C3-4 hydrocarbon components. sII is the most common gas hydrate structure encountered in the field, as it is stable in natural gas mixtures containing small alkanes such as propane or butanes.
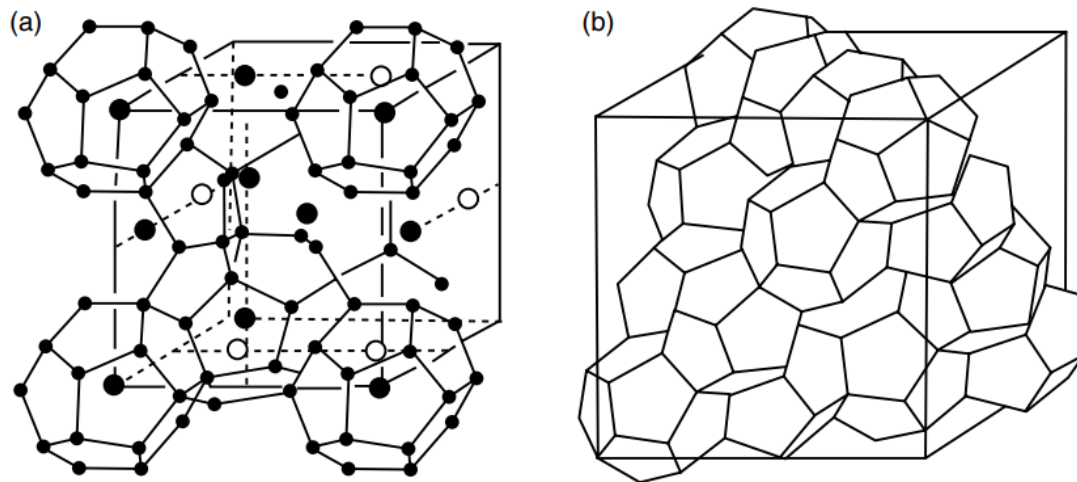
Figure 1.15 Gas hydrate structures: (a) structure I, (b) structure II (Sloan & Koh, 2007, p. 13).

1.3.2. Kinetic Gas Hydrate Inhibitors

While there exist several chemical classes which may be used as a KHI, this chapter will focus on the commonest KHI groups. Polymeric KHI appears to require both hydrophilic and hydrophobic capabilities for good performance, where the hydrophilic/phobic functional groups must be placed directly or adjacent to each other (Dirdal & Kelland, 2020, p. 6981). The hydrophilic functional group is usually made up of amine oxide, amide, or imide groups. (Dirdal & Kelland, 2022, p. 3108). KHI polymers are assumed to kinetically bind onto the hydrate particles during the early stages of nucleation and growth process, keeping the particle from reaching critical size, or by reducing growth rate of particles that already have reached critical size (Kelland et al., 1995, p. 533). The two key KHI properties is said to be that the polymers pendant group must fit into an incomplete, growing cage to anchor the polymer to the crystal surface; and the pendant group spacing on the polymer backbone must match with the spacing of the growing cages on the crystal surface (Koh & Sum, 2010, p. 92). The KHI performance may be improved by the introduction of synergists such as quaternary ammonium salts, which are reported to be strong synergists for Poly(N-vinyl caprolactam) (Kelland et al., 2013, p. 711). There are three main KHI categories: poly(N-vinyllactam), Hyper-branched poly(esteramide), N-Isopropylmethacrylamide (Ke & Kelland, 2016, p. 10016).

1.3.2.1. Poly(N-vinyllactam)

The most common class of commercial KHI polymers is the homo and copolymers of poly(N-vinyllactam). The basic structure of vinyllactam polymers is presented in Figure 1.16. Of these, the six and eight-ring is commercially too expensive, although their KHI

performance has been compared with the commercially available Poly(N-vinyl pyrrolidone) (PVP) and Poly(N-vinyl caprolactam) (PVCap) (Ke & Kelland, 2016, p. 10016; Kelland, 2014, p. 227). It has been shown that KHI performance increases with increasing ring size (O'Reilly et al., 2011, p. 6559). This is thought to be due to lowering of the polymer cloud point caused by increased hydrophobicity from the lactam ring size (Kelland, 2014, p. 227). While PVP belongs to this class of polymers, its performance is superseded by PVCap (Kelland, 2014, p. 227), which is considered one of the best KHI currently available (Dirdal & Kelland, 2022, p. 3108). In comparison to other polymeric KHI such as polyalkyl(meth)acrylamides, PVCap is known to be particularly good at inhibiting hydrate crystal growth. (Dirdal & Kelland, 2020, p. 6981). PVCap is useful for subcooling up to around 9-10 °C (Kelland, 2014, p. 227).
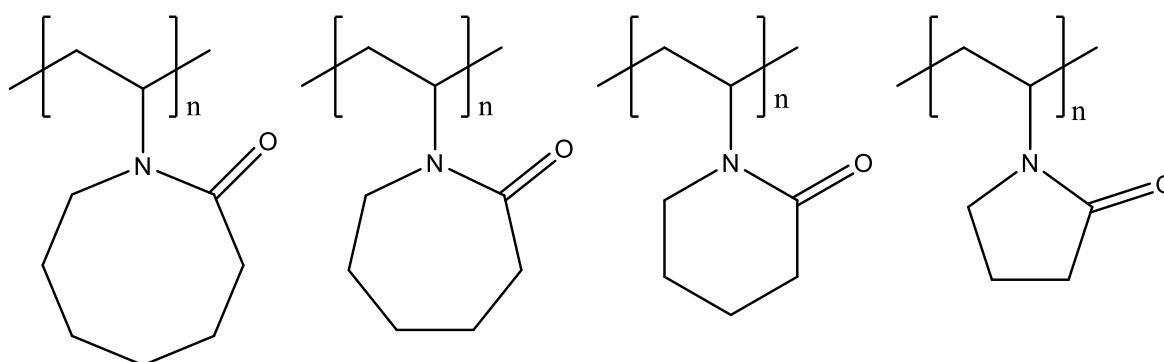
Figure 1.16 Structure of poly(N-vinyllactam) polymers. From left to right: polyvinylazacyclooctanone (PVACO), Polyvinylcaprolactam (PVCap), Polyvinylpiperidone) (PVPip) Polyvinylpyrrolidone (PVP), adapted from (Ke & Kelland, 2016, p. 10016; O'Reilly et al., 2011, p. 6556).

1.3.2.2. Hyper-branched poly(ester amide)

Hyper-branched poly(ester amide) (HPEA) is another class of commercially available KHI polymer. The structure of the ester amide unit is presented in Figure 1.17. These polymers are similarly useful as PVCap for subcooling up to around 10 °C, although some HPEA polymers are claimed to have higher biodegradability than PVCap (Kelland, 2014, p. 230). The tips of HPEA may be modified to make the polymer more or less hydrophilic and is claimed to exhibit increased performance on sI hydrates than PVCap (Ke & Kelland, 2016, p. 10016).
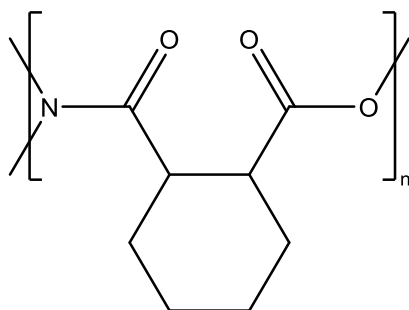
Figure 1.17 Structure of the ester amide unit in hyperbranched poly(ester amide) (HPEA), adapter from (Dirdal & Kelland, 2022, p. 3108).

1.3.2.3. N-Isopropylmethacrylamide
Poly(di)alkyl(meth)acrylamide is a well-studied group of polymeric KHIs (Kelland, 2014, p. 232). KHI polymers based on amide typically have a hydrophobic long acrylic carbon chain (Singh & Suri, 2020, p. 7). Due to their high performance, there have been several patents on amide-based polymers, including polyalkylacrylamides (Singh & Suri, 2020, p. 7). Polymers of the methacrylamide monomers have been shown to exhibit better performance compared with the acrylamide monomers. Placing an extra methyl group on the polyvinyl backbone therefore reduce flexibility of the polymer, which in turn lowers entropy by reducing movement of the pendant alkylamide group in water, and thus improved KHI performance (Kelland, 2014, p. 232). Similar conclusions have been made in other studies where methylated polymers was found to generally perform better than the unalkylated polmyers (Singh & Suri, 2020, p. 17). The best methacrylamide polymer appears to be made from isopropylmethacrylamide (IPMA) (Kelland, 2014, p. 232), such as poly(N-iso-propylmethacrylamide) which is presented in Figure 1.18.
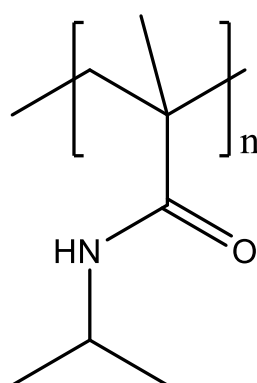
Figure 1.18 Structure of poly(N-iso-propylmethacrylamide), adapted from (Ke & Kelland, 2016, p. 10016).

1.4. Environmental Concern and Green Inhibitors
Production of oil and gas is associated with an extensive amount of different chemicals, which typically ends up in a refinery, waste sand and solids, or wastewater (OECD, 2014, p. 18). Toxic production chemicals may pose a threat to the marine environment (Manfra et al., 2018). It has been reported that the potential for acute toxicity is likely limited to the immediate effluent vicinity in offshore waters. There has also beer reports on how chronic exposure may lead to sub-lethal changes such as endocrine disruption, fecundity, and genetic diversity, among others (Neff et al., 2011, p. 30). The development of green chemicals which exhibit lower toxicity and higher biodegradation has been field of focus by chemical companies for over 20 years, which is thought to be the way of the future to meet both environmental and economic goals (Darling & Rakshpal, 1998, p. 5). In this subchapter, the environmental concerns regarding conventional inhibitors are investigated, and aspiring green inhibitors are reviewed.

1.4.1. Scale Inhibitors
There are increasing concerns with the use of SIs regarding the environmental impact. Along with concerns around toxicity and biodegradation (Mpelwa & Tang, 2019, p. 845), there is also a particular concern about phosphorous based inhibitors, which are easily hydrolysed to orthophosphates (Lattemann & Höpner, 2008, p. 9). Orthophosphates serve as nutrients for primary producers which may lead to eutrophication in the waterbody (Correll, 1998, p. 262). Such concerns has led to the increased interest of many researchers to the development of

environmentally friendly and cost-effective SIs (Mpelwa & Tang, 2019, p. 845). In oilfield applications there have been used green SIs to retard, control, or prevent deposition of scale. Which exhibit acceptable ecological, economical, renewable, and sustainable properties, although these inhibitors have been limited by the biodegradability of some of their components (Mazumder & A, 2020, p. 21).

Due to the increasing environmental concerns, the industry is trying to replace some applications of phosphorous SIs with less organic phosphorus compounds (Mpelwa & Tang, 2019, p. 845). Polyaspartic acid have been identified as a promising green biodegradable polymer SI, based on its versatile properties and biodegradability (Hasson et al., 2011, p. 7606; Mazumder & A, 2020, p. 13). Polymaleic anhydride has also been identified as a biodegradable SI, and were in a study by (Martinod et al., 2008) tested in oil field operations against the performance of phosphino-polycarboxylic acid, which is a phosphonate-based inhibitor. They found that at a concentration of 1 mg/l, the polymaleic acid showed lower efficiency than the phosphonate-based inhibitor for calcium carbonate scaling. Although, it was also found that at a concentration of 4 mg/l the crystal growth was affected by polymaleic acid (Martinod et al., 2008, p. 351). Other polymeric SIs such as polyacrylates, polymaleates, and derivates of these has gained attention in the petroleum industry (Mpelwa & Tang, 2019, p. 845). Although progress is being made, more research is needed to find green SIs which exhibit biodegradable properties with low toxicity and bioaccumulation, that are cost-effective, and pose no threat to the ecosystem and environment (Mazumder & A, 2020, p. 21; Mpelwa & Tang, 2019, p. 846).

1.4.2. Corrosion Inhibitors

Conventional cost-effective SI and CIs widely contains sulfur, phosphorus, or complex aromatic ring structures, which may be environmentally harmful. Based on these concerns inhibitors which exhibit biodegradable and environmentally friendly properties, along with the ability to effectively inhibit scale and corrosion are urgently needed (Zheng et al., 2021, p. 2). Some chemicals may also be highly toxic in marine environments, which has led to an increased focus of current research towards the development of environmentally friendly non-toxic CIs (Tang, 2019, p. 13; Usman & Ali, 2018, p. 18). Incorporation of nanoparticles may enhance the corrosion resistance of various coatings (Rathish et al., 2013, p. 969). In a review by Jain et al. (2020) compounds containing nanoparticles were identified as viable environmentally friendly CIs. The effectiveness of nanoparticles is thought to stop the redox reactions by blocking active sites on the metal surface (Jain et al., 2020, p. 1). They also found that corrosion protection formed by nanocomposite coatings occurred in multiple mechanics. These mechanisms include barrier protection, anodic protection, and smart self-healing protection (Jain et al., 2020, p. 8).

1.4.3. Gas Hydrate Inhibitors

This chapter is adapted from Kelland (2018). Polymers such as PVCap with polyvinyl backbones generally exhibit poor biodegradability (Kelland, 2018, p. 12001). Although many commercial KHI polymers exhibit low toxicity and bioaccumulation, the poor biodegradability can prevent their use in sensitive areas. There have been investigated several methods to reduce or avoid the environmental impact KHI polymers with poor biodegradation. Such as development of biodegradable polymers, recycling of the polymer, degradation and destruction into smaller and benign chemicals, reinjection through well into the formation. Very few commercial KHI polymers exhibit good biodegradability, if discharged into the environment there will therefore always be some concern regarding chronic toxicity from partially degraded products. A graft polymer with a biodegradable

backbone such as polyethylene glycol and pendant caprolactam groups has been considered as one of the best biodegradable KHIs. There has also been development of other KHIs, such as from protein-based products and polypyroglutamates. While it might be possible to design a protein based KHI with high performance, it is considered to currently be economically unviable due to cost of production and size of demand (Kelland, 2018, p. 12009).

1.5. Multi-Functional Inhibitors
As the production of oil and gas often require a variety of different chemical treatments compatibility issues might arise. Incompatibility has been reported between CI and SIs (Lawless et al., 1993, p. 177), and CI and KHIs (Farhadian, Varfolomeev, Semenov, et al., 2020, p. 13718). Due to this, the development of multi-functional inhibitors has been an increasingly researched area in recent years to address compatibility issues (Qasim et al., 2019, p. 10). It has also been pointed out that multi-functional inhibitors for CI and KHIs would increase inhibition efficiency as well as reduce operational costs (Farhadian, Varfolomeev, Semenov, et al., 2020, p. 13717; Qasim et al., 2019, p. 10). In another study it was noted how biodegradable, environmentally friendly SI and CIs with high scale inhibition efficiencies are urgently needed (Zheng et al., 2021, p. 2). In this chapter, we will review existing knowledge surrounding multi-functional inhibitors for scale, gas hydrates, and corrosion.

1.5.1. Scale and Corrosion Inhibitors
SI and CIs are generally incompatible and may behave antagonistically (Mékarbané et al., 2019, p. 2). A reason for this is as described in chapter 1.2.1.4, that CIs may form a film onto the metal surface by interacting with the unoccupied d–orbitals of iron. Hydrophilic and chelating SIs may also sequester iron molecules and cause competitive reactions on the steel surface, resulting in a decrease in inhibition efficiency (Mékarbané et al., 2019, pp. 1–2). To avoid these incompatibility issues among others, multi-functional chemicals with the ability to function as both a CI and SIs has been extensively researched (Lawless et al., 1993, p. 177; Zheng et al., 2021). In a study by (Kohler et al., 2002) polyaspartates was tested as multi-functional inhibitors for corrosion and scale. They found that polyaspartates are noteworthy biodegradable alternatives, but improvements are still needed if they are to substitute currently used inhibitors (Kohler et al., 2002, p. 8). In a relatively recent study by Zheng et al. (2021) chitosan-acrylic acid-polysuccinimide terpolymer (CTS-AA-PSI), which is a derivative of non-phosphorus chitosan, were examined as an environmentally friendly SI and CI. They found that CTS-AA-PSI yielded a scale inhibition rate of 88 % at a concentration of 25 mg/l, and a corrosion inhibition rate of 71 % at a concentration of 500 mg/l (Zheng et al., 2021, p. 13). The biodegradability of CTS-AA-PSI was also found to reach 72 % on the 28th day (Zheng et al., 2021, p. 12). In a study by Mékarbané et al. (2019) the efficiency of a commercially available combined CI and SIs were investigated. While the exact structure of this combined inhibitor is not shared, from the referenced patent by Pou (2014) it seems likely that "Formula A" was tested. Formula A is a combination of the CI Norust® 740 (9 %) and the SI Bellasol® S50 (18 %). The formulation also includes Noramox® C11 (12 %) which is used as compatibility agent, thioglycolic acid (4.5 %) as a CI synergist, and a glycolic solvent based on mono ethylene glycol (q.s. for 100 %). The CI and SI tests by Mékarbané et al. (2019, p. 9) gave inhibition results of 98 % and >97 %, respectively, although an efficiency of around 90 % was listed in the patent (Pou, 2014, p. 5).

1.5.2. Corrosion and Gas Hydrate Inhibitors
Many classic CIs such as imidazolines, quaternary ammonium salts and phosphate esters are antagonistic for the KHI polymers, which severely reduce their KHI performance, as well as

negatively affecting the performance of CI (Kelland et al., 2021, p. 3). Such an incompatibility has been claimed to be due to the adsorption of CI onto the KHI polymeric structure (Kelland et al., 2021, p. 3). In a paper on the perspective of dual CI and KHIs, Qasim et al. (2019) highlights how synthesis of a copolymer for corrosion and gas hydrate inhibition is an emerging field of research, and how it may provide an economical solution to the flow assurance problems (Qasim et al., 2019, p. 17). In a study by Farhadian, Varfolomeev, Rezaeisadat, et al. (2020) a dual inhibitor for corrosion and gas hydrates was synthesise from sunflower oil. The main goal of the study was to introduce a green chemical with a potential for biodegradability, which also overcame incompatibility difficulties. They found that phosphorylated waterborne polyurea/urethane effectively inhibited gas hydrates, and suppressed corrosion in an 2M HCl environment (Farhadian, Varfolomeev, Rezaeisadat, et al., 2020, p. 14). In a study by Farhadian, Varfolomeev, Semenov, et al. (2020) biodegradable substances were chemically modified and tested for their ability to inhibit corrosion and gas hydrates. They found that glucose and sucrose structures modified to contain sulfonate and carboxyl groups exhibited inhibition for both corrosion and gas hydrates (Farhadian, Varfolomeev, Semenov, et al., 2020, p. 13724). In a study by Park et al. (2017) a copolymer of PVCap and acrylic acid was modified with CI groups such as imidazole, quaternary ammonium. While the corrosion efficiency of their product was not determined, their work suggests that a multi-functional polymer was successfully synthesised through synergistic incorporation of the 1-(3-aminopropyl)imidazole (APIM) group into VCap chains (Park et al., 2017, p. 9371). The structure of this copolymer is presented in Figure 1.19.
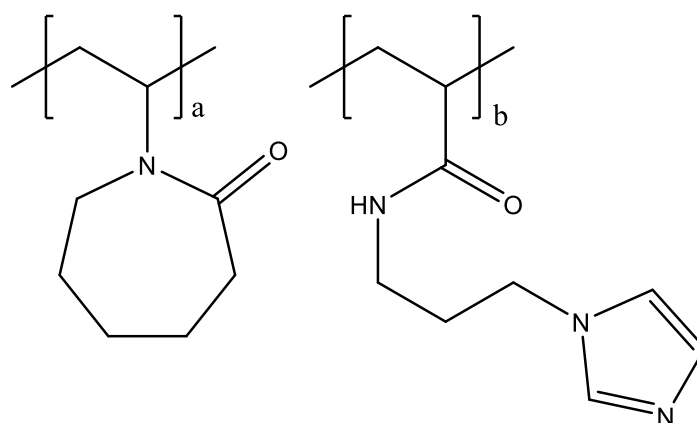
Figure 1.19 Structure of PVCap-co-APIM, adapted from (Park et al., 2017, p. 9365).

Maleic-based copolymers was explored as dual KHI and film-forming CI in a recent study by (Kelland et al., 2021). They found that reacting vinyl acetate:maleic anhydride with cyclohexylamine and 3,3-di-n-butylaminopropylamine gave a terpolymer (VA:MA-60 % cHex-40 % DBAPA) that performed excellent as an KHI and exhibited good CI effect for CO_2 corrosion in 3.6 wt. % brine (Kelland et al., 2021, p. 13). The structure of this terpolymer is presented in Figure 1.20.
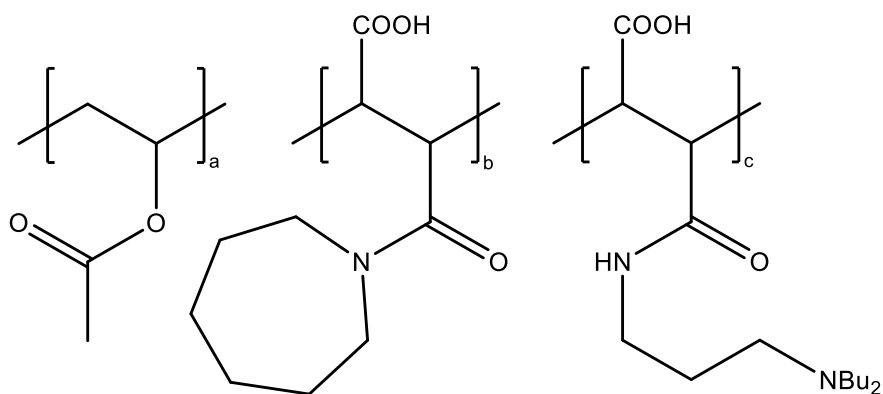
Figure 1.20 Structure of VA:MA-60 % cHex-40 % DBAPA, adapted from (Kelland et al., 2021, p. 6).

1.5.3. Scale and Gas Hydrate Inhibitors

Polyaspartamides was investigated as a possible dual kinetic hydrate and SI in a study by (Chua et al., 2011), which is a class of KHIs that is made from polysuccinimide and exhibit good biodegradability. Several derivatives of polysuccinimide were synthesized and tested as KHI in high-pressure autoclaves with synthetic natural gas and as SI for calcium and barium scale in high-pressure dynamic tube blocking rig. They found that when dosed at several thousand ppm, which is a typical KHI dosage, some polymers showed good scale inhibition for both calcium and barite scale without compromising the KHI performance (Chua et al., 2011, p. 5171).

1.5.4. Scale, Corrosion, and Gas Hydrate Inhibitors

In a review of multi-functional chemicals to treat scale, gas hydrates and corrosion by Kelland et al. (2021) no single product to treat the three issues for a wide range of field conditions was found to be available (Kelland et al., 2021, p. 14). While many CIs are incompatible with commercial KHI polymers, Chua et al. (2011) have shown how derivatives of polyaspartamides works as SI without compromising KHI performance, and because polyaspartates have been shown to work as CI, they argue that a high KHI dose of PSI may help function as a CI in addition to KHI and SI (Chua et al., 2011, p. 5171).

2. Corrosion Testing Methodology

The ability to test corrosion is paramount in the development of a multi-functional inhibitor with the ability to inhibit corrosion, scale, and gas hydrates simultaneously. The research team working on this subject at UiS has long experience with gas hydrate and scale testing, but corrosion testing is still a rather new area and was only introduced to the team through the work of Undheim (2021), which aimed to develop a complete corrosion testing manual. While Undheim (2021) successfully developed a manual for the Gamry MultiPort Electrochemical Cell (Multiport), further development was required to reduce deviation, and increase accuracy and replicability between tests. In this chapter the corrosion method by Undheim (2021) will be replicated and reviewed before changes made to further optimize the method are described. While method optimization is not the main goal of this thesis, every aspect was not explored to its full extent in order to save time for other parts of this thesis. Although, by exploring and utilizing the changes which were made, the method was deemed adequate with an increased level of reliability, accuracy, and replicability. In the end of the chapter all changes made will be summarised. While there was a shift from the MultiPort, used by Undheim (2021) to a smaller version called Gamry EuroCell Electrochemical Cell (EuroCell), the same method can be used for both units with comparable results.

2.1. Method Replication

This exercise was performed to gain good insight into the corrosion testing manual for the MultiPort, developed by Undheim (2021). The relevant theory will be reviewed, and the previously performed experiments will be replicated to both validate the method, as well as investigating the effect of purer CO_2 gas used in sparging of the brine. This subchapter forms the groundwork of optimization attempts which are discussed in subchapter 2.2.

2.1.1. Theory

This subchapter is adapted from Gamry Instruments (2021), unless otherwise noted. Corrosion rate can be determined by an equilibrium between anodic and cathodic electrochemical reactions. In the absence of electrical connections, the equilibrium potential assumed by the metal is the Open-circuit potential, denoted by E_{oc}. The corrosion current is denoted by I_{corr} and is either the value of the anodic or cathodic current at E_{oc}. I_{corr} can be estimated from current-versus-voltage data. From the E_{oc} the voltage is scanned, and the data is fitted to a theoretical model of the corrosion process. The electrochemical processes rates are assumed to be controlled by the kinetics of the electron-transfer reaction at the metal surface. Such a kinetically controlled reaction obeys the Tafel equation, given in Equation (2.1). Where the exchange current is denoted by I_0, the electrode potential is denoted by E, the equilibrium potential is denoted by E_0, and the Tafel constant of the reaction is denoted by β.

$$I = I_0 e^{\frac{2.303(E-E_0)}{\beta}}$$

Equation (2.1)

The Tafel equation describes the behaviour of either the anodic or cathodic reaction. As the anodic and cathode reactions occur simultaneously in a corrosion system, the Tafel equations for both may be combined to form the Butler-Volmer equation, given in Equation (2.2). Where E_{corr} is the corrosion potential in volts.

$$I = I_{corr}\left(e^{\frac{2.303(E-E_{corr})}{\beta_a}} - e^{\frac{-2.303(E-E_{corr})}{\beta_c}}\right)$$

Equation (2.2)

The Butler-Volmer equation can be simplified by restricting the potential to be near E_{corr}, where the current-voltage curve approximates linearity. The slope of this relationship represents the polarization resistance (R_p). Together with an estimate of the β coefficients, an R_p value can be used to generate an estimate of the corrosion current. By approximating the exponential terms in Equation (2.2) with the first two terms of power-series expansion and simplifying, a form of the Stern-Geary equation is formed, as given in Equation (2.3).

$$I_{corr} = \frac{1}{R_p} \frac{\beta_a \beta_c}{2.303\,(\beta_a + \beta_c)}$$
Equation (2.3)

The corrosion current flow may further be related to mass via Faraday's Law in Equation (2.4). Where the charge is denoted by Q, the number of electrons transferred per molecule is denoted by n, Faraday's constant is denoted by F, and the number of moles reacting is denoted by M.

$$Q = nFM$$
Equation (2.4)

The mass of the species that will react with one Faraday of charge is the equivalent weight (EW). By substituting $M = \frac{m}{AW}$ and $EW = \frac{AW}{n}$ into Equation (2.4), where AW is the atomic weight, we get Equation (2.5), where m is the mass of the species that has reacted.

$$m = \frac{(EW)Q}{F}$$
Equation (2.5)

The weight loss of the reacted species may be converted to corrosion rate (CR) by substituting the value of Faraday's constant and modifying Equation (2.5), which results in Equation (2.6). Where I_{corr} is the corrosion current in amperes, K is a constant to define units, EW is the equivalent weight, d is the density, and A is the sample area.

$$CR = \frac{I_{corr} \times K \times EW}{dA}$$
Equation (2.6)

The efficiency of a corrosion inhibitor (CI) may be determined by Equation (2.7), where X_0 is the corrosion rate without a CI and X_1 is the corrosion rate with a CI, adapted from (El-Sayed et al., 2011, p. 6574).

$$\%\eta = \frac{X_0 - X_1}{X_0} \times 100$$
Equation (2.7)

2.1.2. Materials and Methods
The assembly of the Multiport was performed as described by Undheim (2021, p. 18). The blank tests were completed with only brine and added CO_2 gas, the materials used and testing procedure for this exercise was completed as described by Undheim (2021, p. 70). Exceptions for blank testing are that only one metal sample was used, compared to the three samples used in the literature reference. The imidazoline and polymer tests was completed with brine, added CO_2 gas and CI, the materials used and testing procedure for this exercise was completed as described by Undheim (2021, p. 74). Exceptions made to the test are the addition of a new experimental polymer, and the sequence of 15 tests was completed in one sitting for each type, as opposed to performing a minimum of five tests over several sittings. Exceptions which include all tests are the use of purer pressurised CO_2 which now contains

an O_2 concentration of 0.001 ppm in comparison to 0.01 ppm used in the literature reference (Undheim, 2021, p. 112).

2.1.3. Results and Discussions

The corrosion rate for the performed blank and imidazoline tests are presented in an increasing order in Figure 2.1. The blank test shows how corrosion may vary widely within in linear trend with R^2=0.98, over a period of around 4 hours. The lowest and highest recorded corrosion rate was found to be 0.978 and 2.162, respectively. With the addition of 500 ppm imidazoline on a new metal sample, the corrosion was found to be reduced, although perhaps not as much as one would expect from imidazoline. The corrosion rate was found to be mostly stable after the initial two linear polarization resistance (LPR) measurements. The R^2 for all tests with imidazoline was found to be 0.68, although it would be 0.97 with the exclusion of the initial two tests.
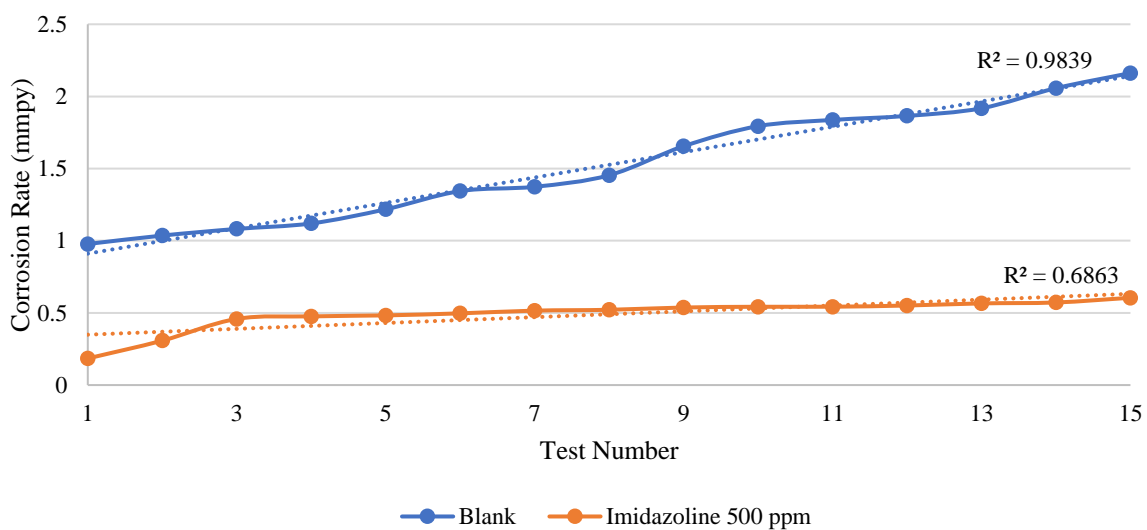
Figure 2.1 Blank and imidazoline corrosion tests.

Corrosion testing was also performed on an experimental polymeric inhibitor. The five tests performed with this polymer is presented and compared with the blank and imidazoline tests in Figure 2.2. The polymer initially exhibits good inhibition, although corrosion rate increases to 1.3 millimetre per year (mmpy) by test number four. While the blank test as described in Figure 2.1 increases linearly, it seems likely that the polymer would remain steady at slightly above 1 mmpy if more tests were performed. Only five tests were performed with this polymer due to time limitations.
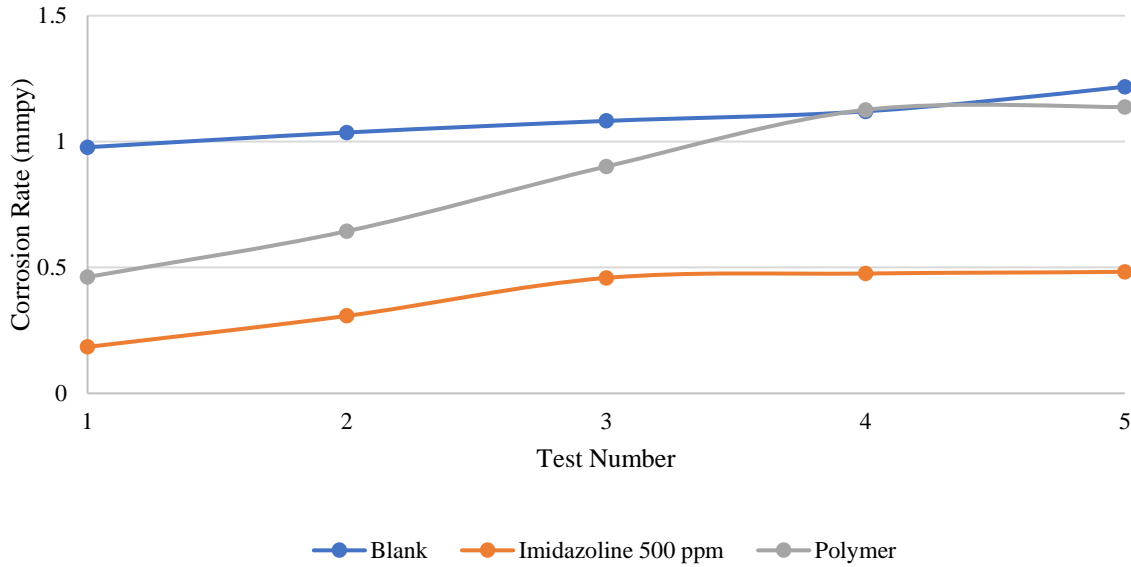
Figure 2.2 Polymeric corrosion inhibitor results compared with blank and imidazoline.

The currently performed imidazoline tests are compared to the results found by Undheim (2021, p. 103) in Figure 2.3. There appear to be quite a difference between the test results where the current tests show a rapid increase in corrosion rate before progressing with minor change, the literature reference shows steadily increasing linear trend with R^2=0.98. Although the same methodology was followed, there are some differences in the way the 15 tests was performed which could explain some of this difference. The literature reference performed three sequences with five tests each sequence, while the current 15 tests was performed in one sitting. The literature reference mentions how replicability challenges was experienced, and how tests performed on different days did not always correlate (Undheim, 2021, p. 91). By fitting the highest results found for 500 ppm imidazoline by Undheim (2021, p. 103) to the graph, we find that these results seem to fit with the current results, as presented in Figure 2.4. This indicates that the method is quite sensitive to how the sequence is conducted, and that performing a longer sequence might be favourable to increase replicability.
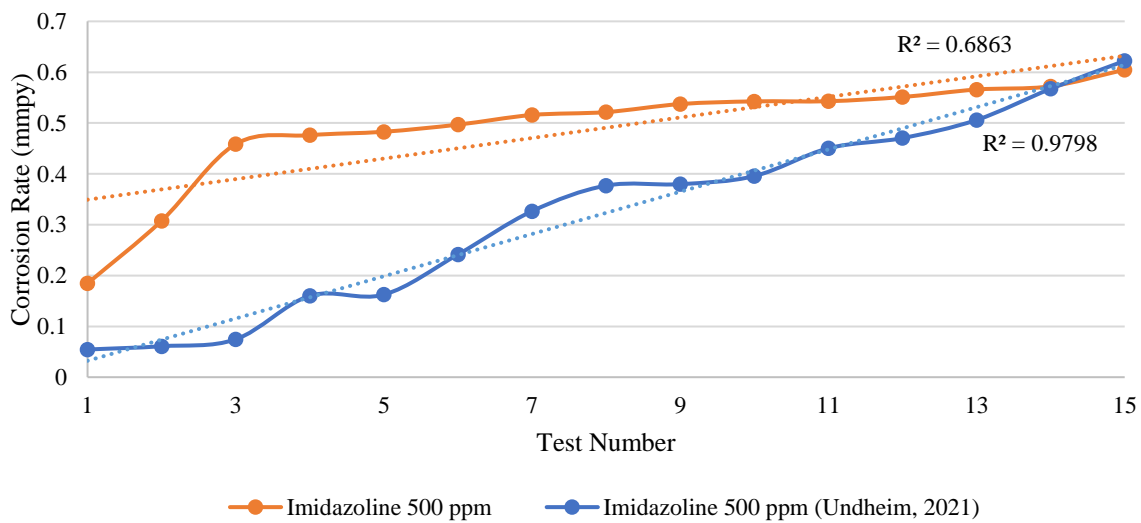
Figure 2.3 Imidazoline tests compared with literature reference results.
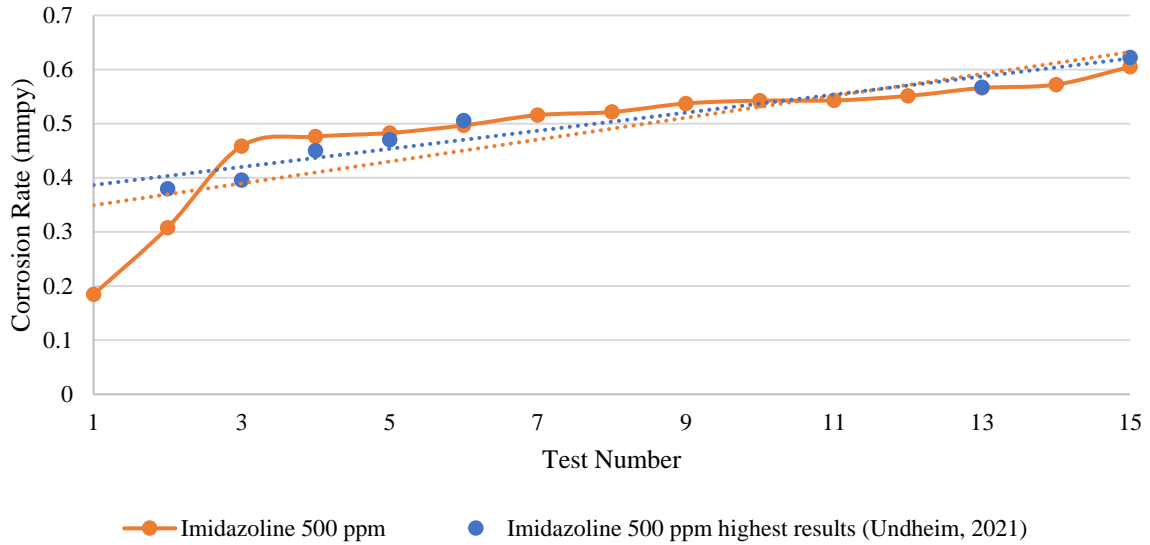
Figure 2.4 Imidazoline tests compared with literature reference, fitted with highest results.

Overall, the current results follow the same trends as found in the literature reference, as presented in Figure 2.5. Both the current blank and imidazoline tests exhibit less variability when plotted on an increasing trend, this may be associated to the lower concentration of O_2 found in the pressurised CO_2, although some degree of deviation persists.
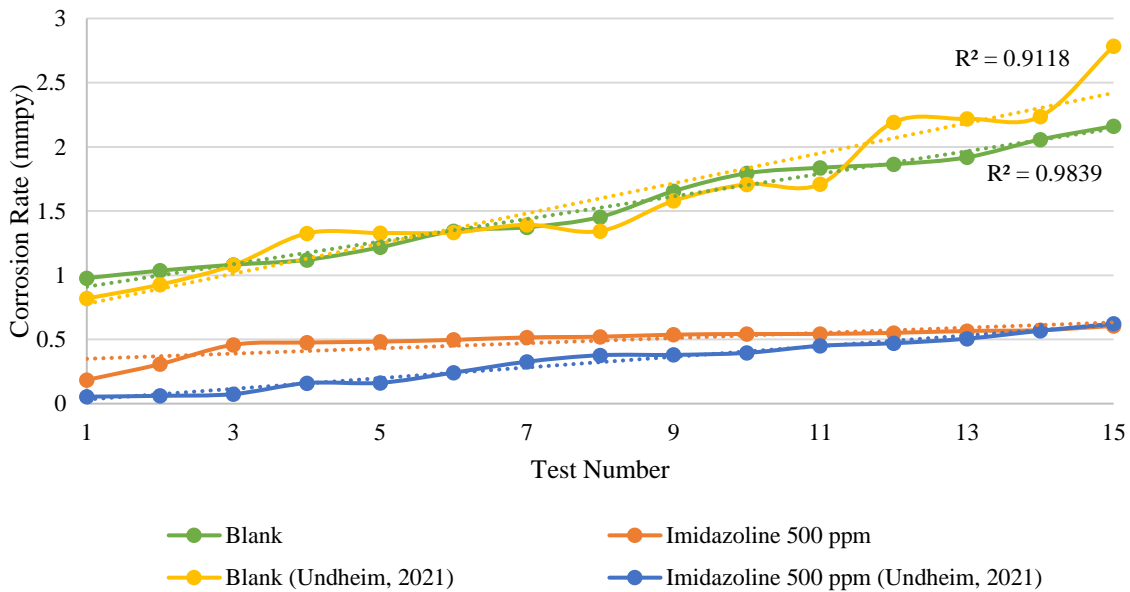
Figure 2.5 Blank and imidazoline compared with literature reference results.

The inhibition efficiency of the tested CIs was calculated with X_0=2.784 and compared with the results for imidazoline in the literature reference in Figure 2.6. Although the current imidazoline tests exhibit lower initial efficiency, the overall trend follows a similar pattern as in the literature reference (Undheim, 2021, p. 82).
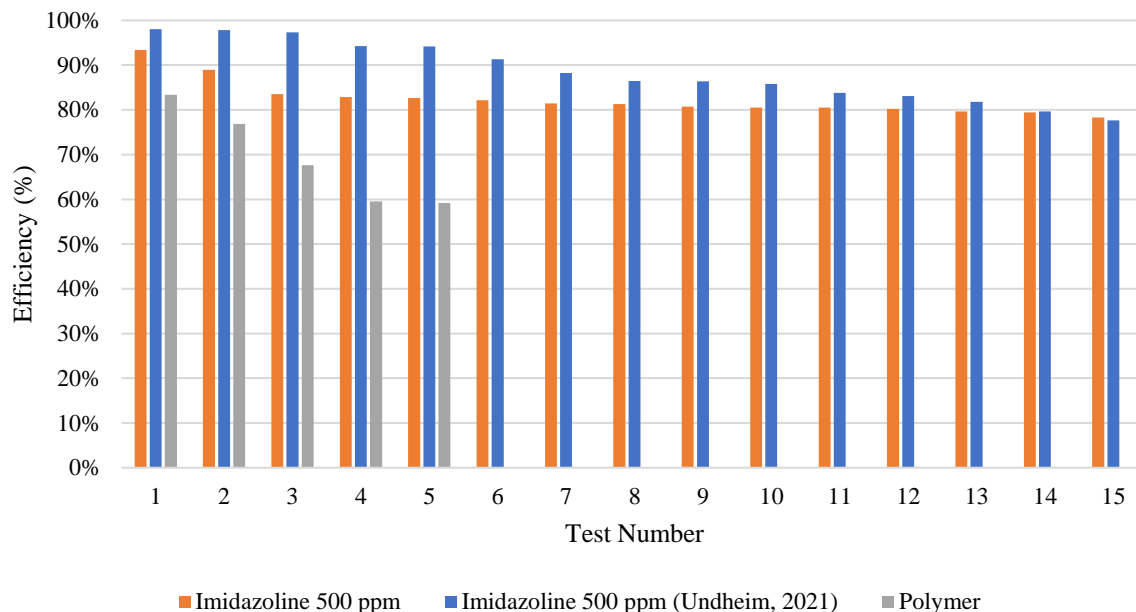
Figure 2.6 Inhibition efficiency comparison.

The average inhibition efficiency and standard deviation (SD) of these was calculated and compared with the results for imidazoline in the literature reference in Figure 2.7. Although the current imidazoline test exhibited lower average efficiency than compared to the literature reference, 82 and 88 % respectively, the SD was also found to be lower, 4 and 7 % respectively. The reduced SD may be attributed to the lower O_2 concentration as previously described. The experimental polymer showed an average efficiency of 69 % with an SD of 11 %.
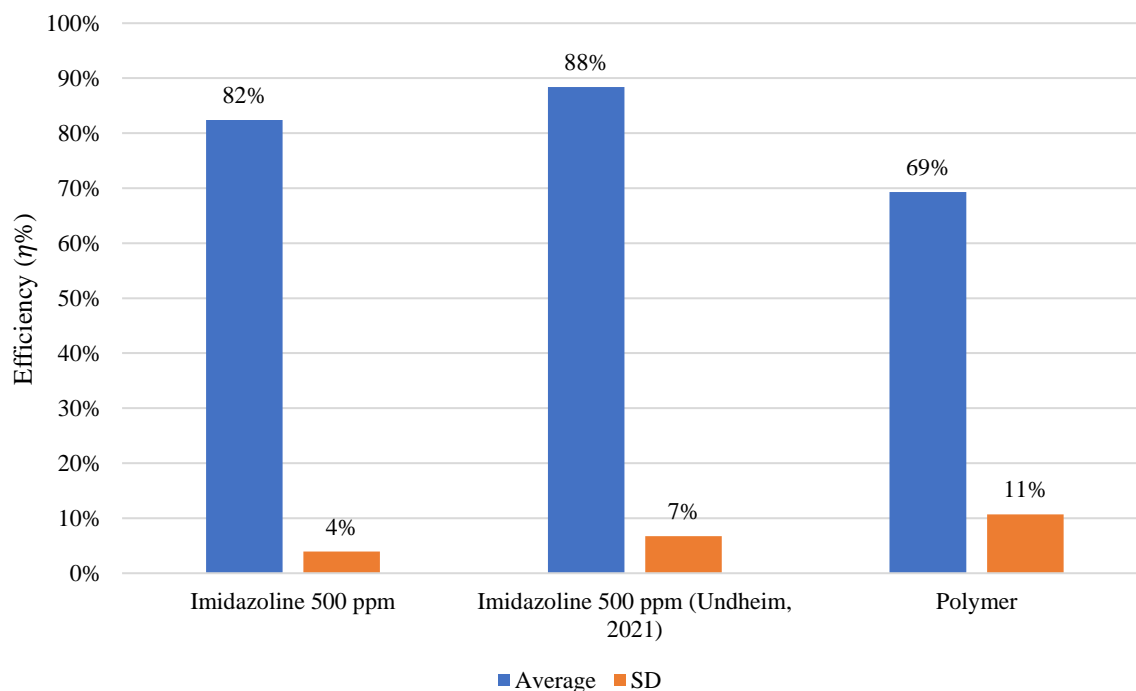
Figure 2.7 Average inhibition efficiency and standard deviation.

2.1.4. Summary
A corrosion baseline was created from a sequence of 15 blank tests without the addition of a CI. These tests showed an $R^2=0.98$, which is an improvement from the literature reference of $R^2=0.91$, this is attributed to the lower O_2 concentration in the pressurised CO_2 gas. Imidazoline was tested at a concentration of 500 ppm and found to exhibit an average efficiency of 82 % with a SD of 4 %. Although the average efficiency was found to be lower than the literature reference possibly due to differences in testing sequence, the SD exhibited a 3 %-point reduction, which is attributed to the lower O_2 concentration. The experimental polymeric inhibitor was tested at 500 ppm and found to exhibit an average efficiency of 69 % with a SD of 11 %. While some of the results seems to be somewhat replicable, there is still high deviation between both the current results in comparison with Undheim (2021), and between the data points within each testing sequence. The attempts to rectify these challenges will be described in subchapter 2.2.

2.2. Method Optimization

While the corrosion testing manual developed by Undheim (2021) gives a good fundamental for further development of the methodology, there are some challenges with the method that are yet to be resolved. Among these we find issues with replicability, reliability, and high deviation to be among the most pressing. Another issue regarding the establishment of a single baseline is that there is no simple way to identify if the environment within the corrosion cell is identical between different sequences. In this subchapter the attempts at rectifying these challenges, as well as other improvements made to the method will be described. This work was conducted through research of relevant literature and speaking with experts within the field such as Prof. Tor Hemmingsen and Amela Keserovic Hoff, PhD.

2.2.1. Initial Modifications
The first approach at attempting to optimize the corrosion testing method described in chapter 2.1 was to include the effects of time, rather than sorting the results in an increasing order. While such sorting of results does have its benefits as it neatly shows the whole range of corrosion in an orderly fashion and allows easy comparison between different results, there are also large uncertainties correlated with this approach. To reduce these uncertainties, it was decided that achieving a stable corrosion rate during baseline tests for each sequence would be paramount in increasing reliability and an accurate comparison between sequences.

As noted by Undheim (2021), scratches in the C1018 steel coupon surface may be revealed by a light wet sanding. These scratches were initially a large concern regarding potential leakage and deviation in results. Although, utilizing an O-ring in combination with the compression gasket seemed counterintuitive as the applied pressure was limited to the O-rings resistance without being squeezed out of position, as mentioned by (Undheim, 2021, p. 29). It seems likely that the reduction in pressure may be the culprit behind some issues related to leakage. The O-ring between the Pyrex tube and compression gasket as shown in (Undheim, 2021, p. 30) was therefore excluded, and leakage was not experienced thereafter.

A tool called Sequence Wizard was found in the Gamry Framework software, which allows LPR tests to be initiated without manual input from the operator. The utilisation of this tool reduced what would otherwise be a very time-consuming workload to a more manageable level. With the Sequence Wizard it was possible to initiate tests more often, and at a more precise time interval without operator input. While this tool was utilized quite early in the optimization process to initiate LPR at specific time intervals and more often, the final sequence was not developed until later, this is therefore presented in subchapter 2.2.10.

2.2.2. Baseline

There were initial attempts to create a new baseline to include the initial changes and because the current container of pressurised CO_2 contains a lower concentration of O_2 than previously used. While we had some initial success in creating a more stable baseline, there were also difficulties associated with localized corrosion. The coupon presented in Figure 2.8 shows precipitation of what is assumed to be ferrous carbonate, although iron(II,III) oxide could also be present, unevenly on the metal surface, this will be referred to as "patching" as it was found to usually occur as patches of various sizes spread across the metal surface.
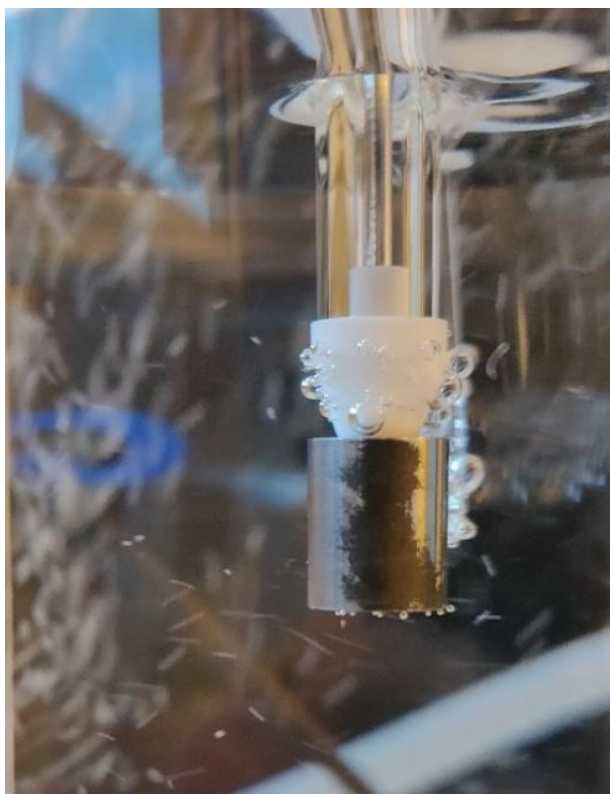
Figure 2.8 Localized corrosion as "patching" on metal surface.

Several coupons were found to possess various degrees of abnormalities and exhibited discrepancies in expected corrosion rate during baseline testing with only brine and CO_2. These coupons were also susceptible to patching and showed high deviation between results. In an effort to improve these tests, there was an attempt to sand the coupon surface with high grit wet sandpaper in order to provide a uniform surface, as proposed by (Undheim, 2021, p. 59). Preliminary results presented in Figure 2.9 seemed to provide both uniform corrosion and high baseline corrosion rates after mechanically sanding the metal surface. Compared with the blank results presented in Figure 2.1, the mechanically sanded coupon seemed like a great success as the corrosion rate was mostly stable throughout the four-hour period of the sequence.
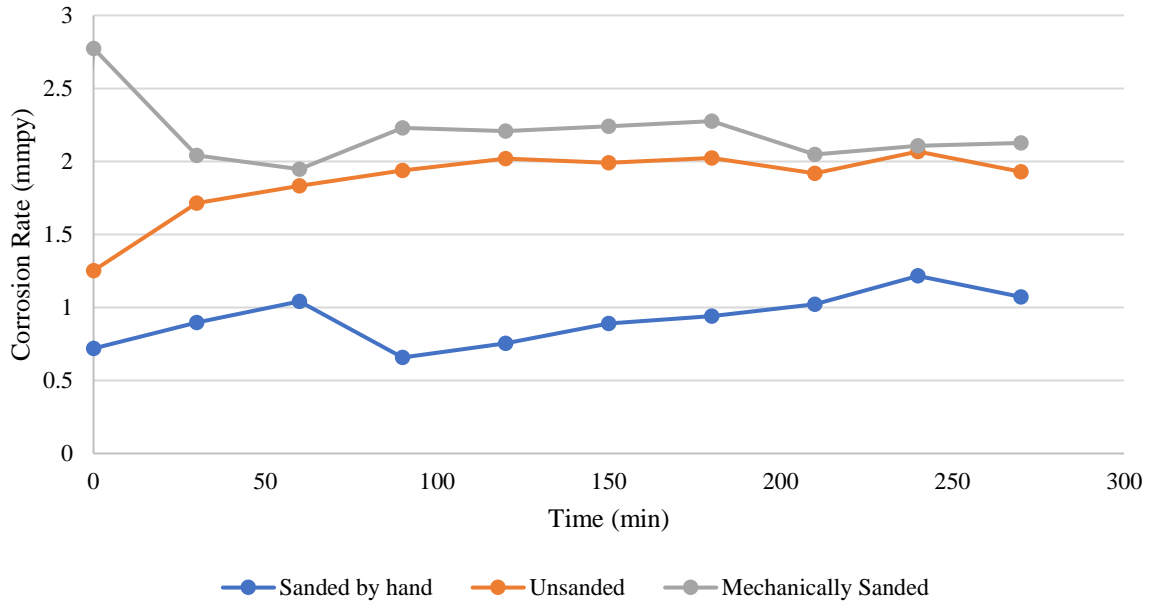
Figure 2.9 Corrosion test results, different surface treatments on a single coupon.

Surface treatment of coupons was investigated further, as it seemed to yield good results. Although, of the results presented in Figure 2.10, only "BaselineCoupon 1" exhibited uniform corrosion, the other three coupons treated in the same manner showed at least some degree of patching and low corrosion rate. After several attempts at replicating this baseline with poor results, the variability between different coupons was started to be questioned. While there will be some degree of variation in the metal matrix, the exact variation to be expected by this factor was unknown.
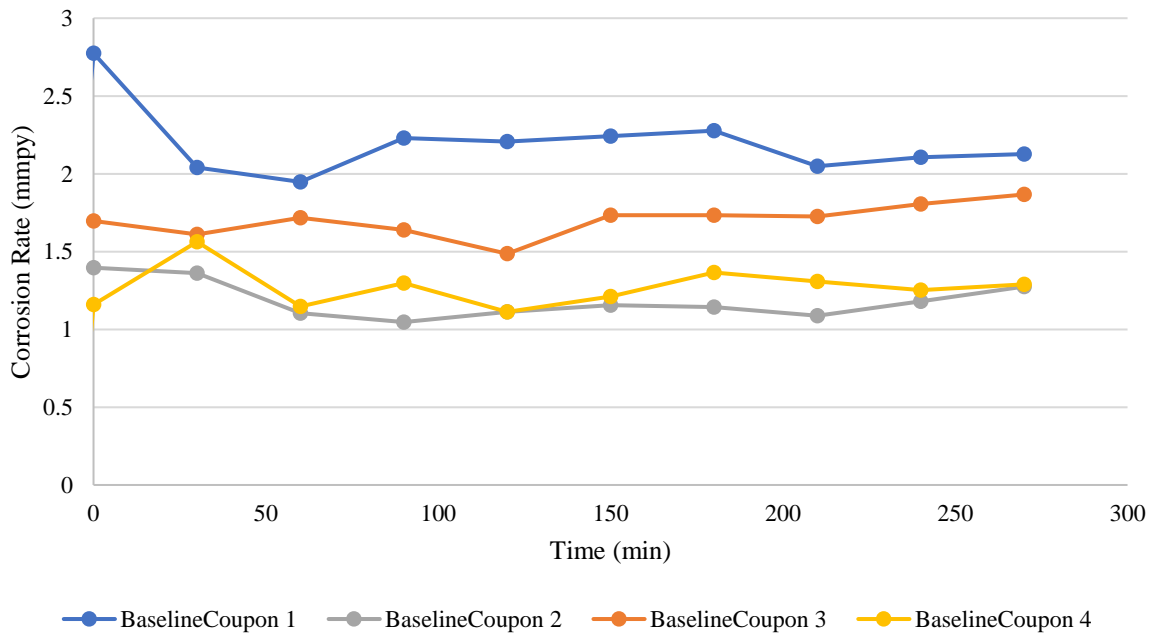
Figure 2.10 Corrosion test results, different coupons, mechanically sanded.

Later results, as presented in Figure 2.11, indicated an inverse relationship, which may be correlated to difficulties in gaining a similar enough surface on the coupons. Two different coupons were used in this test, in comparison to Figure 2.9 where different treatments were applied to the same coupon.
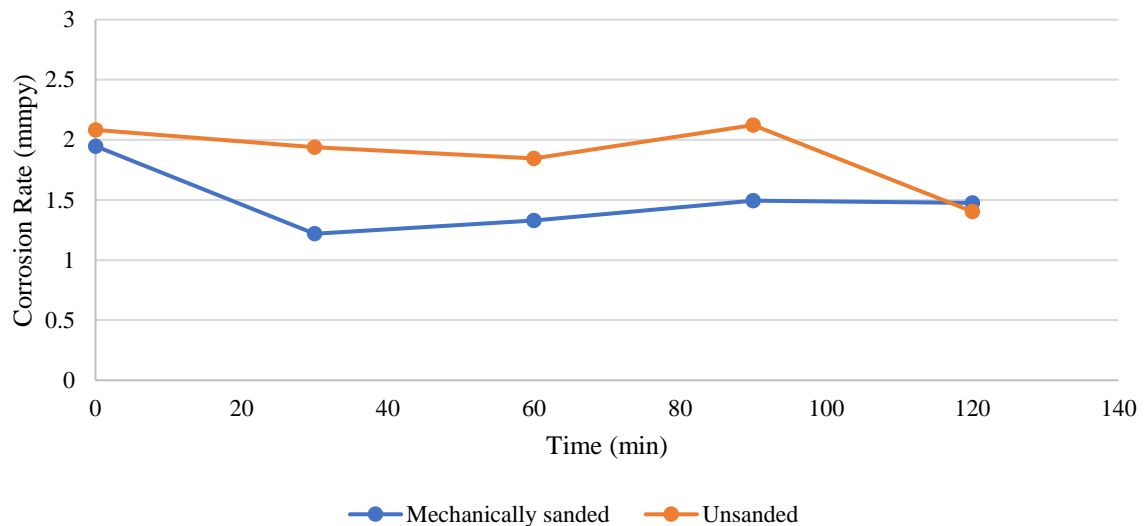
Figure 2.11 Different coupons and different surface treatment.

There were also concerns regarding how large of a variation could be expected from any applied surface treatment, and how results could be made statistically significant with such a variation. In the end it was decided that sanding, especially by hand was too time consuming as well as it being difficult to gain a similar enough surface. From these sanding trials we may conclude that while achieving an identical surface on every coupon possibly would yield good results, this was found to be impossible with our current available equipment. Therefore, it was decided to reduce the surface treatment to only include sonication and washing, as will be further described in chapter 2.2.4.

2.2.3. Sequence Length

There were some suggestions by Undheim (2021, p. 94) regarding possible ways to improve the method. Among these, changes to the sequence length and interval between measurements became easier to do by utilizing the Sequence Wizard tool, which is described further in subchapter 2.2.10. Increased sequence length and reduced time between measurements was also suggested (T. Hemmingsen, personal communication, 4 February 2022; A. Keserovic Hoff, personal communication, 4 February 2022). Initially there was some attempts to investigate if results could be improved by simply increasing the sequence length. Although. the first long sequence test provided poor and unstable results, as presented in Figure 2.12. Due to a computer issue, this test was unfortunately stopped prematurely and restarted in the morning. Nevertheless, it became apparent that simply running for a longer time might not be a simple solution to this issue after all, and that additional optimization is required. While the variation in corrosion rate possibly could be explained by changes in temperature, the room temperature where the cell was placed is thought to be quite consistent. Although, temperature variation is something which could be investigated further in future work, as suggested by (T. Hemmingsen, personal communication, 4 February 2022).
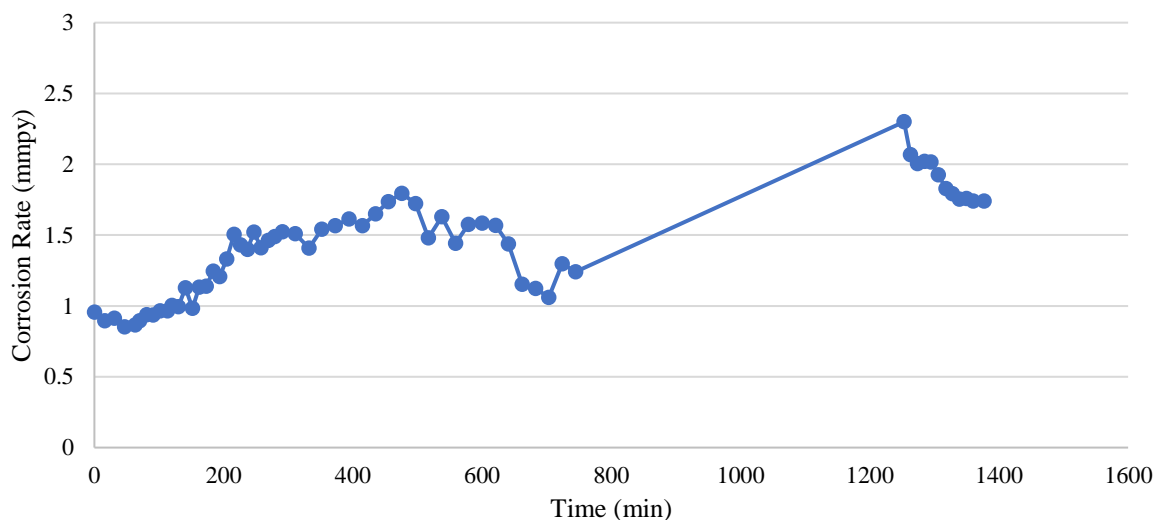
Figure 2.12 Corrosion test baseline sequence overnight, first test.

In an attempt to further investigate whether there is a correlation between stability and the length of the sequence. Two tests were conducted with imidazoline, of which the results are presented in Figure 2.13. Here, imidazoline was injected just prior to the steep reduction in corrosion rate, for both tests. While the overall trend at this point was starting to become closer to the expected results, it was clear that improvements still were to be made.
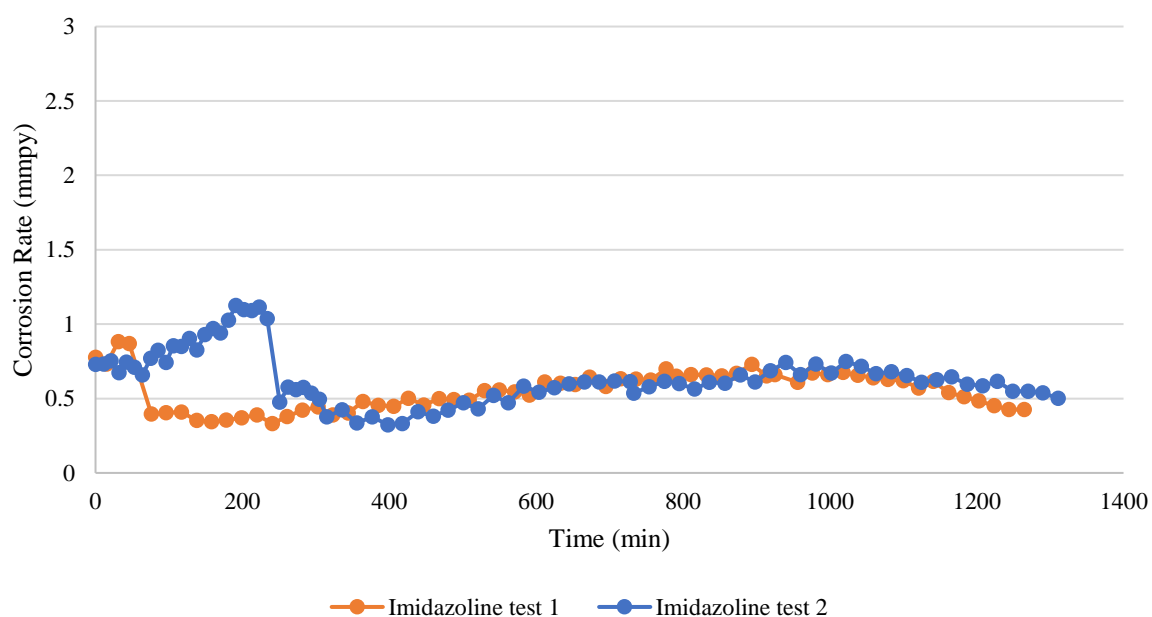
Figure 2.13 Corrosion test sequence overnight, with 500 ppm imidazoline.

2.2.4. Washing
In order to ensure that every trace of film-forming agent is removed from the corrosion cell and corresponding equipment, the washing procedure was optimized. After completion of the overnight sequences, the complete removal of imidazoline was found to be challenging, as a thick film had formed on every internal surface. A 1M HCl solution was therefore used to

protonate imidazoline, making it more water soluble and easier to wash off. While the film seemed to dissipate with the 1M HCl solution, it was decided to utilize a solution of 1:1 2M HCl and i-PrOH to ensure removal of any remaining trace. Although, a 5M HCl solution was also sometimes used. In some cases, a 1:1 solution o 1M NaOH and i-PrOH was used for inhibitors where acid washing was less effective. Although washing procedures change with necessity, the procedure typically followed prior to- and post corrosion testing in this thesis may be found in Appendix A. An alternative to this procedure could be to store most of the glassware submerged in a 1:1 solution of 1M NaOH and i-PrOH, followed by a rinse with DIW, and acetone. The graphite counter electrode was replaced with a platinum wire counter electrode. Washing of the platinum wire consists of rinsing with DIW and acetone before it is submerged in DCM overnight.

The coupons were found to require substantial washing to remove any organic residues. Initially, the coupons were rinsed and sonicated in acetone. Sonication was done by placing the coupon in a centrifuge tube which was partially filled with acetone and fitted with a needle through the cap to avoid build-up of pressure, as seen in Figure 2.14 (a). The centrifuge tube was then submerged in a Branson 2510 Ultrasonic Cleaner, as seen in Figure 2.14 (b) for one hour. After sonication, a screw was inserted into the coupon, which was then attached to an electric drill as seen in Figure 2.15. The coupon was rubbed on tissue paper with acetone, DIW, ethanol, and i-PrOH, as described in Appendix A. There was a suggestion to use a cloth to slightly polish the metal surface (T. Hemmingsen, personal communication, 4 February 2022). While the approach with using a cloth provided good results, it was later found that sonication provided similar results and was easier to apply in a more consistent by new operators. Although, utilization of a cloth for this purpose could be interesting to investigate further in the future. After some time, the baseline corrosion rate was found to be decreasing and patching started to become more common. This was thought to be because of build-up of various contaminants in the centrifuge tube, which was therefore replaced. Following this, the baseline corrosion rate returned to a higher rate, and the coupon showed uniform corrosion. Towards the end of the work, it was found that sonication of the coupon for one hour in i-PrOH rather than acetone yielded the most consistent results. The washing procedures described in this chapter are likely excessive, they may therefore preferably be stepwise reduced in future work to optimize the procedure further.

Figure 2.14 (a) Coupon submerged in acetone in a centrifuge tube. (b) Centrifuge tube containing the coupon submerged in a Branson 2510 Ultrasonic Cleaner.
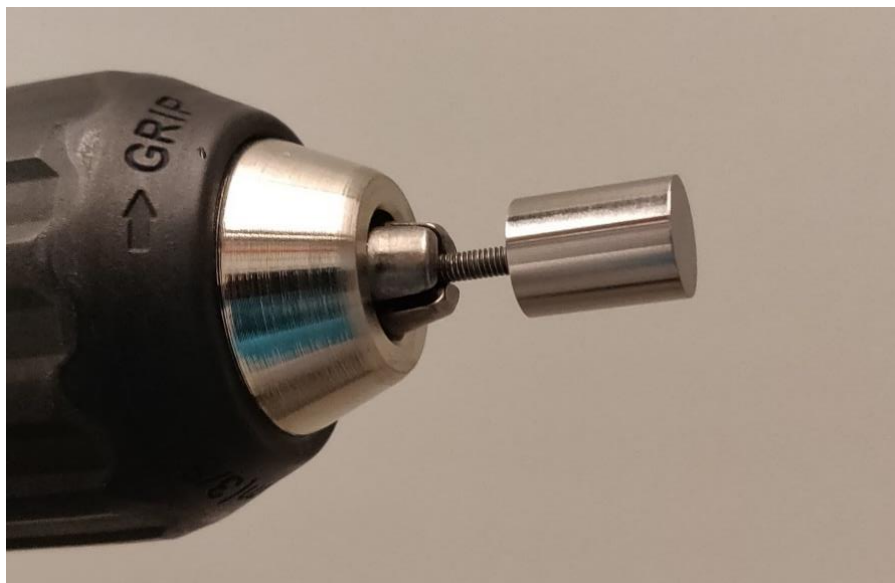
Figure 2.15 Coupon attached to an electric drill by small screw.

2.2.5. Inhibitor Addition

For most inhibitors, dissolution in a small amount of brine before direct addition by a pipette through an open port in the corrosion cell as described by (Undheim, 2021, p. 66) was sufficient. Although, for some particularly smelly compounds such as thioglycolic acid, addition occurred by inserting a needle through a Suba-Seal to reduce the leakage of smell

into the laboratory. This was accompanied by including a discharge tube for the gas flow into a nearby flow hood.

2.2.6. Gas Flow and Foaming
The gas flow into the system was regulated by a Messer Constant 2000 pressure regulator, as described by (Undheim, 2021, p. 33). The start-up procedure should be followed as described by (Messer, n.d.), which is to completely open the gas cylinder valve slowly, and thereafter adjust the pressure by the hand knob, the needle valve may then be slightly opened and adjusted until desired flow is achieved. The shut of procedure described in the same manual is to first close the gas cylinder valve, and thereafter when the pressure regulator has been depressurised, the hand knob should be released, and finally the needle valve should be closed. All pressurised gas should have left the system, and both pressure gauges should display zero.

Some inhibitors added to the corrosion cell was found to be highly effective surfactants, which sometimes caused an overflow of foam into the discharge tube, as presented in Figure 2.16. In the most severe cases the discharge tube became filled with brine and foam. The discharge tube was purged by connecting the inlet and discharge tubes and increasing the gas pressure. The discharge tube was thereafter rinsed with DIW and acetone prior to another CO_2 purge.
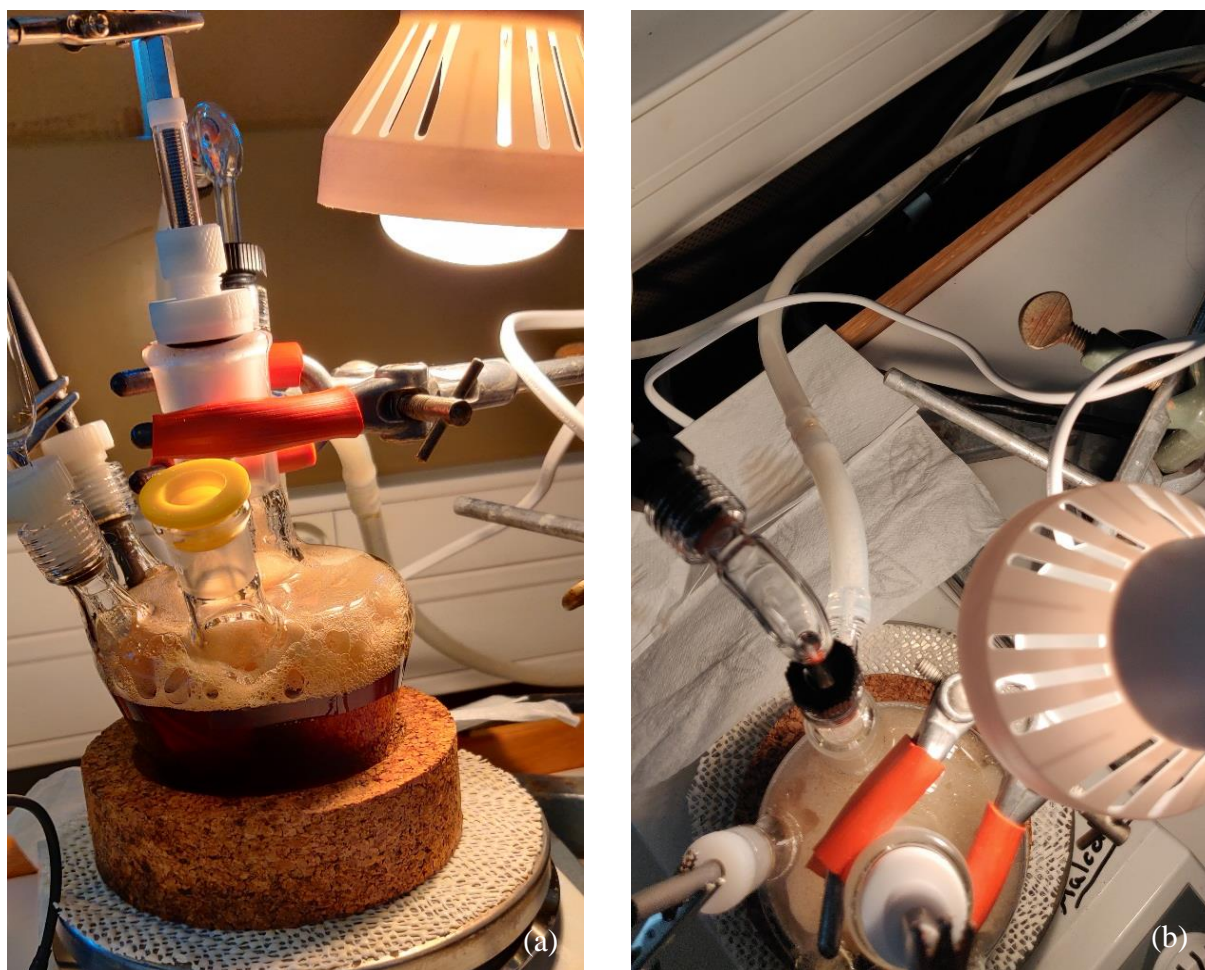
Figure 2.16 (a) EuroCell filled with thick foam. (b) Discharge gas tube partially filled with foam.

The gas flow should be kept at a rate high enough to esnure saturation of the brine, but low enough to avoid overfoaming. Another concern when utilising the EuroCell with only 150 ml brine, is that the compressed CO_2 is quite cold, and a high flowrate may affect the temperature of the brine. Although, this effect has not been investigated any further and might not be of a significant concern due to the overal low gas flow.

2.2.7. Potentiostat Calibration

The potentiostat was calibrated as described by (Gamry Instruments, n.d.). This was done by connecting all the connection clamps to the appropriate connections on the Gamry Instruments Universal Dummy Cell and the black ground connectors to the faraday cage, as seen in Figure 2.17. A calibration script from the Gamry Framework software was thereafter initiated, as seen in Figure 2.18. The Gamry Instruments Universal Dummy Cell used here was borrowed from the Department of Mechanical and Structural Engineering and Materials Science at UiS.

Figure 2.17 Potentiostat calibration with Gamry Instruments Universal Dummy Cell.
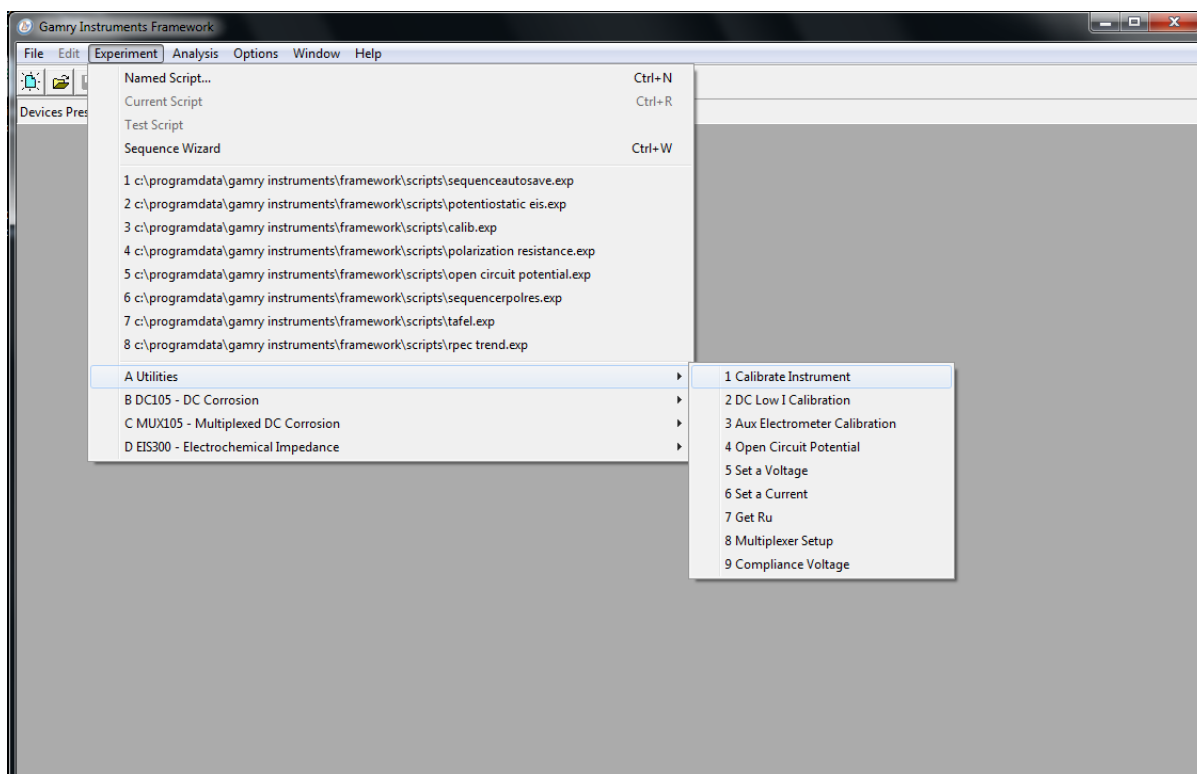
Figure 2.18 Gamry Instruments Framework, initiating calibration.

2.2.8. Reference Electrode and Reference Bridge Tube

Both the reference electrode and reference bridge tube contains a porous glass frit which is susceptible to cracking if allowed to dry, as described by (Gamry Instruments, 2017, pp. 13–14). Therefore, the reference bridge tube is stored filled with brine, and the tip covered by a black plastic sleeve or submerged in a saline solution. The reference electrode should be vented for 30 minutes prior to use, this can be achieved by removing the seal or by inserting a pipette tip to ensure airflow, as seen in Figure 2.19.

Figure 2.19 Reference electrode being ventilated by a pipette tip.

2.2.9. Counter Electrode

As a wide range of different compounds are tested in the corrosion cell, accumulation in the graphite counter electrode became an increasing concern. While the washing procedure used to clean the glassware generally seemed to be adequate in washing the graphite rod, we were reluctant to leave the rod submerged in strong cleaning solutions for a prolonged time. To reduce possible contamination from the graphite rod, as described by (Gamry Instruments, 2017, p. 10), the rod was replaced with a fritted isolation tube containing a 150 mm platinum wire, as described by (Gamry Instruments, 2017, p. 11). By bending the platinum wire out- and down the Pyrex tube, it can easily be connected to the crocodile clamps by clamping them securely onto the tube, as presented in Figure 2.20.

Figure 2.20 Platinum wire counter electrode, connected with clamps outside of Pyrex tube.

2.2.10. Test Sequence

The final test sequence developed in this work includes a two-hour long baseline sequence prior to inhibitor addition, which is then measured for three hours. While it would be beneficial to conduct corrosion testing over several days as suggested by (A. Keserovic Hoff, personal communication, 4 February 2022) and done by other researchers (Abbasov et al., 2013, p. 457; Ferrer & Bennett, 2022, pp. 11–12; Mékarbané et al., 2019, p. 4; Mohamed et al., 2012, p. 60) it was decided to compress the sequence into one workday. The time interval between tests was therefore also reduced from 30 minutes to five minutes. The overall test procedure and parameters is conducted in the same way as described by Undheim (2021). While the full set of changes to the method will be summarised in chapter 2.3, the changes made to the test sequence are as follows:

- Coupon is left in brine for one hour prior to first LPR measurement, as suggested by (T. Hemmingsen, personal communication, 4 February 2022).
- Baseline LPR measurements are taken for at least two hours, may be run longer if corrosion rate is unstable, as suggested by (T. Hemmingsen, personal communication, 4 February 2022).
- Time between measurements is set to five minutes, although this may be increased if sequence length is extended.
- After addition of inhibitor, LPR measurements are taken for three hours.

The Sequence Wizard may be opened by the shortcut "Ctrl+W" or by finding it in the "Experiment" tab, as presented in Figure 2.21.
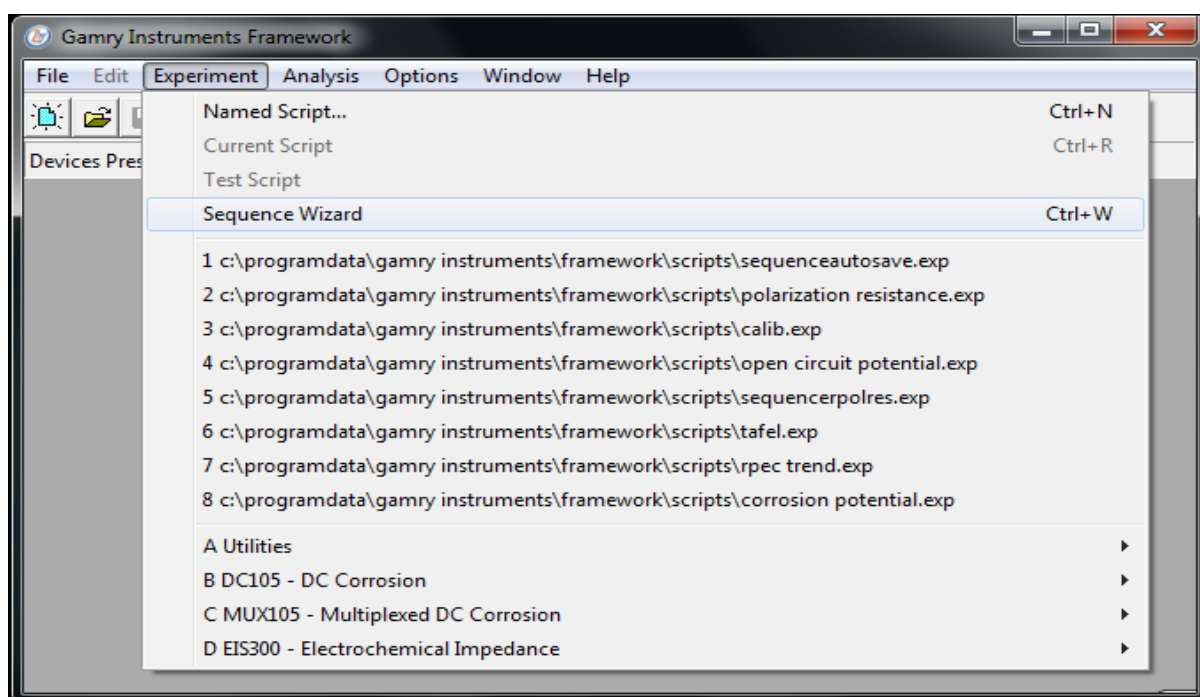
Figure 2.21 Opening the Sequence Wizard.

The sequence presented in Figure 2.22 starts with a one-hour delay before an initial LPR test is conducted to quickly be able to identify if there are any problems. If no clear deviation is identified by the operator, the sequence proceeds to perform LPR tests with a five-minute delay for a duration of two hours. As the baseline sequence comes to an and, there is a one-hour delay to allow enough time for an inhibitor to be injected into the brine. After the operator has injected the inhibitor, the remaining time may be skipped by pressing "skip" or "F2". The sequence then proceeds to perform LPR tests with a five-minute delay for a duration of three hours. The sequence may easily be modified as desired by the operator by adding steps from the left panel or by removing or changing order of steps in the right panel. Parameters such as increasing sequence length or decreasing interval between measurements may be modified by right clicking each step and clicking "Properties" as presented in Figure 2.22. The sequence may be initiated by clicking the "Run Sequence" button.
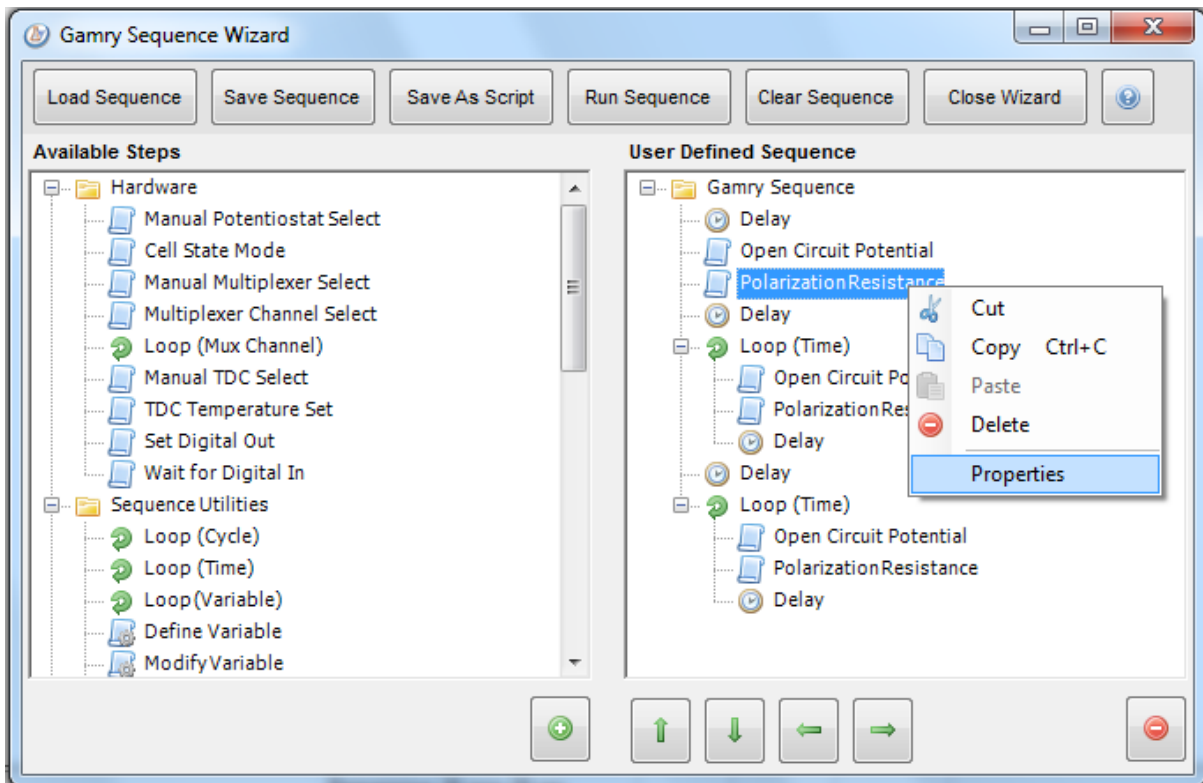
Figure 2.22 Sequence Wizard showing full test sequence.

2.2.11. Method Verification

After implementation, the aforementioned changes into the method a test with 500 ppm imidazoline was initiated, the result from this test is presented in Figure 2.23. Compared to the previous results discussed in chapter 2.1 it seems clear that the new method offers a higher level of both reliability and accuracy. Although, there are still occasional issues regarding patching during the baseline testing which could lead to a lower measured corrosion rate than would be the case with completely uniform corrosion. The efficiency of an inhibitor with this method is calculated by using the average corrosion rate of the last hour prior to addition, and the average corrosion rate of the last hour post addition. In Equation (2.8) the efficiency is calculated in this way by using Equation (2.7).

$$\frac{1.944 \; mmpy \; - \; 0.288 \; mmpy}{1.944 \; mmpy} \times 100 = 85.2 \sim 85 \; \%$$

Equation (2.8)

After most of the optimization work previously described was completed, there was a shift from the Multiport to a smaller model called the EuroCell. The workings of these cells are identical, while the only difference is the size and shape of the cell and corresponding equipment. Empirical data seems to suggest that the baseline corrosion rate of the EuroCell often is slightly lower than for the Multiport, as seen in Figure 2.23. The same phenomena were also observed in later corrosion tests, but the effect is considered small and will not be investigated further due to time limitations. Although, approaches that can be taken to investigate this will be suggested in subchapter 2.2.12.
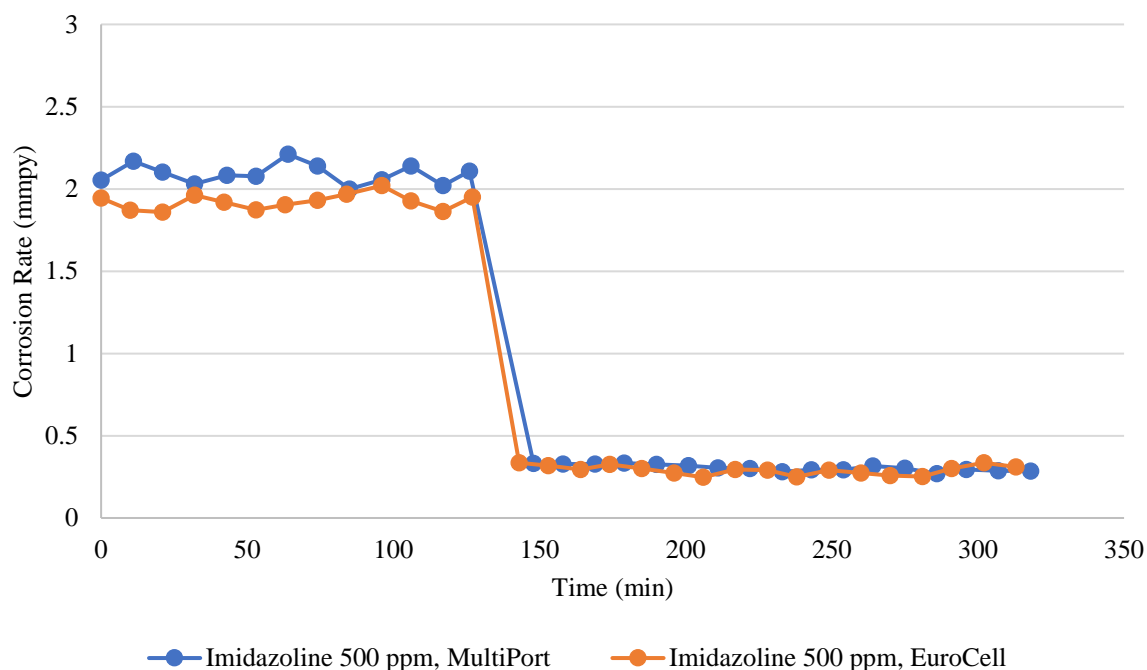
Figure 2.23 Comparison between Multiport and EuroCell imidazoline corrosion results.

2.2.12. Further Optimization

Through this work we have introduced several new aspects into the corrosion testing method and investigated some of the recommendations suggested by Undheim (2021). While the method has been improved, there are still steps that could be taken to optimize the method further:

- The coupon could be cast in Teflon and the end sanded with high grit paper. This would allow the coupons to be used for a much longer period, as suggested by (T. Hemmingsen, personal communication, 4 February 2022).
- Because the volume of the EuroCell is much smaller than the MultiPort, the effect of temperature changes should be investigated by introducing a thermostat into the procedure.
- If the temperature variation is found to of concern, ways to keep it consistent should be investigated.
- The gas regulator could be replaced by an automatic regulator to ensure consistent flowrate.
- Impedance of the reference electrode should be investigated.
- Tafel constants should be explored further, as also proposed by (Undheim, 2021, p. 92).
- The cleaning procedures developed in this work may be somewhat excessive, steps to simplify these should be investigated further.
- Utilizing a potentiostat that can run parallel cells would greatly increase accuracy of the results.
- The accuracy and reliability of the method should be investigated further, e.g., statistically analyse measurements of the same compound, and compare results to similar corrosion testing methods.

- Sequence length could also be investigated further, e.g., results for the same compound could be compared between the current sequence length and a sequence over several days. It is expected that a longer sequence would provide more accurate results, but exactly how much more is currently unknown.
- A different way of injecting inhibitor could also be interesting to investigate, e.g., an inhibitor could be incrementally injected to measure the inhibition effect at different concentrations, which was suggested by (T. Hemmingsen, personal communication, 4 February 2022).
- OCP could be measured during the one-hour period when the working electrode is submerged in brine.
- The necessity of the one-hour stabilization period while the coupon is submerged in brine could be investigated.

2.3. Summary

The method developed by Undheim (2021) does seem to work as intended and provide reasonable results. The purpose of further optimization was to reduce uncertainties related to the use of different coupons and data analysis, while also achieving higher stability and replicability. After conducting over 2500 LPR tests, the method was improved enough to be satisfactory. In comparison with the baseline results reported by Undheim (2021, p. 99), where the corrosion rate found to lie between 0.4 – 2.7 millimetre per year (mmpy). The current method offers more consistent results with lower deviation, as can be seen in Figure 2.24, where five sequences with different coupons exhibit a baseline corrosion rate between 1.8 – 2.2 mmpy, as given by the points for optimized method coupon 1 – 5. While there are still improvements to be made to the method, the optimized method should allow for easier replicability between different tests.
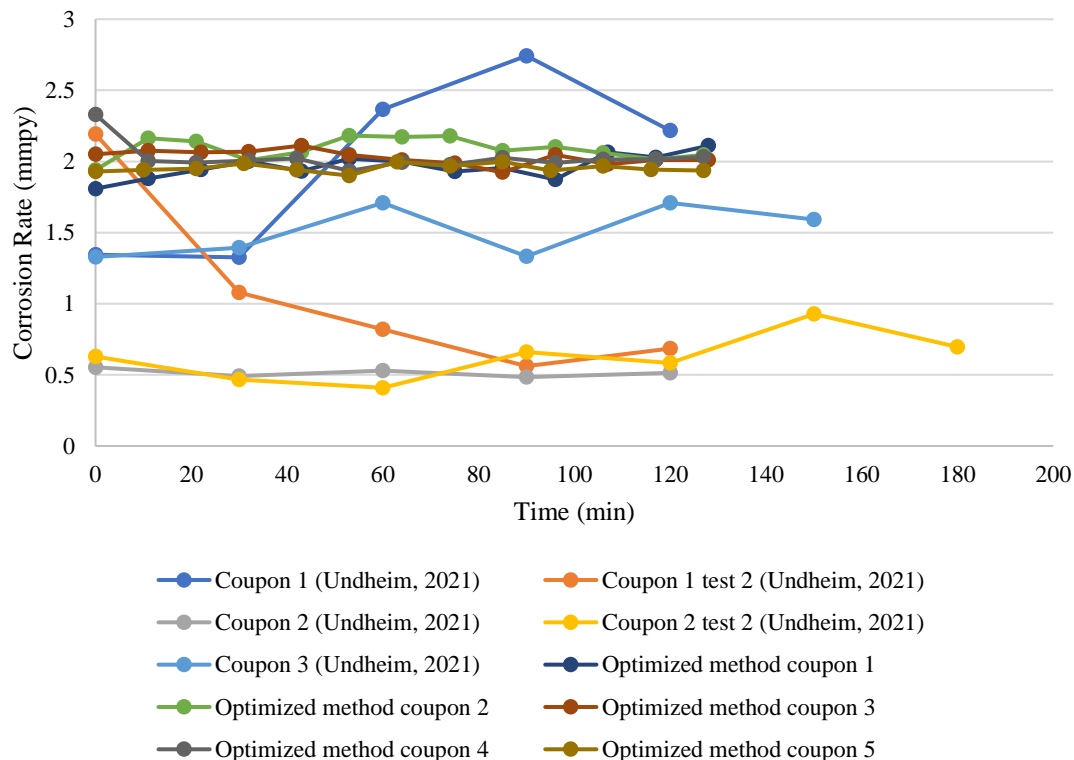
Figure 2.24 Baseline comparison with original method, timestamp data from the literature reference is estimated based on described test procedure.

The optimization changes may be summarised as the following points:

- O-ring was removed from the assembly to ensure a tight seal between the Pyrex tube and the Teflon compression gasket.
- Corrosion results are sorted by time, rather than in an increasing order.
- Sequence length was increased.
- Time between measurements was decreased.
- Coupon sonicated and washed as described in subchapter 2.2.4.
- Corrosion cell with corresponding equipment is acid or base washed as described in subchapter 2.2.4.
- Gas discharge tube was added.
- Potentiostat was calibrated.
- Reference electrode vented for 30 minutes prior to use.
- Reference bridge tube stored in electrolytic solution.
- Graphite counter electrode was replaced by a platinum wire counter electrode.
- The Sequence Wizard was used to initiate the LPR tests with a consistent time interval over a longer duration.
- Coupon submerged in brine for one hour prior to testing.
- Two-hour baseline sequence for each coupon prior to addition of inhibitor.
- Three-hour sequence post inhibitor addition.
- Efficiency calculated by using the average corrosion rate of the last hour prior to addition, and the average corrosion rate of the last hour post addition.

3. Functional Groups as Corrosion Inhibitors

As a step in the development of multi-functional inhibitors, it is paramount to understand which functional groups are efficient as corrosion inhibitor (CI). In this chapter, the different compounds are tested as CI and their results reported and discussed.

3.1. Introduction

Imidazoline is a well-known commercial and highly effective surfactant CI commonly used in flow systems in the oil and gas industry. Inclusion of imidazoline in CI testing with the optimized method described in chapter 2.2 is therefore highly relevant in giving perspective to results from other inhibitors such as those that will be discussed later in chapter 4, as well as a verification of the method itself. Based on the knowledge gained in chapter 1.2 a selection of compounds was tested as CIs.

3.2. Materials and Methods

4,5-dihydro-1H-imidazole (imidazoline) was obtained from MI Swaco. Polyacrylamide was obtained from Sigma-Aldrich. Sodium lignosulfonate (SLS) was obtained from Sigma-Aldrich. Styrene sulfonic acid, sodium salt polymer was obtained from Monomer-Polymer & Dajac Labs, Inc. Luvicap 55W (1:1 Vinylpyrrolidone:vinylcaprolactam copolymer (VP:VCap)) was obtained from BASF. 4,6-Dihydroxy-2-mercaptopyrimidine (2-thiobarbituric acid (TBA)) was obtained from Thermo Scientific. Sodium thiosulfate (STF) was obtained from J.T Baker. Poly(ethylene glycol) was obtained from Sigma-Aldrich. Mercaptosuccinic acid (MSCA) was obtained from Sigma-Aldrich. Thioglycolic acid (TGA) was obtained from Sigma-Aldrich. Butyl thioglycolate (BTG) was obtained from Tokyo Chemical Industry (TCI). Polylysine was obtained from JNC, Japan. Polymaleic anhydride reacted with 3,3-dibutylaminopropylamine (PMA-DBAPA) and derivatives were synthesised at UiS by Dr. Radhakanta Ghosh. All compounds were used directly without further purification. Corrosion testing was carried out as described in in chapter 2.2.10. Where baseline corrosion rate was measured with a five-minute delay for two hours before addition of the inhibitor, which was then measured with a five-minute delay for a period of three-hours. The mild C1018 steel coupons used for corrosion testing was obtained from European Corrosion Supplies.

3.3. Results and Discussion

Imidazoline exhibited good inhibition at both 500 and 100 ppm, which resulted in an efficiency of 85.4±2.2 % and 76.5±1.5 %, respectively, as presented in Table C-1 in Appendix C. Although it must be noted that the result at 500 ppm contains a positive bias due to the higher baseline compared to the other tests with imidazoline. This bias is likely due to the optimization being a work in progress, and tests being conducted at different stages of the optimization. Although, while the difference is reduced by controlling for this bias, such control offers no significant change to the overall ranking of the results.

By introducing 100 ppm each of MCSA and TGA with 500 ppm imidazoline, the efficiency is slightly reduced to 73.8±1.2 % and 75.0±1.8 %, respectively, as given in Figure 3.1. The structures for MCSA and TGA are quite similar, where TGA contains a thiol and carboxylic acid group, and MCSA contains an additional carboxylic acid group. While neither of these synergists exhibited a good synergistic effect with imidazoline, it seems like the additional carboxylic acid group from MCSA does not offer much effect. On the other hand, the thiol functional group might be adsorbing onto the metal, competing with imidazoline for adsorption sites, thus causing the antagonistic effect. While TGA was found to work poorly

as a CI by itself with an efficiency of -29.2±3.6 %, this does not necessarily mean that TGA adsorbs poorly, it could indicate that a hydrophobic film is not formed. imidazoline was found to be sparingly soluble in water, to increase solubility acetic acid was therefore included in a 3:1 mixture of 100 ppm imidazoline to ensure protonation. Imidazoline was easily dissolved in water with this mixture, although the efficiency was reduced to 62.3±2.4 %, from 76.5±1.5 % of 100 ppm imidazoline by itself. This reduction in efficiency is likely due to a shift in the hydrophilic-lipophilic balance (HLB) causing a reduction of the hydrophobicity of the film as water solubility increases. Another reason could be because a larger portion of the chemical is dissolved, ensuring fewer molecules are available to bind to adsorption sites on the steel surface. Imidazoline was also tested at 100 ppm in 90% brine and 10% low aromatic white spirits (LAWS) (10 % toluene, 90 % heptane). This test showed an efficiency of 78.7±2.0 %, which is on par with 100 ppm imidazoline in 100 % brine. The similarity between results is likely correlated to the polarity of LAWS, which are nonpolar solvents, imidazoline was unaffected by the LAWS phase and went straight to the water phase where it was dissolved.

When SLS was used as a synergist at 100 ppm with 500 ppm imidazoline, it exhibited the highest efficiency of the synergists used with imidazoline at 80.4±1.7 %, although still lower than 500 ppm imidazoline alone. The antagonistic effect of SLS could be due to competing adsorption as previously described in this chapter. Although, the increased efficiency compared to other synergists could be caused by the adsorption and film-forming by SLS itself, which will be described later in this chapter.
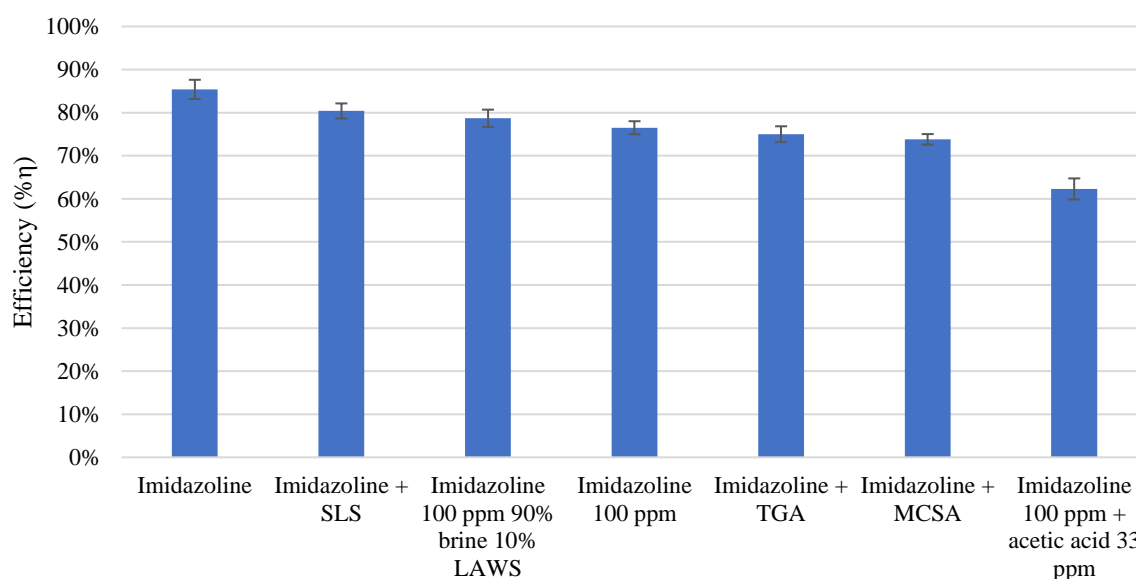
Figure 3.1 Summary corrosion results imidazoline and synergists.

The final compound tested as a synergist with imidazoline in this work was SLS, which was also tested as an inhibitor. By itself, 500 ppm SLS exhibited an efficiency of 95.9±1.6 %, as given in Figure 3.2. The monomer of SLS consists of a sulfur trioxide group at the end of a three-carbon chain, and a methoxy group connected to a benzene ring. The monomers are connected by an ether group between the benzene ring and three-carbon chain. By considering the structure of SLS it seems likely that adsorption could occur through the sulfur trioxide groups, causing the benzene rings and three-carbon chains to from a hydrophilic film on the surface. When introducing 100 ppm TBA as a synergist with 500 ppm SLS, the

efficiency was found to be similar at 94.5±1.8 %. Which could be because SLS easily adsorbs by itself and that TBA is unable to further improve adsorption, possibly due to steric hindrance.

PMA-DBAPA is a polymer with a backbone of polymaleic anhydride, reacted with 3,3-dibutylaminopropylamine (DBAPA) functional groups. The basic polymer PMA-DBAPA, and the amine oxide version which is the polymer reacted with H_2O_2 called PMA-DBAPA-AO was somewhat soluble in water, although some insoluble particles persisted, more so for PMA-DBAPA-AO. The CI efficiency of these polymers was found to be 55.5±2.4 % and 60.2±3.7 %, respectively. Some degree of this efficiency could be explained by the insoluble parts adsorbing onto the metal. PMA-DBAPA in dimethyl ether (DME) was found to be readily soluble in water and exhibited an efficiency similar to the other two tests, albeit lower at 42.3±1.9 %. Overall, it seems that the DBAPA functional group is able to adsorb onto the steel surface and possibly form a film consisting of the polymer backbone.

In contrast to the high efficiency of SLS, sodium thiosulfate (STS) exhibited an efficiency of 45.4±2.0 %. Based on the structure of STS, it seems likely that adsorption onto the metal occurs, creating a barrier from the brine, but as the compound does not contain a hydrocarbon chain, it is probably unable to form a good hydrophobic film by itself. Similarly, polylysine also seems to adsorb onto the metal and creating a barrier, possibly from its two amino groups, exhibiting an efficiency of 40.6±1.8 %. Although, as polylysine contains amino groups on both ends of its monomer, the hydrocarbon chain to form a hydrophobic film is probably very short, and thus less effective, as it is known that for some compounds the hydrocarbon tail length should be around 12 – 18 carbons long for good inhibition.

Luvicap 55W is a copolymer of 1:1 vinylpyrrolidone and vinylcaprolactam, a commonly used commercial KHI, exhibited a CI efficiency of 37.3±5.1 %. While amine containing compounds often seems to adsorb well to the iron in the steel surface, the effect from this polymer was higher than originally expected. If adsorption is similar to that of imidazoline where the amine in the heterocyclic ring adsorbs and the ring lies flat on the surface, one explanation could be that backbone forms the hydrophobic film, separating the metal and the brine. Polyacrylamide consists of a polyethylene backbone with attached primary amide functional groups. Due to the amide group some CI effect was expected, although the results show that the CI effect quite low at an efficiency of 33.2±1.4 %. This could be because only the tip of the function group is likely to adsorb onto the metal, resulting in a majority of the polymer to be moving freely on the metal surface. Poly(ethylene glycol) is a polyether compound where oxygen is the only heteroatom present in the structure. Poly(ethylene glycol) was not expected to show any significant inhibition, which was confirmed by the resulting efficiency of 2.7±2.7 %.
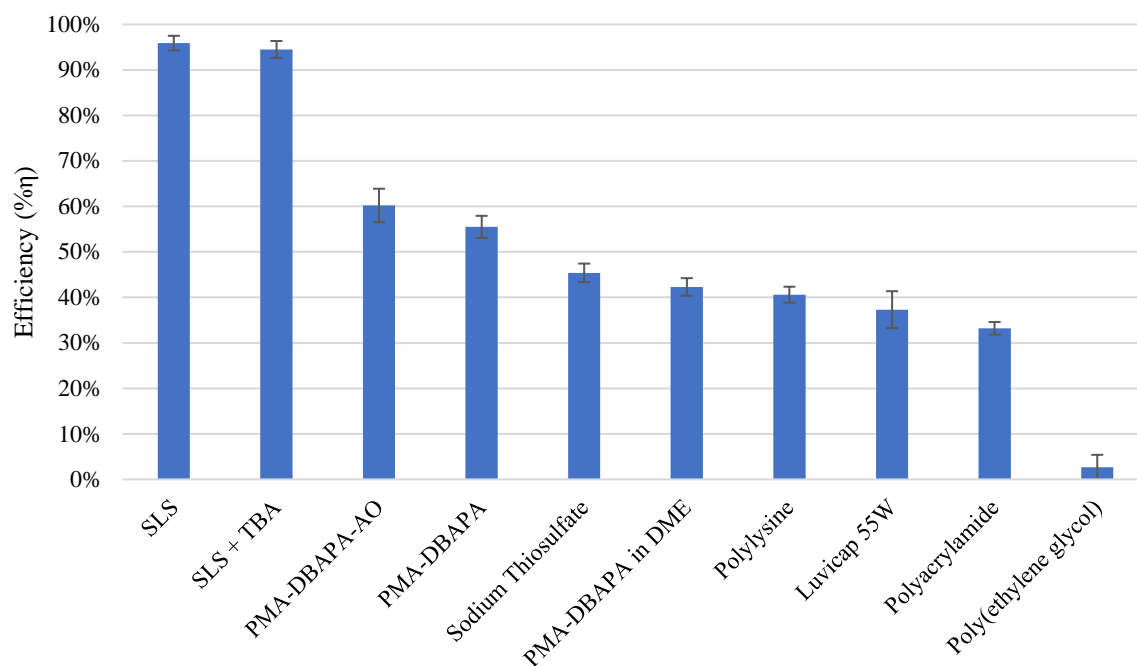
Figure 3.2 Summary corrosion results, excluding imidazoline.

3.4. Conclusion

Imidazoline was tested as CI with the optimised method described in chapter 2.2, both alone with various synergists, and acetic acid. While interesting results were found, none was better than 500 ppm imidazoline by itself which exhibited an efficiency of 85.4±2.2 %. SLS was found to be an efficient CI at 500 ppm with an efficiency of 95.9±1.6 %. The high efficiency of SLS is possibly due to adsorption through the sulfur trioxide groups, causing the benzene rings and three-carbon chains to from a hydrophilic film on the surface.

4. Maleic Anhydride Polymer and Synergists

As a part of the project worked on by Kelland et al. (2021) to develop multi-functional oilfield production chemicals, a new maleic-based copolymer is being explored as a dual gas hydrate and corrosion inhibitor. In this chapter, polymaleic anhydride reacted with 3,3-dibutylaminopropylamine (DBAPA) and vinylcaprolactam (VCap), abbreviated PMA:VCap-DBAPA, are tested as a CI, both by itself and various synergists.

4.1. Introduction

This paragraph is adapted from (Kelland et al., 2021, pp. 5–6). Synthesising polymers of maleic anhydride is an interesting approach as the monomer unit can be reacted and ring-opened with a wide variety of molecules to give it different functional groups for scale, corrosion, or gas hydrate inhibition. Maleic anhydride is made through oxidation of benzene, and its low cost is one of the driving factors for its development as KHI. Polymaleic anhydride may be derivatized by reacting it with amines or alcohol to form polyamides, polyesters, or a mixture of both, as given in Figure 4.1.
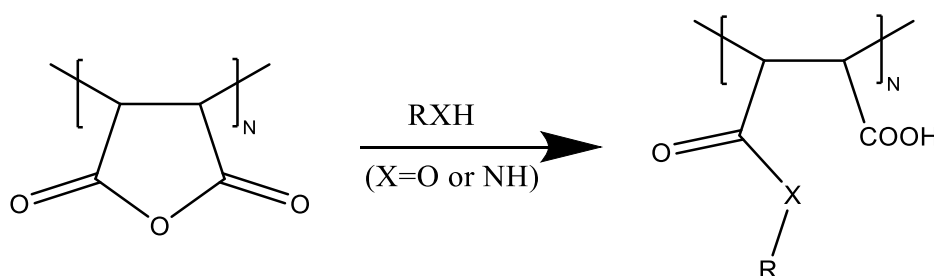
Figure 4.1 Polymaleic anhydride reacted with alcohols and amines, giving polyamide and polyester products, adapted from (Kelland et al., 2021, p. 6).

By reacting maleic anhydride with DBAPA and VCap, the copolymer PMA:VCap-DBAPA may be formed. In water PMA:VCap-DBAPA self-ionises, and reacting it with H_2O_2 will form the amine oxide polymer PMA:VCap-DBAPA-AO, as given in Figure 4.2. The polymer PMA:VCap-DBAPA was also reacted with 3-Acetamidotetrahydro-2-thiophenone (AMT), and glyphosate at a ratio of 20 % relative to DBAPA to form PMA:VCap-(DBAPA:AMT 80:20) and PMA:VCap-(DBAPA:GLYP 80:20), respectively. These polymers are a part of the project to develop multi-functional oilfield production chemicals at UiS. While their KHI results will be reported in another paper, their functionality as a CI will be tested and discussed in this chapter.
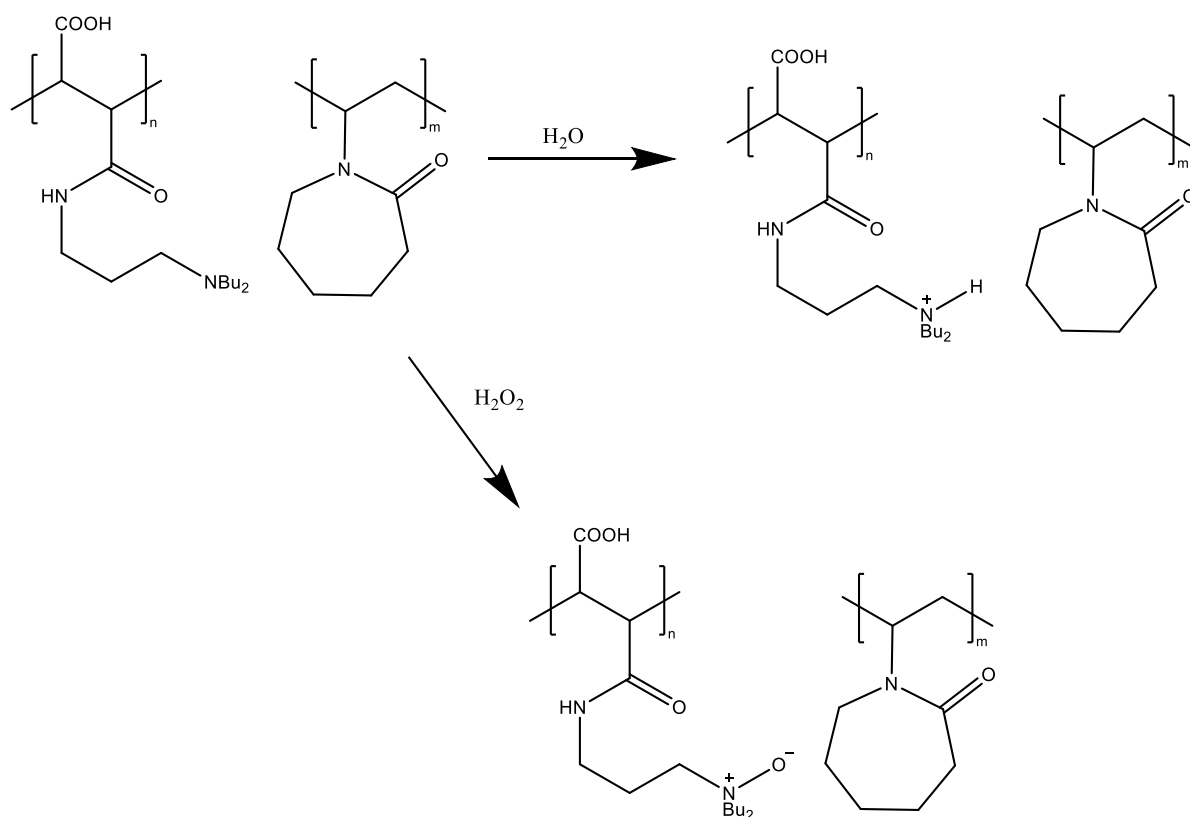
Figure 4.2 Structure of PMA:VCap-DBAPA (top left). Structure of PMA:VCap-DBAPA-AO (bottom).

4.2. Materials and Methods

4,6-Dihydroxy-2-mercaptopyrimidine (2-thiobarbituric acid (TBA)) was obtained from Thermo Scientific. 3-Acetamidotetrahydro-2-thiophenone (AMT) was obtained from Tokyo Chemical Industry (TCI). Guanidine Thiocyanate (GTC) was obtained from Sigma-Aldrich. Thioglycolic acid (TGA) was obtained from Sigma-Aldrich. Butyl Thioglycolate (BTG) was obtained from TCI. Ammonium Thiocyanate (ATC) was obtained from Sigma-Aldrich. Isobutylthiadiazole (IBT) was obtained from TCI. 1-butylimidazole (BID) was obtained from TCI. Mercaptosuccinic acid (MCSA) was obtained from Sigma-Aldrich. Toluene was obtained from VWR. Heptane was obtained from VWR. Polymaleic anhydride reacted with 3,3-dibutylaminopropylamine and N-vinylcaprolactam (PMA:VCap-DBAPA) and derivatives was synthesised at UiS by Janronel Pomicpic. All compounds were used directly without further purification. Corrosion testing was carried out as described in in chapter 2.2.10. Where baseline corrosion rate was measured with a five-minute delay for two hours before addition of the inhibitor, which was then measured with a five-minute delay for a period of three-hours. The mild C1018 steel coupons used for corrosion testing was obtained from European Corrosion Supplies.

4.3. Results and Discussion

Summarisation of the corrosion results relevant to this chapter are presented in Table D-1 in Appendix D. By itself, PMA:VCap-DBAPA at 500 ppm exhibited an efficiency of 18.1 ± 6.6 %. Which may be compared to the similar polymer PMA-DBAPA which was previously discussed in chapter 3 and exhibited an efficiency of 55.5 ± 2.4 %. Based on these results, it seems likely that the addition of VCap offers some degree of steric hinderance, reducing the

polymer's amine groups ability to adsorb onto the steel. The efficiency of PMA:VCap-DBAPA was also tested with various synergists, of which five increased efficiency to above 90 %, a graphical representation of these results is presented in Figure 4.3, where negative results are excluded for simplicity. At a polymer concentration of 2500 ppm with 1000 ppm BTG, which are typical KHI concentrations, an efficiency of 99.7±0.6 % was achieved, although this test was not run for the full three hours due to a high amount of overload errors. While this result is interesting, at more moderate doses of 500 ppm polymer and 100 ppm synergist, BTG and TGA exhibited similar efficiencies of 93.1±1.1 % and 92.2±1.6 %, respectively. The structures of BTG and TGA are also similar, where both compounds contain both a thiol and carboxylic acid functional groups. BTG additionally has a four-member hydrocarbon tail which TGA lacks. A possible reason for this synergistic effect could be by adsorption of thiol to iron in the steel surface through complex formation, and formation of amide by a reaction of amine in DBAPA to the carboxylic acid in TGA or the ether in BTG. By itself, BTG was also found to be an effective CI, as presented in Figure 4.4, which could be explained by the hydrocarbon tail aiding in the formation of a hydrophobic layer on the metal surface. This effectivity also supports the idea of adsorption to steel through thiol, although this is only speculation. While BTG was found to be an efficient CI by itself, the efficiency was similar at 100 and 1000 ppm as with 100 ppm in addition to 500 ppm polymer. Although, as this specific test was conducted by testing 100 ppm for one hour before an additional 900 ppm was injected. Different results might be experienced by injecting 1000 ppm from the initial addition.

At doses of 500 ppm polymer and 100 ppm synergist, both ATC and GTC exhibited the highest efficiencies at 96.0±1.5 % and 96.0±1.4 %, respectively. As there is no significant different in the two results, it seems likely that the guanidinium ion of GTC has little or no effect, and that the synergistic effect is likely due to the introduction of thiocyanate which is present it both compounds. It seems likely that the synergistic effect from thiocyanate could be due to the formation of a complex to bridge the polymer and the iron in the steel surface. Although more research would be needed to precisely determine the mechanism in action. TBA contains two secondary amines and a sulfur group in a heterocyclic structure with two additional carbonyl groups. At the same dose of 500 ppm polymer and 100 ppm synergist, TBA exhibited an efficiency of 94.1±3.2 %. The synergistic effect of TBA is not precisely known, but it seems likely that the sulfur and/or amine groups could adsorb to the steel surface, and the carbonyl groups could be reacting to binding sites in PMA:VCap-DBAPA.

The final synergists IBT, AMT and BID all exhibited antagonistic effects to the polymer, with efficiencies of 8.2±1.5 %, 1.7±3.5 % and -30.92±3.6 % respectively. It seems likely that the three compounds could be competing with the polymer for bonding sites onto the metal, as they all contain several amine- and/or thiol functional groups. The functional groups in these three compounds are all within heterocyclic rings, which could be a reason for steric hinderance and possibly why no synergistic effect was observed.

In comparison to PMA:VCap-DBAPA, the amine oxide version PMA:VCap-DBAPA-AO exhibited an efficiency of 16.3±1.6 %, where the difference between the two is within the margin of error, although the amine oxide version seemed slightly easier to dissolve in water. While the corrosion inhibition efficiency of PMA:VCap-(DBAPA:AMT 80:20) was measured to be 97.7±1.1 %, the polymer was found to be mostly insoluble. Therefore, it seems likely that this high efficiency is caused by the insoluble part attaching onto the metal and creating a physical barrier to the brine. PMA:VCap-(DBAPA:GLYP 80:20) was tested at different concentrations, ranging from 500 to 2500 ppm, with the addition of 1000 ppm TBA

for the final test. By itself PMA:VCap-(DBAPA:GLYP 80:20) exhibited poor protection at all concentrations at a proportional linear relationship. The corrosion inhibition efficiency was measured to be -75.8 ±1.9 % at 2500 ppm and increased to 75.0±2.0 % by the introduction of 1000 ppm TBA. Glyphosate is by itself quite acidic and a corrosive compound, which is probably the cause of the increased corrosion rate experienced during testing. As previously described, TBA was found to be an efficient synergist with PMA:VCap-DBAPA, it seems likely that the increased efficiency here is due to the same mechanism as without the presence of glyphosate.
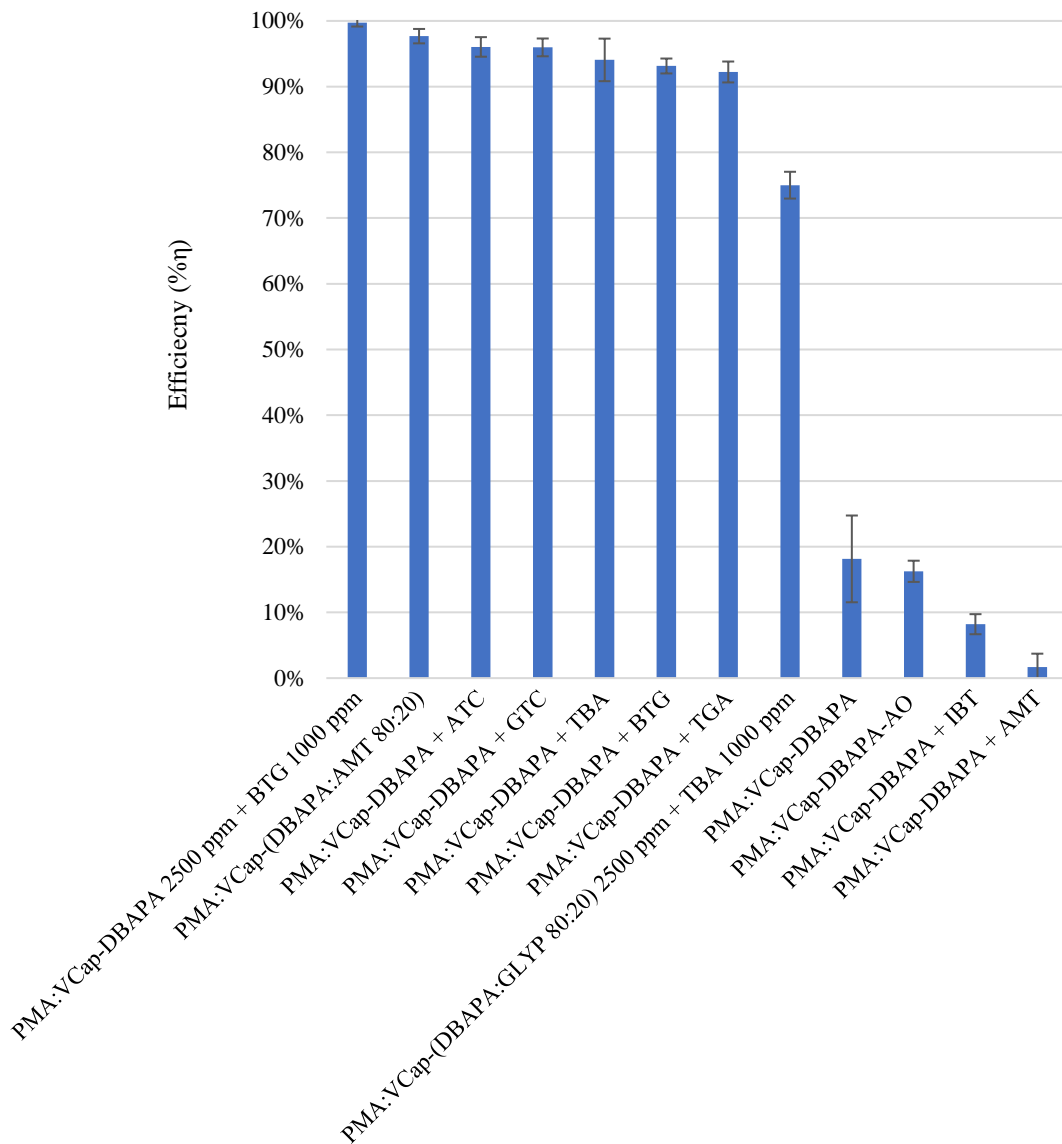
Figure 4.3 Corrosion efficiency summary for polymer and synergists.
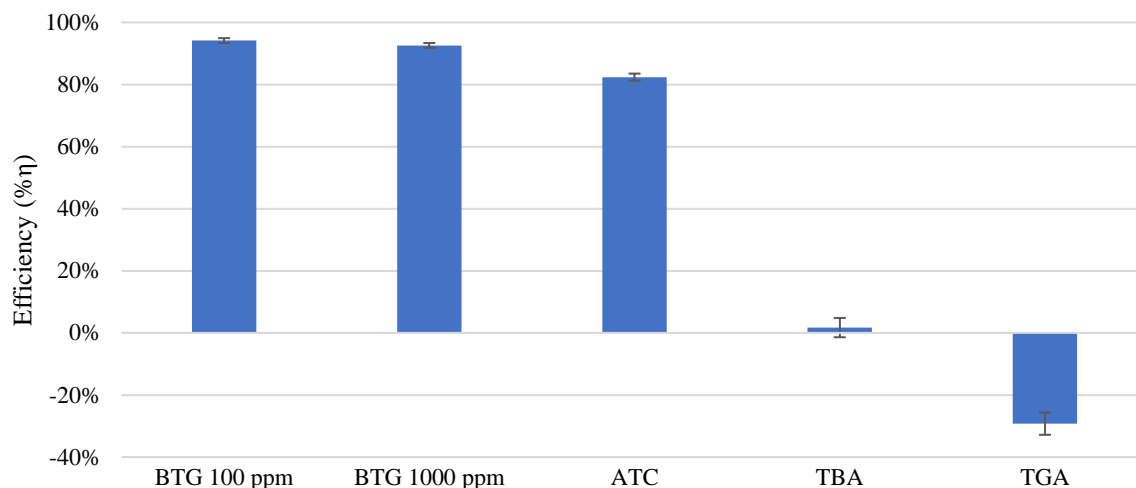
Figure 4.4 Corrosion efficiency summary for synergists.

4.4. Conclusion

The polymers PMA:VCap-DBAPA, PMA:VCap-DBAPA-AO, PMA:VCap-(DBAPA:GLYP 80:20), and PMA:VCap-(DBAPA:AMT 80:20) was tested with the optimized corrosion method described in chapter 2.2. In addition, PMA:VCap-DBAPA, was tested with a selection of synergists in which we were able to achieve a corrosion inhibition efficiency of above 90 % with ATC, GTC, TBA, BTG and TGA. The best result at 500 ppm polymer and 100 ppm synergist was found to be PMA:VCap-DBAPA + ATC which exhibited an efficiency of 96.0±1.5 %. Overall, synergists with thiol functional groups seems to generally provide good synergism with PMA:VCap-DBAPA. While synergists with functional groups embedded within a ring structure generally provides poor synergism with PMA:VCap-DBAPA.

5. Poly(1-oxy-3-lactam vinylene)

The poly(1-oxy-3-lactam vinylene) is of interest as it can be fitted with ring structures which typically exhibit good kinetic gas hydrate inhibition efficiency. In this chapter the synthesis of various poly(1-oxy-3-lactam vinylene) compounds is described, and their functionality as multi-functional inhibitors explored.

5.1. Introduction

As discussed in chapter 1.5, it should be possible to synthesise a multi-functional polymer with abilities to inhibit scale, corrosion, and gas hydrates. Poly(1-oxy-3-lactam vinylene) is an interesting approach, as it can be fitted with caprolactam and piperidone, forming polyoxyvinylcaprolactam (POVCap) and polyoxyvinylpiperidone (POVPip) respectively, as given in Figure 5.1, which shares some similarities to common KHI polymers. Specifically, caprolactam rings are known to attach to hydrate crystal structures (Kelland, 2006, p. 839). The idea for this project is that if POVCap or POVPip works as a kinetic gas hydrate inhibitor (KHI), then the double bond can be opened and fitted with functional groups or copolymerised with effective CI and SI monomers.
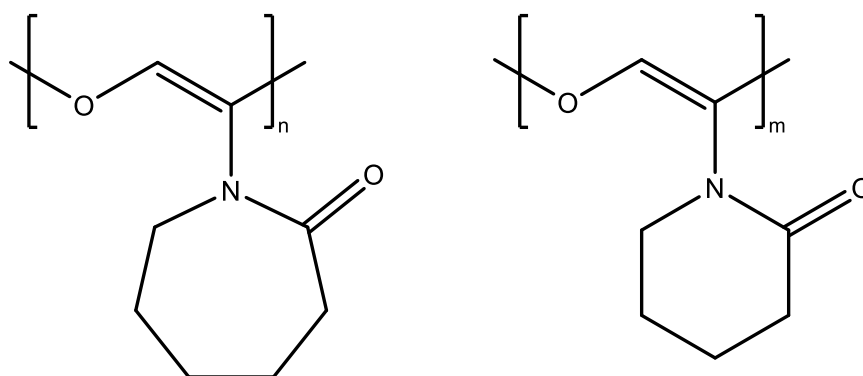
Figure 5.1 Structure of polyoxyvinylcaprolactam (POVCap) (left) and polyoxyvinylpiperidone (POVPip) (right).

It is well known that adding certain solvents may act as synergists to polyvinylcaprolactam (PVCap), and it has been shown that some of these synergists also work with other caprolactam containing polymers, although some may be antagonistic (Dirdal & Kelland, 2022, pp. 3115–3116). Therefore, it was of interest to test some of these synergists with copolymers containing POVCap to investigate if a similar synergism can be achieved.

5.2. Materials and methods

Iso-butyl glycol ether (iBGE) was obtained from VWR. 2,4,7,9-Tetramethyl-5-decyne-4,7-diol (TDD) was obtained from VWR. 2-Piperidone was obtained from Tokyo Chemical Industry (TCI). 2-Pyrrolidone was obtained from Merck. 4-Methyl-1-pentanol (MPO) was obtained from TCI. Anhydrous magnesium sulfate was obtained from Merck. Anhydrous potassium carbonate was obtained from VWR. Azobisisobutyronitrile (AIBN) was obtained from Sigma-Aldrich. Chloroacetyl chloride was obtained from Sigma-Aldrich. Chloroform was obtained from VWR. Deuterated chloroform was obtained from Cambridge Isotope Laboratories. Dichloromethane was obtained from Sigma-Aldrich. Hexabutylguanidinium chloride (HBGC) was synthesised at UiS. Iodine monochloride (ICI) was obtained from Thermo Scientific. Luvicap 55W (1:1 Vinylpyrrolidone:vinylcaprolactam copolymer

(VP:VCap)) was obtained from BASF, Germany. Luvicap EG (Polyvinylcaprolactam (PVCap)) was obtained from BASF, Germany. N,N-Dimethylhydrazine (DMH) was obtained from Sigma-Aldrich. Tetrapentylammonium bromide (TPAB) was obtained from VWR. Thioglycolic acid (TGA) was obtained from Sigma-Aldrich. Toluene was obtained from VWR. Tributyl amine oxide in i-PrOH (TAO) was synthesised at UiS. Tri-n-pentylamine oxide (TPeAO) was synthesised at UiS by Dr. Radhakanta Ghosh. ε-Caprolactam was obtained from Merck. All compounds were used directly without further purification.

A Bruker Ascend NMR 400 MHz spectrometer was used to record nuclear magnetic resonance (NMR) spectrum in deuterated chloroform. Gel permeation chromatography (GPC) was conducted by Prof. Hiroharu Ajiro at NAIST, Japan. OECD306 seawater test for biodegradability was conducted by Hong Lin, with the method as described by (Mady et al., 2019, p. 6201). By using the OxiTop Control manometric system (WTW, Germany) the biological oxygen demand (BOD) was measured over a period of 28 days. The measured BOD was compared with the calculated theoretical oxygen demand (ThOD) values to calculate the %-biodegradability. Sodium benzoate was used as a positive control at 100 ppm, as this is a known readily biodegradable compound. Corrosion testing was carried out as described in in chapter 2.2.10. Where baseline corrosion rate was measured with a five-minute delay for two hours before addition of the inhibitor, which was then measured with a five-minute delay for a period of three-hours. The mild C1018 steel coupons used for corrosion testing was obtained from European Corrosion Supplies. The cloud point was found by heating a solution of dissolved polymer at 2500 ppm to >80 ℃ and noting the temperature when the solution became cloudy.

KHI testing was conducted by Dr. Radhakanta Ghosh and Erik Dirdal, using a rocking cell rig with synthetic natural gas (SNG), as described by (Kelland et al., 2021, p. 6). With this SNG mixture, as given in Table 5.1, sII hydrates are formed as the preferred thermodynamically stable phase. The 40 ml steel cells were filled with 20 ml solution at a polymer concentration of 2500 ppm polymer. The cells were initially flushed to displace air prior to pressurization with SNG at 76 bars. Cooling was then initiated from 20.5 to 2 ℃ at a rate of 1 ℃/h while cells were rocking. The slow constant cooling test method was used. Onset of hydrate formation was taken to be at the first sign of decrease in pressure not caused by a decrease in temperature. The temperature at this pressure decrease was denoted as To, and the temperature when hydrate formation was at its most rapid was denoted as Ta. Some indication of the polymers ability to inhibit crystal growth can be given by the value To-Ta.

Table 5.1 Synthetic natural gas mixture.

Component	Mol %
Methane	80.40
Ethane	10.30
Propane	5.00
Isobutane	1.65
n-butane	0.72
CO_2	1.82
N_2	0.11

5.3. Synthesis

The synthesis of poly(1-oxy-3-lactam vinylenes) was based on the patent by Mathias & Moore (1987). ε-Caprolactam and chloroacetyl chloride was mixed in a mole ratio of 2:1.126

in toluene under nitrogen in ice bath. The solution was allowed to come slowly to room temperature over one hour and left to react for 24 hours. The solution containing caprolactam hydrochloride was filtered, and toluene evaporated off. This gave 1-(2-chloroacetyl) caprolactam at a yield of 85 %. The same method was used to prepare 1-(2-chloroacetyl) pyrrolidone and 1-(2-chloroacetyl) piperidone.

Polymerization of the monomers was done by adding a given amount of monomer into a Schlenk flask which was heated in an oil bath at 100 °C for four hours under 20 mbar vacuum. The resulting polymer was used directly without further purification. The same method was used to polymerize copolymers of polyoxyvinylcaprolactam (POVCap) and polyoxyvinylpiperidone (POVPip). The cloud point for POVPip was found to be >80 °C.^{1}H NMR spectrum for POVCap is presented in Figure G-1 in Appendix G. ^{1}H NMR spectrum for POVPip is presented in Figure G-2 in Appendix G. ^{1}H NMR spectrum for copolymer OVPip:OVCap 60:40 is presented in Figure H-1 in Appendix H. ^{1}H NMR spectrum for copolymer OVPip:OVCap 62:38 is presented in Figure H-2 in Appendix H. Proposed synthesis steps for POVCap are presented in Figure 5.2.
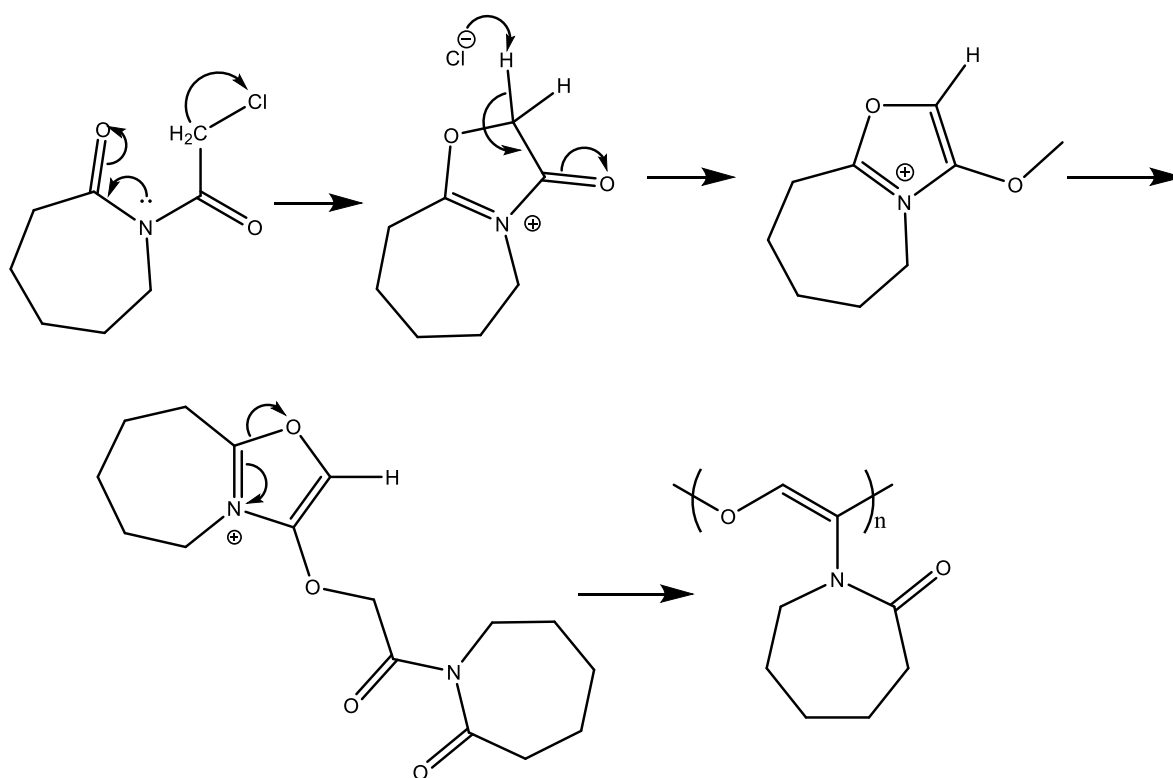
Figure 5.2 Synthesis of polyoxyvinylcaprolactam, adapted from (Mathias & Moore, 1987, p. 2).

In an attempt to make POVCap water soluble, POVCap (500 mg, 2.637 mmol) and AIBN (15 mg, 0.091 mmol) was dissolved in 10 ml i-PrOH together with TGA (243 mg, 2.647 mmol) under nitrogen, and heated for 24 hours at 60 °C. The final product was a highly viscous yellow liquid, which was insoluble in water. In another attempt to make POVCap water soluble, POVCap (970 mg, 5.115 mmol) was dissolved in dichloromethane under nitrogen. A 0.2 M ICl (830 mg, 5.115 mmol) solution in dichloromethane was added dropwise until colour remained consistent. The solution was left in darkness to react for two hours. The intermediate had precipitated and attached to the flask walls. The solution was decanted off,

and the intermediate was rinsed with dichloromethane. The intermediate (31 mg, 0.090 mmol) was further dissolved in chloroform, and DMH (11 mg, 0.180 mmol) was added at a 1:2 mole ratio until the colour dissipated. The solvent was then evaporated off and the final product collected, which was insoluble in water. There was also an attempt where the intermediate (30 mg, 0.087 mmol) was added to an aqueous NaOH (3 mg, 0.087 mmol) solution and left to react for 24 hours at room temperature. The solvent was evaporated off and the product collected, which was insoluble in water. The same reaction was repeated where the intermediate (400 mg, 1.157 mmol) was added to an aqueous 0.1 M NaOH solution. The NaOH solution was incrementally added over the course of 48 hours at room temperature, until a mole ratio of 1:2 intermediate to NaOH (93 mg, 2.315 mmol) was reached, While the product was found to be water soluble, NMR results suggested that the polymer had monomerised.

5.4. Results and Discussion

Copolymers of POVCap and POVPip was synthesised and tested as CI, KHI, and biodegradability. In this subchapter these results will be presented. The biodegradability of the OVPip:OVCap 1:1 copolymer was tested. The resulting BOD28 values from this test are presented in Table 5.2. OVPip:OVCap 1:1 exhibits a biodegradation of 8.63 ± 1.78 % for N into NH_4, 7.24 ± 1.5 % for N into NO_2 and 6.87 ± 1.42 % N into NO_3. In comparison sodium benzoate exhibited a BOD28 of 79.44 ± 1.44 % for all three tests. The low biodegradation is likely due to the lack of easily cleavable groups in the polymer backbone.

Table 5.2 Biodegradability results.

Compound	% Biodegradability (± %SE)		
	N into NH_4	N into NO_2	N into NO_3
Sodium benzoate	79.44 ± 1.44 %	79.44 ± 1.44 %	79.44 ± 1.44 %
OVPip:OVCap 1:1	8.63 ± 1.78 %	7.24 ± 1.5 %	6.87 ± 1.42 %

Samples for a selection of the polymers and copolymers was shipped to Japan for gel permeation chromatography (GPC) testing, of which the results are presented in Figure 5.3. POVPip by itself exhibited a number average molecular weight (M_n) of 1000 g/mol. From the graph a trend of increasing M_n can be seen in correlation with increasing POVCap content. In contrast to POVPip, POVCap by itself exhibited a number average molecular weight (M_n) of 2700 g/mol. While the M_n of the tested copolymers does not follow a perfect linear trend, the deviation could be due to a small sample size or inhomogeneous polymerisation of the copolymers.
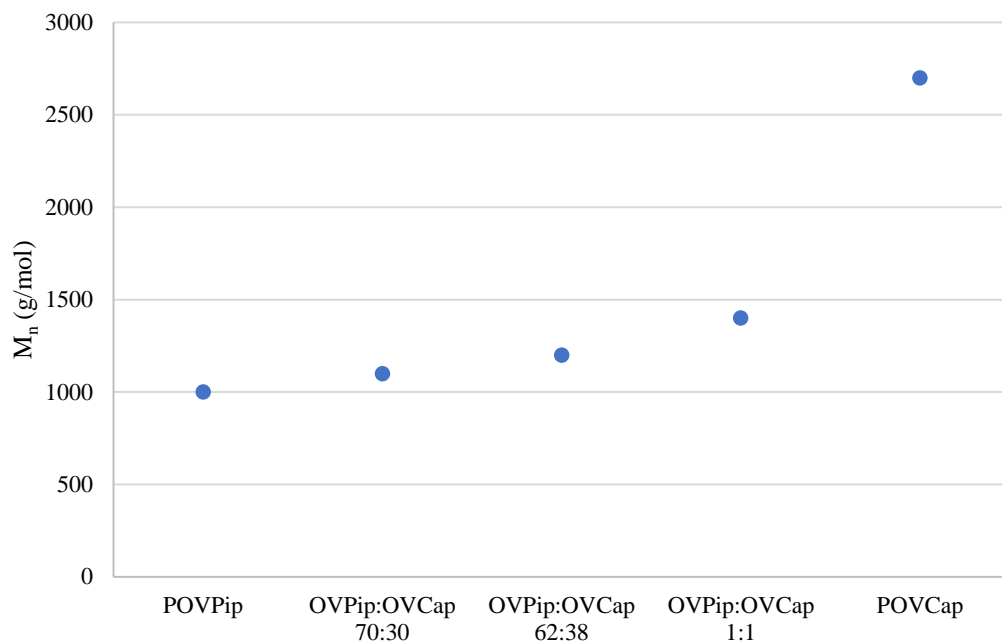
Figure 5.3 GPC results in THF with polymethyl methacrylate (PMMA) standards.

The OVPip:OVCap 60:40 copolymer and pure POVPip was tested as CIs, of which the results are presented in Table C-1 in Appendix C. OVPip:OVCap 60:40 was found to exhibit an efficiency of 22.6±1.5 %. As the copolymer was somewhat slow to dissolve, it was left for 24h before the test was repeated, this time the efficiency was found to be 74.4±1.6 %, but this is assumed to be because of the insoluble part attaching to the metal. Later tests with only POVPip also confirms that the efficiency is low at 15.4±3.6 %. The addition of POVCap which by itself is insoluble in water and does not contain additional functional groups different from the POVPip which could aid adsorption. Therefore, it seems likely that the heightened efficiency is caused by insoluble parts attaching onto the metal. The copolymer of POVCap and POVPip shares many similarities with the VP:VCap 1:1 copolymer in its single amine group and ring structures of different sizes. In comparison to the efficiency of the VP:VCap 1:1 copolymer which was found to be 37.3±4.1 % as discussed in chapter 3, the results for both the copolymer and POVPip are remarkably low. Assuming that the product is pure, the difference except for the ring sizes is the addition of an ether and a C=C double bond in the polymer backbone. Thus, it seems likely that the additional electronegativity of the ether is either affecting the polarity of the backbone and the hydrophilic-lipophilic balance (HLB) of the polymer. The oxygen may also be adsorbing to the steel causing the polymer to lie somewhat flat on the surface without forming a hydrophobic film.

The KHI results of the range of copolymers that was synthesised and tested in this chapter are summarised in Table E-1 in Appendix D. With only DIW To_{Avg} was found to be 17.3±0.4 ℃, and Ta_{Avg} was found to be 17.1±0.3 ℃. By addition of PVCap and VP:VCap copolymer the To_{Avg} was reduced to 9.0±0.1 ℃ and 7.1±0.2 ℃, respectively, and the Ta_{Avg} was reduced to 7.9±0.1 ℃, and 5.9±0.2 ℃, respectively. These results mark an upper and lower limit for where the experimental copolymers are expected to lie within.

Similar to POVCap, copolymers with >50 % POVCap was also found to be insoluble in water, and therefore not tested as KHI. Copolymers ranging from 50 to 0 % POVCap are presented in Figure 5.4, sorted by POVPip content. With POVPip content of 50, 60 and 62 %,

the onset temperature To_{Avg} are quite similar of 13.3±0.2 ℃, 13.7±0.4 ℃, and 13.0±0.2 ℃, respectively. By introducing a 2 %-point increase in POVPip concentration, the POVCap (36 %) + POVPip (64 %) copolymer showed the lowest To_{Avg} of the test at 11.6±0.1 ℃. While the To_{Avg} remains at 12.1±0.1 and 12.2±0.2 ℃ for the copolymers with 70 and 74 % POVPip content, respectively. The To_{Avg} reached 13.9±0.2 ℃ at POVPip content of both 83 and 100 %. From these results it seems likely that at POVPip content <64 % the reduced efficiency could be caused by the somewhat lowered solubility, and at >83 %, the caprolactam content is probably too low to efficiently anchor into the growing crystal matrix inhibiting further growth.
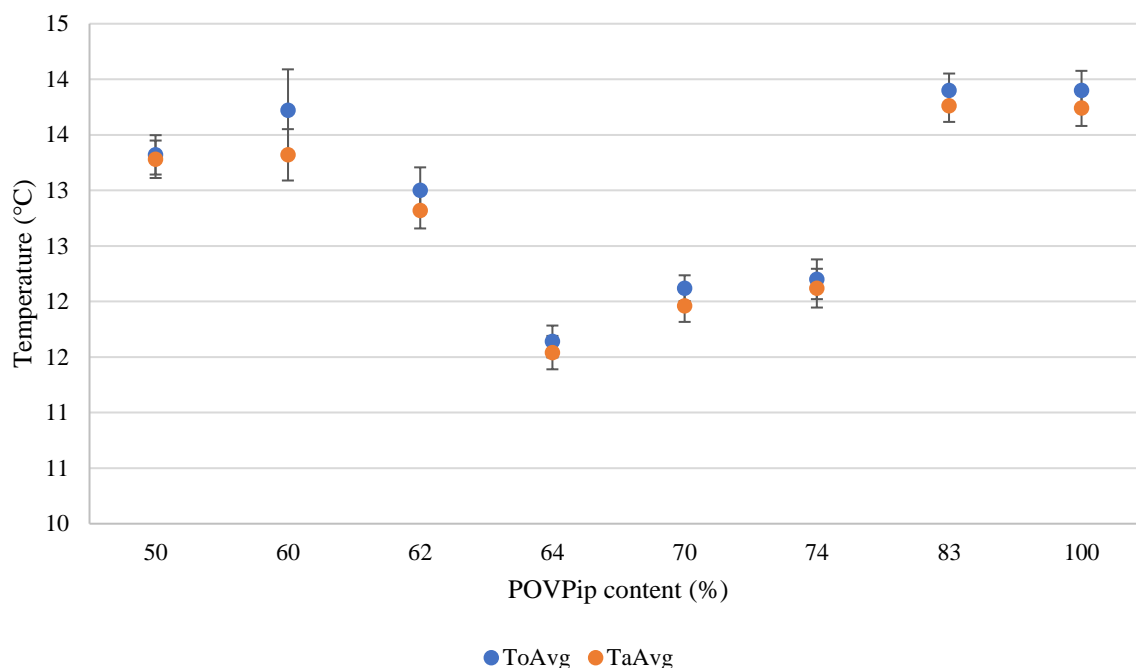
Figure 5.4 To/Ta KHI results for copolymers at 2500 ppm, sorted by POVPip content.

While the OVPip:OVCap 64:36 copolymer would have been the obvious choice for synergist testing as it exhibited the lowest To_{Avg}, logistical problems ensured that there was not enough precursor for additional synthesis within the time limit. Synergist testing was therefore carried out on the OVPip:OVCap 62:38 copolymer which was previously synthesised in sufficient amounts. The complete KHI results are graphically presented in Figure F-1 in Appendix F.

The addition of MPO showed a severe antagonistic effect and resulted in a To_{Avg} of 16.3±0.1 ℃, which is nearly the same level as DIW, although, the Ta_{Avg} for MPO was found to be 12.7±0.1 ℃, giving MPO a To_{Avg}-Ta_{Avg} value of 3.6. The addition of iBGE also exhibited a high To_{Avg}, which was 15.4±0.2 ℃, although its Ta_{Avg} value can be considered identical at 15.3±0.1 ℃. Similar results were also found with TDD which yielded a To_{Avg} of 15.0±0.2 ℃ and Ta_{Avg} of 14.8±0.2 ℃. The introduction of HBGC, while yielding a To_{Avg} of 14.8±0.1 ℃, its Ta_{Avg} was among the lowest of the test at 9.6±0.5 ℃, giving HBGC a To_{Avg}-Ta_{Avg} value of 5.2. Introduction of TAO exhibited a To_{Avg} of 14.3±0.2 ℃ and a Ta_{Avg} of 11.8±0.2 ℃, giving a To_{Avg}-Ta_{Avg} value of 2.5. Only two synergists gave a lower To_{Avg} value than pure POVPip, these are TPAB and TPeAO. TPAB exhibited a To_{Avg} of 13.7±0.1 ℃ and a Ta_{Avg} of 12.4±0.1 ℃. While TPeAO exhibited To_{Avg} of 12.3±0.2 ℃ and Ta_{Avg} of 11.2±0.1 ℃, making it the

only synergist which outperformed the OVPip:OVCap 62:38 copolymer by itself, albeit only slightly. Precisely why these compounds do not provide good synergism with the copolymer is unknown, but it seems clear that there is more to the synergistic effect than just having caprolactam rings. Perhaps the additional of ether, C=C double bonds or the piperidone ring structure has an effect.

The OVPip:OVCap 62:38 copolymer was also tested at different concentrations of 1000, 2500 and 5000 ppm, as given in Figure 5.5. At 1000 ppm the copolymer exhibited a To_{Avg} of 14.4±0.1 ℃ and a Ta_{Avg} of 14.2±0.1 ℃, giving a To_{Avg}-Ta_{Avg} value of 0.1. Increasing the concentration to 2500 ppm exhibited a To_{Avg} of 13.0±0.2 ℃ and a Ta_{Avg} of 12.8±0.2 ℃, giving a To_{Avg}-Ta_{Avg} value of 0.2. Finally, at the highest concentration of 5000 ppm, the copolymer exhibited a To_{Avg} of 11.5±0.2 ℃ and a Ta_{Avg} of 11.3±0.2 ℃, giving a To_{Avg}-Ta_{Avg} value of 0.1. These results indicate a linear relationship where a higher dose increases the hydrate inhibition. This trend is likely correlated to the increased availibility of caprolactam rings to anchor into the growing crystal matrix. Although, it must be noted that the 5000-ppm result given here is equal to that of OVPip:OVCap 64:36 at 2500 ppm, whch is likely due to the differences in solubility between the two copolymers.
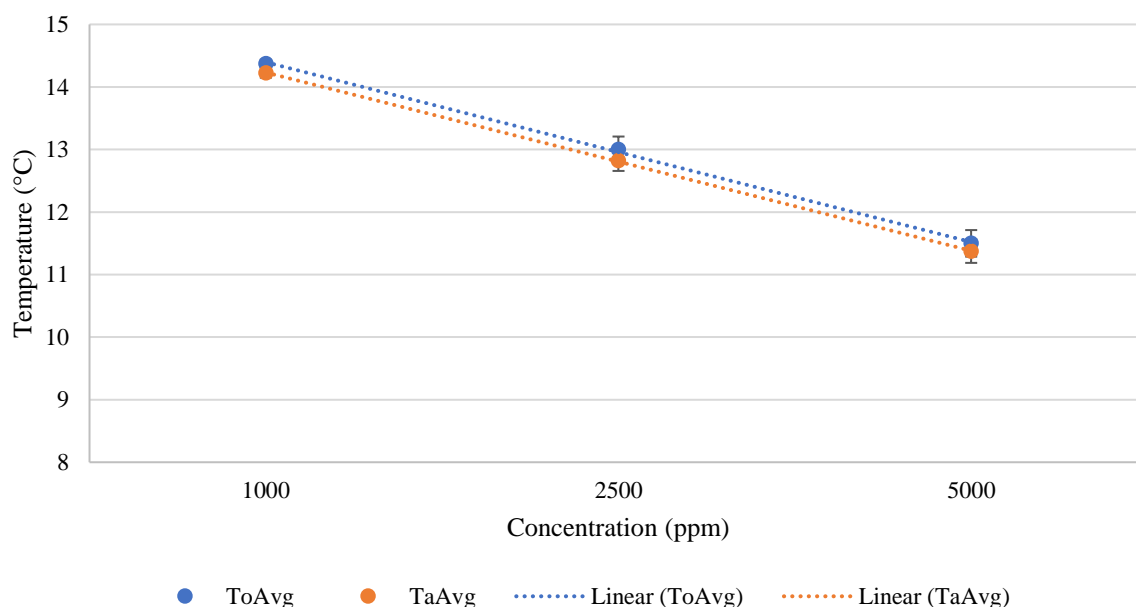
Figure 5.5 KHI concentration test OVPip:OVCap 62:38.

5.5. Conclusion

Synthesis of POVCap and POVPip was successful, while polymerisation of 1-(2-chloroacetyl) pyrrolidone was unsuccessful. It was found that POVCap is insoluble in water, while POVPip is soluble in water. A range of copolymers of POVCap and POVPip was synthesised and tested as a KHI. It was found that the OVPip:OVCap 64:36 copolymer exhibited a hydrate onset temperature of 11.6±0.1 ℃, although the CI results were subpar with an efficiency of 15.4±3.6 % for pure POVPip. None of the synergists tested managed to achieve a similar synergism as with other caprolactam containing KHI polymers.

6. Hyperbranched Polyamine Containing Imidazolidine Rings

In this chapter, the synthesis of hyperbranched polyamine containing imidazolidine rings will be presented and discussed.

6.1. Introduction

Based on the knowledge regarding functional groups from chapter 1.2 and 3, hyperbranched polyamine containing imidazolidine rings was an interesting approach in its many amine groups and ring structures, which are given in Figure 6.1.
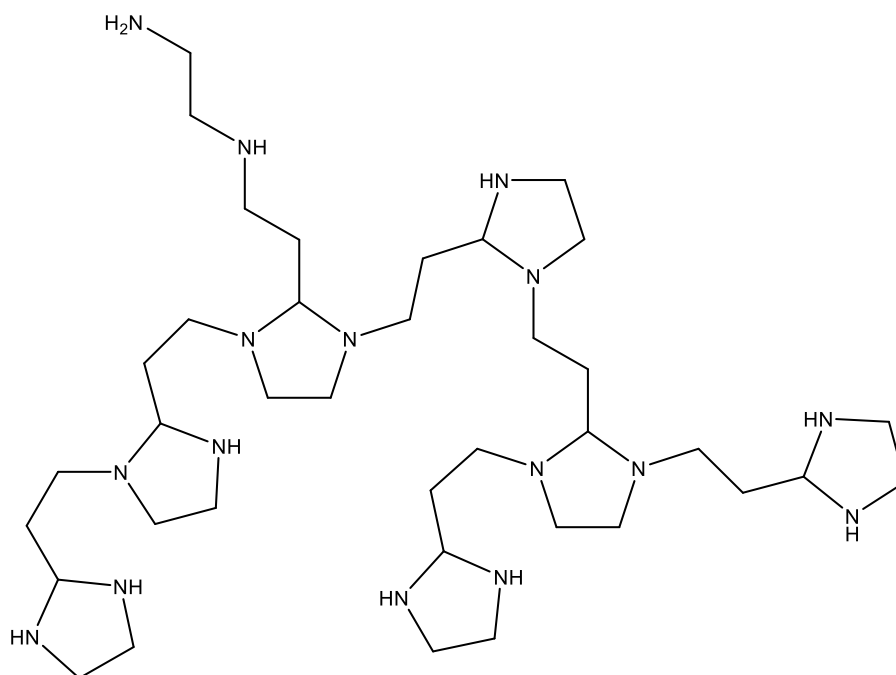
Figure 6.1 Structure of hyperbranched polyamine containing imidazolidine rings, adapted from (Liu et al., 2007, p. 703).

6.2. Materials and Methods

Acrolein diethyl acetal was obtained from Tokyo Chemical Industry (TCI). Ethylenediamine was obtained from Sigma-Aldrich. Diethyl ether was obtained from VWR. Dichloromethane was obtained from Sigma-Aldrich. Chloroform was obtained from VWR. Anhydrous potassium carbonate was obtained from VWR. 1-Bromobutane was obtained from Merck. Hydrogen peroxide was obtained from VWR. Isobutyronitrile (i-PrCN) was obtained from Merck All compounds were used directly without further purification. Deuterated chloroform was obtained from Cambridge Isotope Laboratories. A Bruker Ascend NMR 400 MHz spectrometer was used to record nuclear magnetic resonance (NMR) spectrum in deuterated chloroform.

6.3. Synthesis

The synthesis of hyperbranched polyamine containing imidazolidine rings was based on Liu et al. (2007) where acrolein diethyl acetal (6.50 g, 0.050 mol), was added dropwise to a stirred solution of ethylenediamine (3.00 g, 0.050 mol) at a mole ratio of 1:1, in 25 ml chloroform at room temperature. An excess amount of anhydrous magnesium sulfate (7.00 g, 0.058 mol) was added to remove water that formed during the reaction. The solution was left to react for 24h, as the acrolein diethyl acetal was assumed to be less reactive than pure

acrolein, and magnesium as filtered from the reactant. Precipitation of the product in diethyl ether as described by (Liu et al., 2007) was unsuccessful. Although a layer of white and yellow precipitate was found to slowly form on the inside of the flask. The precipitate was collected and weighed at 1.084 g, which corresponds to a yield of 3 %, assuming that this is product.

The above synthesis was repeated with dichloromethane as solvent, rather than chloroform. The attempts to precipitate the product from chloroform was also attempted on the dichloromethane solution without any solid formation. The last attempt was to reflux the synthesis solution at 65 °C for 24h, rather than letting the product form at room temperature. Similar attempts at precipitation were conducted on the refluxed chloroform solution without any meaningful results.

In an effort to see if there was anything worthwhile in the product, the precipitate (150 mg, 0.201 mmol), 1-bromobutane (743 mg, 5.420 mmol) and anhydrous potassium carbonate (33 mg, 0.239 mmol) was dissolved in 10 ml i-PrCN in an RBF and refluxed under nitrogen at 117.8 °C for 53h. The solution was filtered, and i-PrCN was evaporated off until only a highly viscous fluid remained. This product was dissolved in 10 ml i-PrOH and reacted with a slight excess of H_2O_2 (190 mg, 5.583 mmol) for and left to react for 24h. The solvent was evaporated off, and NMR taken of the product, which indicated that the reaction was unsuccessful.

By introducing an excess amount of diethyl ether before evaporation of solvent, a small amount of highly viscous fluid was found to remain. Although, the NMR results from this product was not similar as to the NMR results reported by Liu et al. (2007). Heating the diethyl ether to its boiling point prior to introduction of the chloroform solution was also attempted, but this did not yield any different results from the room temperature diethyl ether. In another attempt, the chloroform was left in room temperature for several days to slowly evaporate, this left a white solid on the internal surface of the flask. The NMR results from this product was also not similar to the reported NMR spectrum. A final attempt was to leave the chloroform and diethyl ether solution in sub-zero conditions over several days prior to evaporation of the solvent, but this did not yield any different results.

6.4. Conclusion
Several attempts at synthesising the hyperbranched polyamine containing imidazolidine rings were performed, although none proved successful. It seems likely that the acrolein diethyl acetal either did not react or that the product followed the vapor phase during evaporation of solvent.

7. Financial Overview

A financial overview of the estimated chemicals consumed through the work of this thesis may be found in Table 7.1, and materials consumed in Table 7.2. The CO_2 consumption is unknown, but with the amount of corrosion testing completed in this work the consumption can be assumed to be of a substantial amount. The consumption of synthetic natural gas was approximated by (E. G. Dirdal, personal communication, 2 June 2022).

Table 7.1 Approximation of consumed chemicals.

Compound	Amount consumed		
	mg	ml	m^3
Ammonium thiocyanate	90		
Dichloromethane		500	
1-Bromobutane	850		
2,4,7,9-Tetramethyl-5-decyne-4,7-diol	210		
2-Amino-5-mercapto-1,3,4-thiadiazole	95		
2-Piperidone	25000		
2-Propanol	900		
3-Acetamidotetrahydro-2-thiophenone	15		
4,5-Dihydro-1H-imidazole	500		
4,6-Dihydroxy-2-mercaptopyrimidine	245		
4-Methyl-1-pentanol	210		
Acetic acid	25		
Acrolein diethyl acetal		50	
Anhydrous magnesium sulfate	25000		
Anhydrous potassium carbonate	40		
Butyl thioglycolate	315		
Chloroacetyl chloride		50	
Chloroform		300	
Carbon dioxide			Unknown
Deuterium oxide		5	
Deionized water		200000	
Deuterated chloroform	20		
Diethyl ether		500	
Ethylenediamine		15	
Guanidine thiocyanate	15		
Hydrochloric acid 37.5 %		1500	
Hexabutylguanidinium chloride	210		
Hydrogen peroxide 30 %		50	
Iodine monochloride		10	
Iso-butyl glycol ether	210		
Isobutyronitrile		150	
Luvicap 55W	75		
Mercaptosuccinic acid	90		
N,N-Dimethylhydrazine		0.5	
Nitrogen			0.02
Sodium chloride brine 3.5 %		30000	

Table 7.1 (continued) Approximation of consumed chemicals.

Compound	Amount consumed		
	mg	ml	m^3
Sodium hydroxide	120000		
PMA:VCap-DBAPA and derivates	2500		
PMA-DBAPA and derivates	225		
Poly(ethylene glycol)	75		
Polyacrylamide	75		
Polylysine	75		
Pyrrolidone	2.5		
Sodium lignosulfonate	165		
Sodium thiosulfate	15		
Styrene sulfonic acid	15		
Synthetic natural gas			0.12
Tetrapentylammonium bromide	210		
Thioglycolic acid	115		
Toluene		400	
Tributyl amine oxide in i-PrOH	210		
Tri-n-pentylamine oxide	210		

Table 7.2 Approximation of consumed items.

Item	Amount consumed
C1018 steel coupon	380
Centrifugal tube	5
Needle 100 mm	70
Needle 50 mm	40
Nitrile gloves L	3000
Pasteur pipette 125 mm	120
Pasteur pipette 225 mm	60
Pipette tips 0.1 ml	15
Pipette tips 1 ml	50
Pipette tips 5 ml	100
Syringe 1 ml	30
Syringe 12 ml	20
Syringe 5 ml	60

8. Environmental Accounts

Through the work of this thesis, many hours have been spent on corrosion testing and synthesis. An overview of the approximate operational hours may be found in Table 8.1. While the power requirement for each equipment is unknown, the overall electricity consumption has likely been quite high, as a high amount of work has been completed. In addition to the power consumption by this equipment, there has been electricity consumption by the production of approximately ice (10 l), and deionized water (200 l). In addition, and a small amount of polymer samples was sent to Japan for gel permeation chromatography testing. There is also electricity consumption associated with the consumed chemicals as described in chapter 7, although the precise amount is unknown.

While the chemicals used for corrosion testing cannot be recycled due to impurities. The waste from the completion of a test was always collected and disposed of as organic waste according to the rules of the laboratory. As some of these compounds pose environmental toxicity and low biodegradability, it was paramount to not let any of these compounds into the sewer system.

Table 8.1 Approximate operational hours.

Equipment	Hours
Bruker Ascend NMR 400 MHz spectrometer	10
Computer + potentiostat	1200
Rotary evaporator	65
Branson 2510 Ultrasonic Cleaner	50
Magnetic stirrer	1400
Hot plate for oil bath	100

9. References

Abbasov, V. M., Abd El-Lateef, H. M., Aliyeva, L. I., Qasimov, E. E., Ismayilov, I. T., & Khalaf, M. M. (2013). *A Study of the Corrosion Inhibition of Mild Steel C1018 in CO₂-Saturated Brine Using Some Novel Surfactants Based on Corn Oil.* https://doi.org/10.1016/j.ejpe.2013.11.002

Ali Fathima Sabirneeza, A., Geethanjali, R., & Subhashini, S. (2015). Polymeric Corrosion Inhibitors for Iron and Its Alloys: A Review. *Chemical Engineering Communications*, *202*(2), 232–244. https://doi.org/10.1080/00986445.2014.934448

Al-Shihry, S. S., Sayed, A. R., & Abd El-Lateef, H. M. (2020). Design and Assessment of a Novel Poly(urethane-semicarbazides) Containing Thiadiazoles on the Backbone of the Polymers as Inhibitors for Steel Pipelines Corrosion in CO₂-saturated Oilfield Water. *Journal of Molecular Structure*, *1201*, 127223. https://doi.org/10.1016/j.molstruc.2019.127223

Askari, M., Aliofkhazraei, M., Ghaffari, S., & Hajizadeh, A. (2018). Film Former Corrosion Inhibitors for Oil and Gas Pipelines—A Technical Review. *Journal of Natural Gas Science and Engineering*, *58*, 92–114. https://doi.org/10.1016/j.jngse.2018.07.025

Bajpai, D., & Tyagi, V. K. (2006). Fatty Imidazolines: Chemistry, Synthesis, Properties and Their Industrial Applications. *Journal of Oleo Science*, *55*(7), 319–329. https://doi.org/10.5650/jos.55.319

Belton, G. R. (1976). Langmuir Adsorption, the Gibbs Adsorption Isotherm, and Interfacial Kinetics in Liquid Metal Systems. *Metallurgical and Materials Transactions B*, *7B*, 35–42. https://doi.org/10.1007/BF02652817

Chilingar, G. V., Mourhatch, R., & Al-Qahtani, G. (2008). CHAPTER 6—SCALING. In *The Fundamentals of Corrosion and Scaling for Petroleum & Environmental Engineers* (pp. 117–139). Gulf Publishing Company. https://doi.org/10.1016/B978-1-933762-30-2.50012-4

Chua, P. C., Sæbø, M., Lunde, A., & Kelland, M. A. (2011). Dual Kinetic Hydrate Inhibition and Scale Inhibition by Polyaspartamides. *Energy & Fuels*, *25*(11), 5165–5172. https://doi.org/10.1021/ef201007c

Correll, D. L. (1998). The Role of Phosphorus in the Eutrophication of Receiving Waters: A Review. *Journal of Environmental Quality*, *27*(2), 261. https://doi.org/10.2134/jeq1998.00472425002700020004x

Dada, A. O., Olalekan, A. P., Olatunya, A. M., & Dada, O. (2012). Langmuir, Freundlich, Temkin and Dubinin–Radushkevich Isotherms Studies of Equilibrium Sorption of Zn²⁺ Unto Phosphoric Acid Modified Rice Husk. *IOSR Journal of Applied Chemistry*, *3*(1), 38–45. https://doi.org/10.9790/5736-0313845

Darling, D., & Rakshpal, R. (1998, March 22). Green Chemistry Applied to Corrosion and Scale Inhibitors. *CORROSION98*. http://onepetro.org/NACECORR/proceedings/CORR98/All-CORR98/NACE-98207/127691

Dirdal, E. G. (2022, June 2). [Personal communication].

Dirdal, E. G., & Kelland, M. A. (2020). Synthesis and Investigation of Polymers of 2-Methacrylamido-caprolactam as Kinetic Hydrate Inhibitors. *Energy & Fuels*, *34*(6), 6981–6990. https://doi.org/10.1021/acs.energyfuels.0c00929

Dirdal, E. G., & Kelland, M. A. (2022). Alternative Lactam-Based Kinetic Hydrate Inhibitors-Investigation of Polymers of 2-Methacrylamido-caprolactam. *Energy & Fuels*, *36*(6), 3107–3118. https://doi.org/10.1021/acs.energyfuels.2c00208

Edwards, A., Osborne, C., Webster, S., Klenerman, D., Joseph, M., Ostovar, P., & Doyle, M. (1994). Mechanistic Studies of the Corrosion Inhibitor Oleic Imidazoline. *Corrosion Science*, *36*(2), 315–325. https://doi.org/10.1016/0010-938X(94)90160-0

EL-Haddad, M. N. (2014). Hydroxyethylcellulose used as an Eco-Friendly Inhibitor for 1018 C-Steel Corrosion in 3.5% NaCl Solution. *Carbohydrate Polymers*, *112*, 595–602. https://doi.org/10.1016/j.carbpol.2014.06.032

El-Sayed, A.-R., Mohran, H. S., & Abd El-Lateef, H. M. (2011). Inhibitive Action of Ferricyanide Complex Anion on Both Corrosion and Passivation of Zinc and Zinc–Nickel Alloy in the Alkaline Solution. *Journal of Power Sources*, *196*(15), 6573–6582. https://doi.org/10.1016/j.jpowsour.2011.03.057

Farhadian, A., Varfolomeev, M. A., Rezaeisadat, M., Semenov, A. P., & Stoporev, A. S. (2020). Toward a Bio-Based Hybrid Inhibition of Gas Hydrate and Corrosion for Flow Assurance. *Energy*, *210*, 118549. https://doi.org/10.1016/j.energy.2020.118549

Farhadian, A., Varfolomeev, M. A., Semenov, A. P., Mendgaziev, R. I., & Stoporev, A. S. (2020). Dual-Function Synergists Based on Glucose and Sucrose for Gas Hydrate and Corrosion Inhibition. *Energy & Fuels*, *34*(11), 13717–13727. https://doi.org/10.1021/acs.energyfuels.0c02436

Ferrer, A., & Bennett, B. (2022). Remediating Oilfield Deposition from the Laboratory Bench to the Field – Development of a Multifunctional Product. *IPTC-22249-MS*, 17. https://doi.org/10.2523/IPTC-22249-MS

Foss, M., Gulbrandsen, E., & Sjöblom, J. (2010). Oil Wetting and Carbon Dioxide Corrosion Inhibition of Carbon Steel with Ferric Corrosion Products Deposits. *Corrosion*, *66*(2), 025005-025005–025011. https://doi.org/10.5006/1.3319662

Galio, A., & Dariva, C. (2014). Corrosion Inhibitors – Principles, Mechanisms and Applications. In M. Aliofkhazraei (Ed.), *Developments in Corrosion Protection* (pp. 365–380). https:/doi.org/10.5772/57255

Gamry Instruments. (n.d.). *Getting Started with Electrochemical Corrosion Measurement*. Retrieved 12 December 2021, from https://www.gamry.com/application-notes/corrosion-coatings/basics-of-electrochemical-corrosion-measurements/

Gamry Instruments. (n.d.). *Potentiostat Calibration with Dummy Cell*. Potentiostat Calibration. Retrieved 2 April 2022, from https://www.gamry.com/support/technical-support/troubleshooting/troubleshooting-walkthrough/potentiostat-calibration/

Gamry Instruments. (2017). *EuroCell Operator's Manual*. https://www.gamry.com/assets/Uploads/EuroCell-Kit-Manual.pdf

Gao, X., Liu, S., Lu, H., Gao, F., & Ma, H. (2015). Corrosion Inhibition of Iron in Acidic Solutions by Monoalkyl Phosphate Esters with Different Chain Lengths. *Industrial & Engineering Chemistry Research*, *54*(7), 1941–1952. https://doi.org/10.1021/ie503508h

Ghorbani, N., Wilson, M. C. T., Kapur, N., Fleming, N., Tjomsland, T., & Neville, A. (2017). Adsorption of Polyphosphinocarboxylic Acid (PPCA) Scale Inhibitor on Carbon Nanotubes (CNTs): A Prospective Method for Enhanced Oilfield Scale Prevention. *Journal of Petroleum Science and Engineering*, *150*, 305–311. https://doi.org/10.1016/j.petrol.2016.12.016

Hasson, D., Shemer, H., & Sher, A. (2011). State of the Art of Friendly "Green" Scale Control Inhibitors: A Review Article. *Industrial & Engineering Chemistry Research*, *50*(12), 7601–7607. https://doi.org/10.1021/ie200370v

Hemmingsen, T. (2022, February 4). [Personal communication].

Heydari, M., & Javidi, M. (2012). Corrosion Inhibition and Adsorption Behaviour of an Amido-Imidazoline Derivative on API 5L X52 Steel in CO_2-Saturated Solution and

Synergistic Effect of Iodide Ions. *Corrosion Science*, *61*, 148–155. https://doi.org/10.1016/j.corsci.2012.04.034

Jaal, R. A., Ismail, M. C., & Ariwahjoedi, B. (2014). A Review of CO_2 Corrosion Inhibition by Imidazoline-based Inhibitor. *MATEC Web of Conferences*, *13*, 05012. https://doi.org/10.1051/matecconf/20141305012

Jain, P., Patidar, B., & Bhawsar, J. (2020). Potential of Nanoparticles as a Corrosion Inhibitor: A Review. *Journal of Bio- and Tribo-Corrosion*, *6*(2), 43. https://doi.org/10.1007/s40735-020-00335-0

Kamal, M. S. (2018). Oilfield Scale Formation and Chemical Removal: A review. *Journal of Petroleum Science and Engineering*, *171*, 127–139. https://doi.org/10.1016/j.petrol.2018.07.037

Ke, W., & Kelland, M. A. (2016). Kinetic Hydrate Inhibitor Studies for Gas Hydrate Systems: A Review of Experimental Equipment and Test Methods. *Energy & Fuels*, *30*(12), 10015–10028. https://doi.org/10.1021/acs.energyfuels.6b02739

Kelland, M. A. (2006). History of the Development of Low Dosage Hydrate Inhibitors. *Energy & Fuels*, *20*(3), 825–847. https://doi.org/10.1021/ef050427x

Kelland, M. A. (2014). *Production Chemicals for the Oil and Gas Industry* (2nd ed.). CRC Press.

Kelland, M. A. (2018). A Review of Kinetic Hydrate Inhibitors from an Environmental Perspective. *Energy & Fuels*, *32*(12), 12001–12012. https://doi.org/10.1021/acs.energyfuels.8b03363

Kelland, M. A., Moi, N., & Howarth, M. (2013). Breakthrough in Synergists for Kinetic Hydrate Inhibitor Polymers, Hexaalkylguanidinium Salts: Tetrahydrofuran Hydrate Crystal Growth Inhibition and Synergism with Polyvinylcaprolactam. *Energy & Fuels*, *27*(2), 711–716. https://doi.org/10.1021/ef301718c

Kelland, M. A., Pomicpic, J., Ghosh, R., Undheim, C., Hemmingsen, T. H., Zhang, Q., Varfolomeev, M. A., Pavelyev, R. S., & Vinogradova, S. S. (2021). Multi-Functional Oilfield Production Chemicals: Maleic-Based Polymers for Gas Hydrate and Corrosion Inhibition. *IOP Conference Series: Materials Science and Engineering*, *1201*(1), 012081. https://doi.org/10.1088/1757-899X/1201/1/012081

Kelland, M. A., Svartaas, T. M., & Dybvik, L. (1995). Studies on New Gas Hydrate Inhibitors. *Society of Petroleum Engineers*. https://doi.org/10.2118/30420-MS

Keserovic Hoff, A. (2022, February 4). [Personal communication].

Koch, G., Varney, J., Thompson, N., Moghissi, O., Gould, M., & Payer, J. (2016). *International Measures of Prevention, Application and Economics of Corrosion Technology*. NACE. http://impact.nace.org/documents/Nace-International-Report.pdf

Koh, C. A., & Sum, A. (2010). *Natural Gas Hydrates in Flow Assurance*. Gulf Professional Publishing. https://books.google.no/books?id=HJJcnIX7q3MC

Kohler, N., Courbin, G., Estievenart, C., & Ropital, F. (2002). Polyaspartates: Biodegradable Alternates to Polyacrylates or Noteworthy Multifunctional Inhibitors? *CORROSION02*, 20. https://onepetro.org/NACECORR/proceedings/CORR02/All-CORR02/NACE-02411/114715

Kvarekvål, J., & Moloney, J. (2017). Sour Corrosion. In *Trends in Oil and Gas Corrosion Research and Technologies* (pp. 113–147). Elsevier. https://doi.org/10.1016/B978-0-08-101105-8.00006-1

Lattemann, S., & Höpner, T. (2008). Environmental Impact and Impact Assessment of Seawater Desalination. *Desalination*, *220*(1), 1–15. https://doi.org/10.1016/j.desal.2007.03.009

Lawless, T. A., Bourne, H. M., Bolton, J. R., & Services, A. P. (1993). *Examining the Potential for Corrosion lnhibitor and Scale lnhibitor Compatibility in a Multifunctional Squeeze Strategy*. 10. https://doi.org/10.2118/25167-MS

Liu, J., Ren, C., Yang, Z., & Shi, W. (2007). Novel Route for Synthesizing Hyperbranched Polyamine. *Journal of Polymer Science Part A: Polymer Chemistry*, *45*(4), 699–708. https://doi.org/10.1002/pola.21839

Ma, M., Zhang, Y., Guo, Z., & Gu, N. (2013). Facile Synthesis of Ultrathin Magnetic Iron Oxide Nanoplates by Schikorr Reaction. *Nanoscale Research Letters*, *8*(1), 16. https://doi.org/10.1186/1556-276X-8-16

MacAdam, J., & Jarvis, P. (2015). Chapter 1 - Water-Formed Scales and Deposits: Types, Characteristics, and Relevant Industries. In Z. Amjad & K. D. Demadis (Eds.), *Mineral Scales and Deposits* (pp. 3–23). Elsevier. https://doi.org/10.1016/B978-0-444-63228-9.00001-2

Mady, M. F., Malmin, H., & Kelland, M. A. (2019). Sulfonated Nonpolymeric Aminophosphonate Scale Inhibitors—Improving the Compatibility and Biodegradability. *Energy & Fuels*, *33*(7), 6197–6204. https://doi.org/10.1021/acs.energyfuels.9b01032

Manfra, L., Cianelli, D., Di Mento, R., & Zambianchi, E. (2018). Numerical-Ecotoxicological Approach to Assess Potential Risk Associated with Oilfield Production Chemicals Discharged into the Sea. *Environmental Science and Pollution Research*, *25*(18), 18213–18219. https://doi.org/10.1007/s11356-018-2355-x

Martinod, A., Euvrard, M., Foissy, A., & Neville, A. (2008). Progressing the Understanding of Chemical Inhibition of Mineral Scale by Green Inhibitors. *Desalination*, *220*(1), 345–352. https://doi.org/10.1016/j.desal.2007.01.039

Mathias, L. J., & Moore, D. R. (1987). *POLY(1-OXY-3-LACTAM WINYLENE)* (U.S. Patent No. 4,644,050).

Mazumder, J., & A, M. (2020). A Review of Green Scale Inhibitors: Process, Types, Mechanism and Properties. *Coatings*, *10*(10), 928. https://doi.org/10.3390/coatings10100928

Mékarbané, P., Alonzo, D., Moser, F., & Larrouy, G. (2019). Development of Combined Corrosion and Scale Inhibitors. *CORROSION19*. https://onepetro.org/NACECORR/proceedings/CORR19/All-CORR19/NACE-2019-12960/127201

Messer. (n.d.). *Instructions for Use Constant 2000 Pressure Regulator for Gas Cylinder*. https://cdn.manomano.com/files/pdf/2727485.pdf

Migahed, M. A., elgendy, Amr., EL-Rabiei, M. M., Nady, H., & Zaki, E. G. (2018). Novel Gemini Cationic Surfactants as Anti-Corrosion for X-65 Steel Dissolution in Oilfield Produced Water Under Sweet Conditions: Combined Experimental and Computational Investigations. *Journal of Molecular Structure*, *1159*, 10–22. https://doi.org/10.1016/j.molstruc.2018.01.033

Mohamed, H., El-Lateef, H., Abbasov, V., Aliyeva, L., & Ismayilov, T. (2012). Corrosion Protection of Steel Pipelines Against CO_2 Corrosion-A Review. *Chem. J.*, *2*. https://www.researchgate.net/publication/267557833

Mpelwa, M., & Tang, S.-F. (2019). State of the Art of Synthetic Threshold Scale Inhibitors for Mineral Scaling in the Petroleum Industry: A Review. *Petroleum Science*, *16*(4), 830–849. https://doi.org/10.1007/s12182-019-0299-5

Neff, J., Lee, K., & DeBlois, E. M. (2011). Produced Water: Overview of Composition, Fates, and Effects. In K. Lee & J. Neff (Eds.), *Produced Water: Environmental Risks and Advances in Mitigation Technologies* (pp. 3–54). Springer. https://doi.org/10.1007/978-1-4614-0046-2_1

Obot, I. B. (2009). Synergistic Effect of Nizoral and Iodide Ions on the Corrosion Inhibition of Mild Steel in Sulphuric Acid Solution: *Portugaliae Electrochimica Acta*, *27*(5), 539–553. https://doi.org/10.4152/pea.200905539

OECD. (2014). *Chemicals Used in Oil Well Production*. https://www.oecd-ilibrary.org/content/publication/9789264220966-en

Oguzie, E. E., Li, Y., & Wang, F. H. (2007). Corrosion Inhibition and Adsorption Behavior of Methionine on Mild Steel in Sulfuric Acid and Synergistic Effect of Iodide Ion. *Journal of Colloid and Interface Science*, *310*(1), 90–98. https://doi.org/10.1016/j.jcis.2007.01.038

Olajire, A. A. (2015). A Review of Oilfield Scale Management Technology for Oil and Gas Production. *Journal of Petroleum Science and Engineering*, *135*, 723–737. https://doi.org/10.1016/j.petrol.2015.09.011

Olvera-Martínez, M. E., Mendoza-Flores, J., & Genesca, J. (2015). CO_2 Corrosion Control in Steel Pipelines. Influence of Turbulent Flow on the Performance of Corrosion Inhibitors. *Journal of Loss Prevention in the Process Industries*, *35*, 19–28. https://doi.org/10.1016/j.jlp.2015.03.006

O'Reilly, R., Ieong, N. S., Chua, P. C., & Kelland, M. A. (2011). Crystal Growth Inhibition of Tetrahydrofuran Hydrate with Poly(N-vinyl piperidone) and Other Poly(N-vinyl lactam) Homopolymers. *Chemical Engineering Science*, *66*(24), 6555–6560. https://doi.org/10.1016/j.ces.2011.09.010

Palumbo, G., Górny, M., & Banaś, J. (2019). Corrosion Inhibition of Pipeline Carbon Steel (N80) in CO_2-Saturated Chloride (0.5 M of KCl) Solution Using Gum Arabic as a Possible Environmentally Friendly Corrosion Inhibitor for Shale Gas Industry. *Journal of Materials Engineering and Performance*, *28*(10), 6458–6470. https://doi.org/10.1007/s11665-019-04379-3

Palumbo, G., Kollbek, K., Wirecka, R., Bernasik, A., & Górny, M. (2020). Effect of CO_2 Partial Pressure on the Corrosion Inhibition of N80 Carbon Steel by Gum Arabic in a CO_2-Water Saline Environment for Shale Oil and Gas Industry. *Materials*, *13*(19), 4245. https://doi.org/10.3390/ma13194245

Park, J., Kim, H., Sheng, Q., Wood, C. D., & Seo, Y. (2017). Kinetic Hydrate Inhibition Performance of Poly(vinyl caprolactam) Modified with Corrosion Inhibitor Groups. *Energy & Fuels*, *31*(9), 9363–9373. https://doi.org/10.1021/acs.energyfuels.7b01956

Pou, T. E. (2014). *Bifunctional Anti-Deposit and Anti-Corrosion Additives* (United States Patent No. US20140216748A1). https://patents.google.com/patent/US20140216748A1/en?oq=Patent+US2014216748A

Qasim, A., Khan, M. S., Lal, B., & Shariff, A. M. (2019). A Perspective on Dual Purpose Gas Hydrate and Corrosion Inhibitors for Flow Assurance. *Journal of Petroleum Science and Engineering*, *183*, 106418. https://doi.org/10.1016/j.petrol.2019.106418

Rathish, R. J., Dorothy, R., Joany, R. M., & Pandiarajan, M. (2013). Corrosion Resistance of Nanoparticle—Incorporated Nano Coatings. *European Chemical Bulletin*, *2*(12), 965–970. https://doi.org/10.17628/ECB.2013.2.965-970

Santos, B. A. F., Serenario, M. E. D., Souza, R. C., Oliveira, J. R., Vaz, G. L., Gomes, J. A. C. P., & Bueno, A. H. S. (2021). The Electrolyte Renewal Effect on the Corrosion Mechanisms of API X65 Carbon Steel Under Sweet and Sour Environments. *Journal of Petroleum Science and Engineering*, *199*, 108347. https://doi.org/10.1016/j.petrol.2021.108347

Shemer, H., & Hasson, D. (2015). Characterization of the Inhibitory Effectiveness of Environmentally Friendly Anti-Scalants. *Desalination and Water Treatment*, *55*(13), 3478–3484. https://doi.org/10.1080/19443994.2014.939493

Singh, A., Lin, Y., Zhu, C., Wu, Y., & Ebenso, E. E. (2015). Use of HPHT Autoclave to Determine Corrosion Inhibition Effect of Poly(methyl methacrylate-co-N-vinyl-2-pyrrolidone) on Carbon Steels in 3.5% NaCl Solution Saturated with CO_2. *Chinese Journal of Polymer Science*, *33*(2), 339–348. https://doi.org/10.1007/s10118-015-1587-1

Singh, A., & Suri, A. (2020). A Review on Gas Hydrates and Kinetic Hydrate Inhibitors Based on Acrylamides. *Journal of Natural Gas Science and Engineering*, *83*, 103539. https://doi.org/10.1016/j.jngse.2020.103539

Sloan, E. D., & Koh, C. A. (2007). *Clathrate Hydrates of Natural Gases* (3rd ed.). CRC Press. https://doi.org/10.1201/9781420008494

Sum, A. K., Koh, C. A., & Sloan, E. D. (2012). Developing a Comprehensive Understanding and Model of Hydrate in Multiphase Flow: From Laboratory Measurements to Field Applications. *Energy & Fuels*, *26*(7), 4046–4052. https://doi.org/10.1021/ef300191e

Tang, Z. (2019). A Review of Corrosion Inhibitors for Rust Preventative Fluids. *Current Opinion in Solid State and Materials Science*, *23*(4), 100759. https://doi.org/10.1016/j.cossms.2019.06.003

Tiu, B. D. B., & Advincula, R. C. (2015). Polymeric Corrosion Inhibitors for The Oil and Gas Industry: Design Principles and Mechanism. Reactive and Functional Polymers. *Reactive and Functional Polymers*, *95*, 25–45. https://doi.org/10.1016/j.reactfunctpolym.2015.08.006

Undheim, C. (2021). *An Established Manual for Corrosion Testing and Corrosion Inhibitor Analysis* [University of Stavanger]. Bachelor Thesis. https://hdl.handle.net/11250/2774276

Usman, B. J., & Ali, S. A. (2018). Carbon Dioxide Corrosion Inhibitors: A Review. *Arabian Journal for Science and Engineering*, *43*(1), 1–22. https://doi.org/10.1007/s13369-017-2949-5

Yu, H., Wu, J. H., Wang, H. R., Wang, J. T., & Huang, G. S. (2006). Corrosion Inhibition of Mild Steel by Polyhydric Alcohol Phosphate Ester (PAPE) in Natural Sea Water. *Corrosion Engineering, Science and Technology*, *41*(3), 259–262. https://doi.org/10.1179/174327806X111207

Zhang, J., Liu, J., Yu, W., Yan, Y., You, L., & Liu, L. (2010). Molecular Modeling of the Inhibition Mechanism of 1-(2-aminoethyl)-2-alkyl-imidazoline. *Corrosion Science*, *52*(6), 2059–2065. https://doi.org/10.1016/j.corsci.2010.02.018

Zhang, P., Kan, A. T., & Tomson, M. B. (2015). Chapter 24—Oil Field Mineral Scale Control. In Z. Amjad & K. D. Demadis (Eds.), *Mineral Scales and Deposits* (pp. 603–617). Elsevier. https://doi.org/10.1016/B978-0-444-63228-9.00024-3

Zheng, Y., Gao, Y., Li, H., Yan, M., Zhao, J., & Liu, Z. (2021). Chitosan-Acrylic Acid-Polysuccinimide Terpolymer as Environmentally Friendly Scale and Corrosion Inhibitor in Artificial Seawater. *Desalination*, *520*, 115367. https://doi.org/10.1016/j.desal.2021.115367

Zhukov, A. Y., Stolov, M. A., & Varfolomeev, M. A. (2017). *Use of Kinetic Inhibitors of Gas Hydrate Formation in Oil and Gas Production Processes: Current State and Prospects of Development*. https://doi.org/10.1007/s10553-017-0814-6

Appendix A
EuroCell kit washing procedures.

Washing procedures for the EuroCell, gas bubbler, reference bridge tube, sample holder, counter electrode isolation tube, and pill magnet:

1. Rinse with water.
2. Rinse with acetone.
3. Rinse with DIW.
4. Apply acid or basic solution thoroughly.
5. Wipe gently with tissue paper if needed.
6. Rinse with DIW.
7. Rinse with acetone.
8. Rinse with DIW.

Repeat the above sequence before and after corrosion testing. The EuroCell may be left filled with an acidic or basic solution and containing glassware and Teflon components overnight to ensure removal any remaining inhibitor. The reference bridge tube should be stored filled with brine, and the tip submerged in brine or a 1M HCl solution.

Washing of coupon:

1. Rinse with acetone.
2. Submerge coupon in i-PrOH and sonicate for one hour.
3. Rinse with acetone.
4. Rinse with DIW.
5. Apply acetone to tissue paper and wipe coupon surface thoroughly.
6. Rinse with DIW.
7. Apply DIW to tissue paper and wipe coupon surface thoroughly.
8. Rinse with DIW.
9. Apply ethanol to tissue paper and wipe coupon surface thoroughly.
10. Rinse with DIW.
11. Apply i-PrOH to tissue paper and wipe coupon surface thoroughly.
12. Rinse with DIW.
13. Rinse with acetone.
14. Rinse with DIW.

After assembly, the working electrode with attached coupon should be rinsed with acetone and DIW prior to insertion into the EuroCell.

Washing of platinum wire counter electrode:

1. Apply DIW to tissue paper and gently wipe the platinum wire gently.
2. Apply acetone to tissue paper and gently wipe the platinum wire gently.

The platinum wire may be submerged in DCM overnight after testing. Let the wire dry before inserting into the counter electrode isolation tube.

Appendix B

Corrosion test procedure for Gamry EuroCell with brine, added CO_2 and corrosion inhibitor.

1. Initiate sonication of coupon in i-PrOH for one hour.
2. Wash the EuroCell, gas bubbler, reference bridge tube, and pill magnet as described in Appendix A.
3. Place the EuroCell on a magnetic stirrer and secure with a three-fingered clamp attached to a stand, as described in (Gamry Instruments, 2017, p. 5).
4. Add 150 ml 3.5 wt. % NaCl brine and pill magnet to the EuroCell.
5. Set magnetic stirrer to 200 rpm.
6. Assemble EuroCell gas bubbler as described in (Gamry Instruments, 2017, p. 8)
7. Insert EuroCell gas bubbler into the EuroCell and attach inlet and outlet gas hose as described in (Gamry Instruments, 2017, pp. 9–10)
8. Close all open ports in the EuroCell.
9. Open gas valves until pressure reaches 0.5 – 1 bar and sparge brine with CO_2.
10. Replace brine in the reference bridge tube, and assemble as described in (Gamry Instruments, 2017, p. 13) ensure no bubbles are present inside. If the reference bridge tube was stored in 1 M HCl, it should be kept in brine for a minimum of 30 minutes prior to insertion into the EuroCell.
11. Open ventilation hole on reference electrode as described by (Gamry Instruments, 2017, p. 14), and place in reference bridge tube.
12. Wash coupon as described in Appendix A.
13. Open the Sequence Wizard and create or open a sequence as described in chapter 2.2.10, and give each step unique names.
14. Wash and assemble counter electrode as described in (Gamry Instruments, 2017, p. 10), and insert it into the EuroCell.
15. If brine has sparged for minimum 40 minutes and pH is 4 – 5, wash and assemble the sample holder as described in (Gamry Instruments, 2017, p. 15).
16. Attach connection clamps; white on reference, blue/green on sample holder, red/orange on counter electrode.
17. Initiate the LPR sequence.

After the last measurement has been taken, the corrosion cell can be disassembled and washed as described in Appendix A. The reference electrode and bridge tube should be stored as described in chapter 2.2.8.

If using the sequence as described in chapter 2.2.10, the following steps will also apply:
18. After initiation of the sequence, the coupon will stabilize in brine for one hour.
19. An initial LPR test will be conducted. A corrosion rate around 2 mmpy is expected with the setup in this thesis. Large deviation from this may be due to contamination, leakage, poor brine, low temperature, high pH, bad connection, or something else. Consult the troubleshooting section in the operator's manual (Gamry Instruments, 2017, pp. 19–20).
20. The sequence will form a baseline over the course of two hours.
21. A one-hour delay to allow an inhibitor to be injected into the EuroCell.
22. The remaining time may be skipped by pressing "F2" or "Skip".
23. The sequence will run for three hours.

After the last measurement has been taken, the corrosion cell can be disassembled and washed as described in Appendix A. The reference electrode and bridge tube should be stored as described in subchapter 2.2.8.

Appendix C

Summary corrosion results for chapters 3 and 5.

Table C-1 Summary corrosion test results.

Inhibitor	Synergist	$C_{Inhibitor}$ (ppm)	$C_{Synergist}$ (ppm)	$CR_{Baseline}$ (mmpy)	$SD_{Baseline}$	$CR_{Inhibitor}$ (mmpy)	$SD_{Inhibitor}$	Efficiency ($\%\eta\pm\%SE$)	Soluble in water
Imidazoline	MCSA	500	100	1.783	0.031	0.467	0.012	73.8±1.2	Yes
Imidazoline	SLS	500	100	1.876	0.048	0.368	0.012	80.4±1.7	Yes
Imidazoline	TGA	500	100	1.845	0.028	0.461	0.036	75±1.8	Yes
Imidazoline		500		2.089	0.061	0.306	0.017	85.4±2.2	Yes
Imidazoline		100		1.818	0.021	0.427	0.031	76.5±1.5	Yes
Imidazoline + acetic acid 3:1 mix		100		1.942	0.045	0.733	0.040	62.3±2.4	Yes
Imidazoline 90 % brine 10 % LAWS		100		1.892	0.020	0.403	0.049	78.7±2.0	Yes
SLS	TBA	500	100	2.025	0.056	0.111	0.009	94.5±1.8	Yes
SLS		500		2.136	0.049	0.087	0.006	95.9±1.6	Yes
Luvicap 55W (1:1 VP:VCap copolymer)		500		2.034	0.090	1.275	0.051	37.3±4.1	Yes
PMA-DBAPA		500		2.079	0.065	0.925	0.019	55.5±2.4	No
PMA-DBAPA in DME		500		1.860	0.019	1.072	0.048	42.3±1.9	Yes
PMA-DBAPA-AO		500		2.150	0.080	0.855	0.048	60.2±3.7	Yes
Poly(ethylene glycol)		500		1.826	0.063	1.776	0.031	2.7±2.7	Yes
Polyacrylamide		500		1.842	0.035	1.231	0.013	33.2±1.4	Yes
Polylysine		500		1.862	0.025	1.107	0.035	40.6±1.8	Yes
OVPip:OVCap 60:40		500		1.791	0.020	1.386	0.031	22.6±1.5	No
OVPip:OVCap 60:40 (24h)		500		1.791	0.020	0.458	0.037	74.4±1.6	No
POVPip		500		1.789	0.024	1.513	0.099	15.4±3.6	Yes
Styrene sulfonic acid		500		1.912	0.028	2.163	0.033	-13.1±1.8	Yes
	STF		500	1.712	0.035	0.934	0.035	45.4±2.0	Yes
	MCSA		500	1.928	0.034	2.357	0.025	-22.3±1.7	Yes
	TBA		500	1.994	0.089	1.960	0.018	1.7±3.1	Yes
	TGA		500	2.080	0.057	2.688	0.068	-29.2±3.6	Yes

Abbreviations: BTG: Butyl thioglycolate. MCSA: Mercaptosuccinic acid. SLS: Sodium lignosulfonate. STF: Sodium thiosulfate. TBA: 2-Thiobarbituric acid. TGA: Thioglycolic acid. LAWS: Low aromatic white spirit (10 % toluene, 90 % heptane).

Appendix D

Summary corrosion results for chapter 4.

Table D-1 Summary corrosion results for PMA:VCap-DBAPA and synergists.

Inhibitor	Synergist	$C_{Inhibitor}$ (ppm)	$C_{Synergist}$ (ppm)	$CR_{Baseline}$ (mmpy)	$SD_{Baseline}$	$CR_{Inhibitor}$ (mmpy)	$SD_{Inhibitor}$	Efficiency (%η±%SE)	Soluble in water
PMA:VCap-(DBAPA:GLYP 80:20)	TBA	2500	1000	2.009	0.021	0.502	0.049	75.0±2.0	Yes
PMA:VCap-(DBAPA:GLYP 80:20)		500		2.009	0.021	2.634	0.033	-31.1±1.6	Yes
PMA:VCap-(DBAPA:GLYP 80:20)		1000		2.009	0.021	3.111	0.061	-54.8±2.4	Yes
PMA:VCap-(DBAPA:GLYP 80:20)		2500		2.009	0.021	3.531	0.043	-75.8±1.9	Yes
PMA:VCap-(DBAPA:AMT 80:20)		500		1.842	0.034	0.042	0.004	97.7±1.1	No
PMA:VCap-DBAPA	AMT	500	100	1.921	0.035	1.889	0.035	1.7±2.0	Yes
PMA:VCap-DBAPA	ATC	500	100	1.922	0.039	0.076	0.013	96.0±1.5	Yes
PMA:VCap-DBAPA	BID	500	100	1.932	0.023	2.529	0.102	-30.9±3.6	Yes
PMA:VCap-DBAPA	BTG	2500	1000	1.844	0.015	0.005	0.005	99.7±0.6	Yes
PMA:VCap-DBAPA	BTG	500	100	1.851	0.030	0.126	0.009	93.1±1.1	Yes
PMA:VCap-DBAPA	GTC	500	100	1.855	0.040	0.074	0.007	96.0±1.4	Yes
PMA:VCap-DBAPA	IBT	500	100	1.865	0.031	1.712	0.022	8.2±1.5	Yes
PMA:VCap-DBAPA	TBA	500	100	1.895	0.101	0.112	0.011	94.1±3.2	Yes
PMA:VCap-DBAPA	TGA	500	100	1.836	0.051	0.142	0.004	92.2±1.6	Yes
PMA:VCap-DBAPA		500		1.962	0.176	1.605	0.053	18.1±6.6	Yes
PMA:VCap-DBAPA-AO		500		1.973	0.026	1.652	0.030	16.3±1.6	Yes
	ATC		500	1.909	0.026	0.336	0.015	82.4±1.2	Yes
	BTG		100	1.759	0.012	0.102	0.015	94.2±0.8	Yes
	BTG		1000	1.759	0.012	0.130	0.014	92.5±0.8	Yes
	TBA		500	1.994	0.089	1.959	0.018	1.7±3.1	Yes
	TGA		500	2.080	0.057	2.688	0.068	-29.2±3.6	Yes

Abbreviations: AMT: 3-Acetamidotetrahydro-2-thiophenone. ATC: Ammonium thiocyanate. BID: 1-Butylimidazole. BTG: Butyl thioglycolate. GTC: Guanidine thiocyanate. IBT: Isobutylthiadiazole. TBA: 2-Thiobarbituric acid. TGA: Thioglycolic acid.

Appendix E

Summary KHI results for chapter 5.

Table E-1 Summary KHI results for copolymer and commercial KHI polymers.

Inhibitor	$C_{Inhibitor}$ (ppm)	$C_{Synergist}$ (ppm)	To_{Cell} 1	To_{Cell} 2	To_{Cell} 3	To_{Cell} 4	To_{Cell} 5	To_{Avg}	Ta_{Cell} 1	Ta_{Cell} 2	Ta_{Cell} 3	Ta_{Cell} 4	Ta_{Cell} 5	Ta_{Avg}	To_{Avg} - Ta_{Avg}
DIW			18.2	17.1	16.5	16.6	18.0	17.3	17.9	17.0	16.3	16.5	17.9	17.1	0.2
Luvicap 55W (1:1 VP:VCap copolymer)	2500		6.8	6.9	7.1	6.6	8.0	7.1	5.7	5.8	5.8	5.8	6.6	5.9	1.1
Luvicap EG (PVCap)	2500		8.8	8.7	9.3	8.8	9.2	9.0	7.8	7.9	8.1	7.7	8.2	7.9	1.0
OVPip:OVCap 1:1	2500		13.0	14.0	13.1	13.2	13.3	13.3	12.9	13.9	13.1	13.2	13.3	13.3	0.0
OVPip:OVCap 60:40	2500		13.4	12.7	14.1	14.9	13.5	13.7	13.2	12.5	13.8	13.7	13.4	13.3	0.4
OVPip:OVCap 62:38	1000		14.2		14.5	14.4	14.4	14.4	14		14.4	14.3	14.2	14.2	0.1
OVPip:OVCap 62:38	2500		12.8	12.6	12.9	12.9	13.8	13.0	12.7	12.4	12.8	12.8	13.4	12.8	0.2
OVPip:OVCap 62:38	5000		10.9		11.9	11.6	11.6	11.5	10.8		11.8	11.5	11.4	11.4	0.1
OVPip:OVCap 62:38 + HBGC	2500	5000	14.4	14.8	15.3	14.8	14.8	14.8	10.0	7.7	10.7	9.5	10.2	9.6	5.2
OVPip:OVCap 62:38 + iBGE	2500	5000	15.1	15.7	15.8	14.6	15.8	15.4	15.0	15.6	15.7	14.5	15.7	15.3	0.1
OVPip:OVCap 62:38 + MPO	2500	5000	16.4		16.4	15.9	16.5	16.3	12.7		12.8	12.5	12.7	12.7	3.6
OVPip:OVCap 62:38 + TAO	2500	5000	14.1		14.9	14.0	14.1	14.3	12.0		12.2	11.4	11.7	11.8	2.5
OVPip:OVCap 62:38 + TDD	2500	5000	14.7	14.6	15.0	15.5	15.3	15.0	14.5	14.3	14.7	15.3	15.1	14.8	0.2
OVPip:OVCap 62:38 + TPAB	2500	5000	13.7		13.9	13.8	13.5	13.7	12.3		12.6	12.4	12.2	12.4	1.4
OVPip:OVCap 62:38 + TPeAO	2500	5000	12.1		12.7	11.7	12.5	12.3	11.1		11.4	10.8	11.3	11.2	1.1
OVPip:OVCap 64:36	2500		11.7	11.8	11.8	11.1	11.4	11.6	11.6	11.7	11.8	10.9	11.3	11.5	0.1
OVPip:OVCap 70:30	2500		12.4	11.7	12.2	12.1	12.2	12.1	12.2	11.4	12.1	12.0	12.1	12.0	0.2
OVPip:OVCap 74:26	2500		12.1	12.0	12.9	11.9	12.1	12.2	12.0	12.0	12.8	11.8	12.0	12.1	0.1
OVPip:OVCap 83:17	2500		13.7	13.5	14.4	13.9	14.0	13.9	13.5	13.4	14.2	13.8	13.9	13.8	0.1
POVPip	2500		13.3	14.0	14.4	13.9	13.9	13.9	13.2	13.8	14.2	13.7	13.8	13.7	0.2

Abbreviations: DIW: Deionized water. HBGC: Hexabutylguanidinium chloride. iBGE: Iso-butyl glycol ether. MPO: 4-Methyl-1-pentanol. TAO: Tributyl amine oxide in i-PrOH. TDD: 2,4,7,9-Tetramethyl-5-decyne-4,7-diol. TPAB: Tetrapentylammonium bromide. TPeAO: Tri-n-pentylamine oxide.

Appendix F

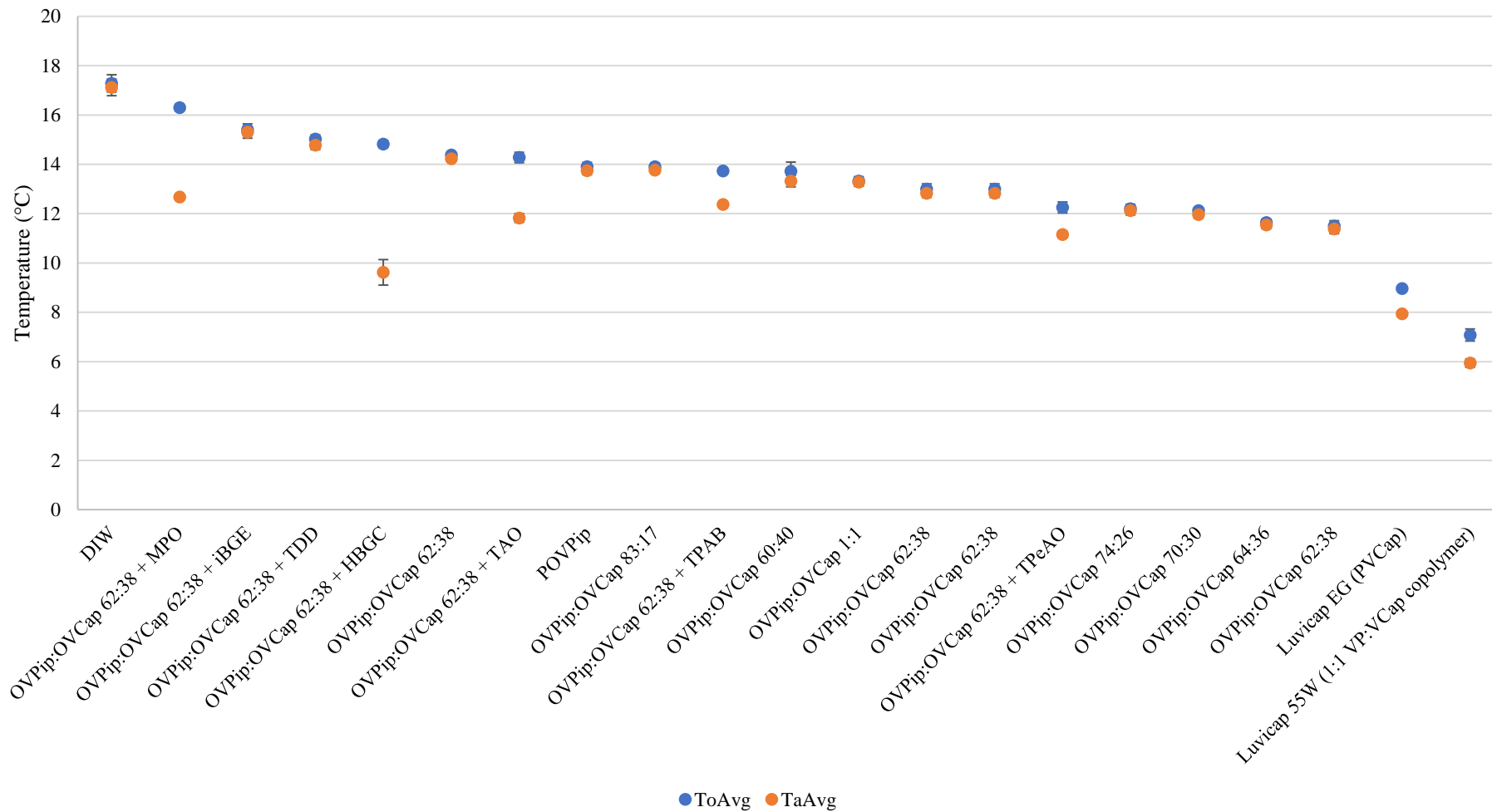Graphical presentation of KHI results for chapter 5.

Figure F-1 To/Ta KHI results for copolymer and commercial KHI polymers.

Appendix G

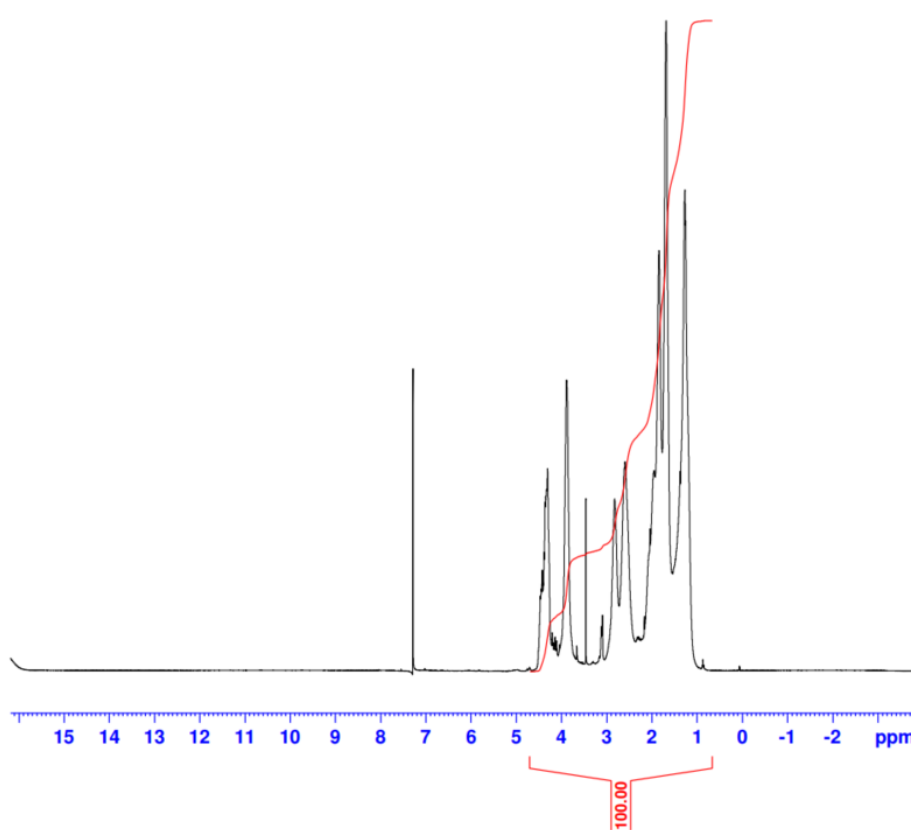Measured ^{1}H NMR spectrum for POVCap and POVPip in deuterated chloroform.
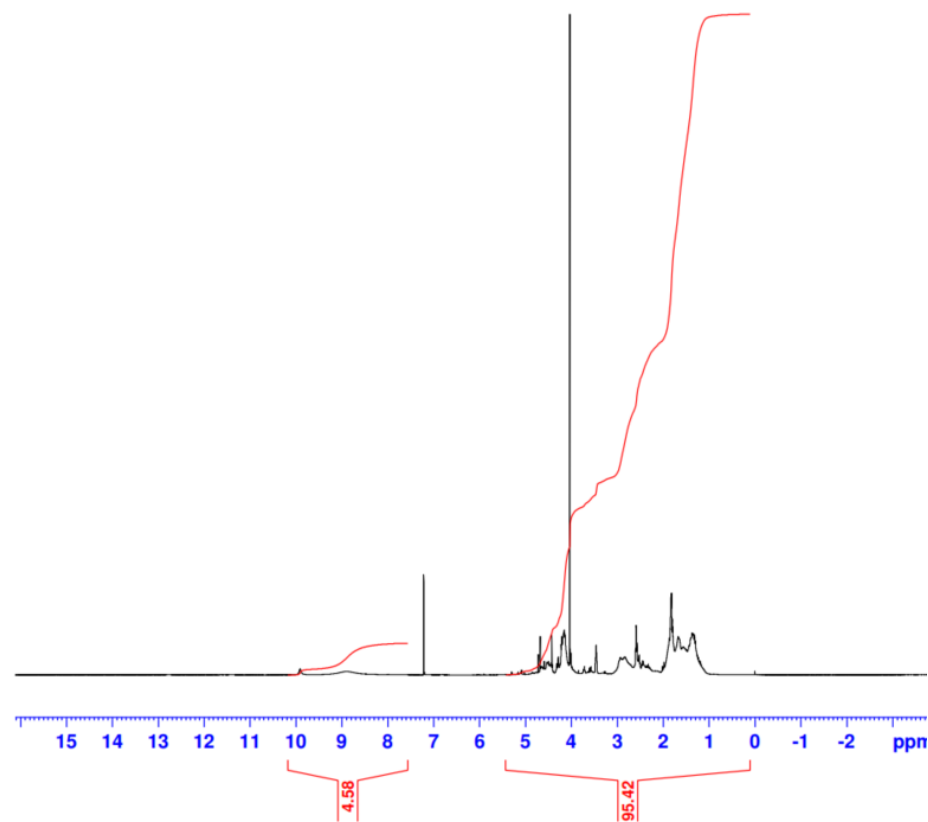

Figure G-1 ^{1}H NMR spectrum for POVCap.

Figure G-2 ^{1}H NMR spectrum for POVPip.

Appendix H

Measured ^{1}H NMR spectrum for copolymers OVPip:OVCap 70:30 and OVPip:OVCap 62:38 in deuterated chloroform.
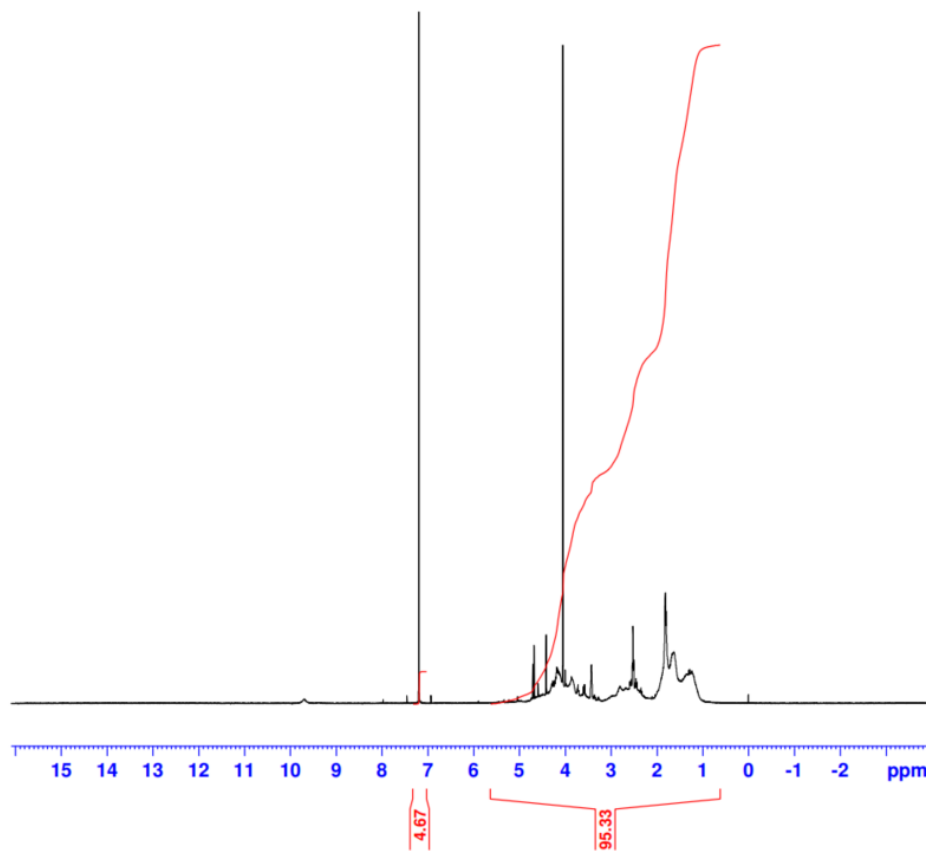

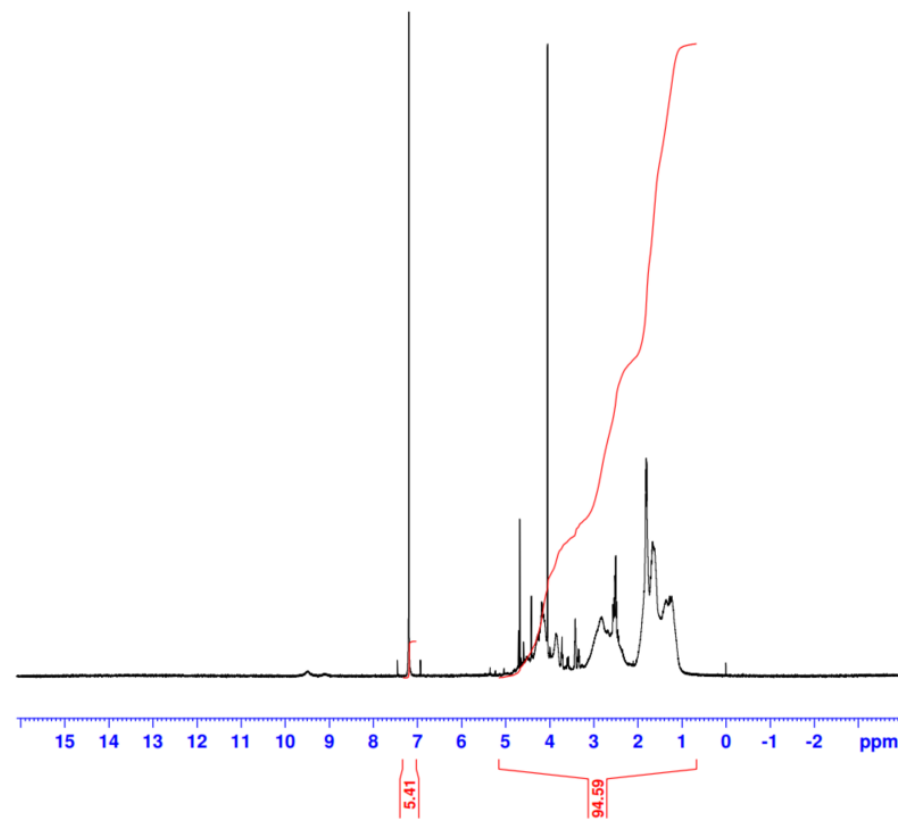*Figure H-1 ^{1}H NMR spectrum for OVPip:OVCap 70:30.*

Figure H-2 ^{1}H NMR spectrum for OVPip:OVCap 62:38.